Materials Today Advances 12 (2021) 100164

Contents lists available at ScienceDirect

Materials Today Advances

journal homepage: www.journals.elsevier.com/materials-today-advances/

Water-repellent surfaces of metallic glasses: fabrication and application

Z. Li [a, b], J. Ma [a, *]

[a] Shenzhen Key Laboratory of High Performance Nontraditional Manufacturing, College of Mechatronics and Control Engineering, Shenzhen University, Shenzhen, 518060, China

[b] College of Physics and Optoelectronic Engineering, Shenzhen University, Shenzhen, 518060, China

ARTICLE INFO

Article history:
Received 7 July 2021
Received in revised form
17 August 2021
Accepted 18 August 2021
Available online xxx

Keywords:
Water-repellent surface
Metallic glass
Fabrication approaches
Critical evaluations
Cutting-edge applications

ABSTRACT

Water-repellent surfaces based on advanced materials have broad applications in various fields. The amorphous structure and flexible element compositions make metallic glasses (MGs) suitable for multifunctional surfaces' design. Recent progresses in the fabrication and application of MG water-repellent surfaces are comprehensively reviewed. A variety of fabrication approaches are presented including thin film MG coating and bulk MG surface patterning as well as other potential methods based on manipulation of one-dimensional MGs. Considering the surface wetting kinetics and the metastable atomic structure, the evaluations on stability and durability of MG surfaces in real environment are discussed. Several critical evaluations of MG functional surfaces have been proposed for the design and fabrication, focusing on the size effect and external stimuli influence on the surface wettability and amorphous structure evolutions. On the basis of the systematic evaluations, the cutting-edge and potential applications of MG water-repellent surfaces are then discussed. Current challenges faced in practical applications and the prospects on the future developments are addressed to facilitate further research/investigations on MG functional surfaces.

1. Introduction

The water-repellent (hydrophobic or superhydrophobic) surfaces have been widely found in nature including the lotus leaves [1,2], flower petals [3,4], nepenthes [5,6], butterfly wings [7,8], insects compound eyes [9,10], water-strider legs [11,12], etc. These functional surfaces have recently drawn great attention owing to the potential utility in the emerging fields including anti-icing [13,14], drag reduction [15,16], self-cleaning [17,18], fluid transportation [19,20], battery and fuel cell applications [21,22]. As one of the most important aspects in the surface and interface science, the water-repellent property has a significant influence on some other crucial surface functions like corrosion inhibition [23], anti-bacteria [24], catalytic activity [25], biocompatibility [26], etc. Therefore, the research efforts for the fabrication and application of water-repellent surfaces have always been carried on for obtaining the fundamental understanding of functional surfaces [27–29]. It was found that the natural water-repellent surfaces have two basic features: low surface free energy and special surface geometrical structures. The classical theories of surface wettability have been developed by researchers to describe the contact conditions and tensions between interfacial surfaces (solid–liquid, liquid–vapor, and vapor–solid). Young's model [30], Wenzel model [31], and Cassie-Baxter model [32] were established respectively to rationalize the different wetting states considering the influence of surface morphology on contact modes, including the perfectly smooth surface contact, the rough surface with complete liquid penetration, and the rough surface with air trapped in solid–liquid interface. On the basis of these theories, to achieve enhanced water-repellent behavior, the micro-/nanostructures on the surface must keep air layer between water droplet and solid surface, so that they are partially contacted to provide a compound interface of material surface and air for water droplet. Inspired by nature, a variety of fabrication approaches have been proposed to prepare the artificial water-repellent surfaces with special structures on different substrate materials like ceramics, silicon, polymers, and metals [33]. To fabricate robust functional surfaces, the mechanical properties, chemical properties, corrosion resistance as well as the formability of the substrate materials should be fully taken into

* Corresponding author.
E-mail address: majiang@szu.edu.cn (J. Ma).

https://doi.org/10.1016/j.mtadv.2021.100164

account. Considerable efforts have been made to utilize the advanced materials as functional surface substrates in recent years.

Metallic glasses (MGs) known as amorphous alloys are usually fabricated by extremely fast quenching of melted metal at a sufficiently rapid cooling rate such as 10^3−10^6 K/s to bypass the regimes of nucleation and crystallization, so that the metals with vitrified state can be obtained [34−37]. In contrast to the crystalline metals, the MGs have an amorphous structure of the atomic arrangement and no crystal defects like dislocations and grain boundaries, which is beneficial to achieve higher strength, larger elasticity and better corrosion resistance [38−40]. In addition, a wonderful property is that the metallic glasses (MGs) show superplastic behavior with a low viscosity in the supercooled liquid regions (SCLRs), e.g. 10^3 Pa·s for zircon (Zr)-based MGs [41], this unique feature indicates that the material can be shaped into the micro-/nanostructures down to sub-10 nm levels under relatively moderate temperature and pressure [42−46]. The excellent formability of MGs provides access to plenty of approaches for fabricating structures in different scales for functional surfaces [47−50]. Various kinds of MGs have been developed on the basis of the compositions of zircon (Zr), iron (Fe), lanthanum (La), titanium (Ti), magnesium (Mg), cobalt (Co), copper (Cu), cerium (Ce), palladium (Pd), platinum (Pt), silver (Ag), etc. [38,40] As multicomponent alloys, the material compositions can be tuned in a broad range under the synthesis rules of MGs [51,52] to acquire different intrinsic characteristics, like the antibiosis with Ag and Cu [53,54], and the catalysis or degradation with Pt, Pd, and Fe [55−60]. Some of the MGs have a much lower surface free energy than the conventional metals, for example the water contact angle (CA) of the smooth surface of $Pd_{40}Cu_{30}Ni_{10}P_{20}$ MG has been detected as 98.8 degrees [61], which means the original surface of this kind of MG is hydrophobic, while most of the crystalline metals are inherently hydrophilic [62]. Therefore, MGs have advantages both in structure formability and composition flexibility to be substrate materials with superior mechanical properties for the fabrication of water-repellent surfaces.

This article focuses on the recent progresses in the fabrication and application for water-repellent surfaces of MGs. The bottom-up fabrication routes on the basis of the coating of thin film metallic glasses (TFMGs), and the top-down routes on the basis of surface patterning of bulk metallic glasses (BMGs) including thermoplastic forming, subtractive machining, chemical etching and dealloying, are systematically reviewed and discussed to give an overview of the present situations of fabrication processes. In addition to the approaches on the basis of TFMGs (2D) and BMGs (3D), the potential fabrication methods by manipulation of 1D MGs like micro-/nanoparticles and rods are also suggested. The critical evaluations of MG functional surfaces concerning the stability and durability, including the wetting kinetics, amorphous structure evolutions, mechanical properties, wear and corrosion resistance are proposed, hoping to promote the application of MG functional surfaces in the real environments, such as the cutting-edge fields presented in this paper. On the basis of this comprehensive review, the current challenges and future research focus of the design, fabrication and practical application for the water-repellent surfaces of MGs are further addressed.

2. Fabrication approaches of water-repellent surfaces

From the biological inspirations and wettability theories, the construction of specific surface micro-/nanostructures and surface modification by low-surface-energy materials are generally involved in the fabrication of the artificial water-repellent surfaces. For the MGs substrate with tunable composition and excellent formability, the principal existing forms prepared by different processes are the thin films and bulk counterparts. Correspondingly, the coating of thin film MGs and surface patterning of bulk MGs combined with surface modification are currently the main implementing approaches for water-repellent surfaces. Various fabrication methods have been carried out to obtain the thin films and specific surface textures of MGs with hydrophobic or superhydrophobic properties.

2.1. Coating of thin film metallic glasses

Thin film metallic glasses (TFMGs), as the 2D-MGs, were the earliest form of amorphous alloy fabricated by vapor deposition [34,63] and electrodeposition [64]. Because of the different formation processes, the local atomic structures of TFMGs is quite distinct with that of the rapid quenched bulk metallic glasses (BMG) [65], and the TFMGs with high level of disorder and excess free volume retain the superior mechanical properties of MGs and exhibit ultrastable amorphous atomic structure [66], meanwhile tending to be more ductile at room temperature and more flexible in the elemental compositions than their 3D counterparts [67−70]. A variety of fabrication routes for TFMGs have been conducted to extend their potential functional applications including water-repellent surfaces in diverse fields.

2.1.1. Sputtering

Sputtering process currently has become the most widely adopted approach to fabricate TFMGs with special micro/nano morphology and properties like biocompatibility [71], antibiosis [72], optical reflectivity [73] and excellent mechanical behaviors [74,75]. The principal fabrication process is using the argon ion accelerated by electric field to bombard the single alloy or multiple elemental targets, causing the sputtering of target material particles on the substrate, and then forming thin films. The high cooling rate (e.g. 10^9 K/s) of vapor-solid quenching ensures the formation of amorphous TFMGs with a large range of compositions [76,77]. Chu et al. [78,79] prepared a series of Zr-based thin films with the thickness less than 500 nm on stainless substrates by pulse magnetron sputtering. The smooth TFMGs with a surface roughness of 1 nm exhibited hydrophobicity as the water contact angle (CA) was above 90 degrees, indicating that the inherent low surface free energy of the fabricated TFMGs was achieved. In addition, the microhardness and corrosion resistance of the films were found both higher than the conventional metals. Zeman et al. [80] fabricated a binary amorphous thin film by co sputtering of Zr and Cu targets within a wide tunable composition range. The TFMGs were smoother and denser without columnar microstructures in the cross-section comparing to the pure elemental films. This can be a reason enhancing the hydrophobicity of the TFMGs (CA = 108 degrees), since the wettability is significantly affected by surface structures. The influence of the extra elements' addition in the Zr−Cu TFMGs on the surface properties has also been studied. It was found that with the increase of hafnium (Hf) fraction in the ternary amorphous films, the water contact angle slightly increased while the surface roughness decreased down to an extremely low value of 0.2 nm [81]. A further addition of Al or Si by co sputtering resulted into the quaternary TFMGs with hydrophobic surface as well as enhanced mechanical properties and thermal stability [82]. These improvements may be attributed to the fact that the added elements increased the covalent component and the average bond energy, indicating that the wettability of TFMGs can be regulated by the addition of mixed compositions.

The water-repellent TFMGs have always been concerned with and pursued in the biomedical applications in recent years. Chiang et al. [83] adopted the sputtering process to transform the Zr-based BMG target to TFMGs and the obtained films exhibited a good antimicrobial effect. In spite of these surface physical properties, the metal ions release of TFMGs also plays an important role in the antimicrobial abilities. The Cu-bearing TFMGs coated on dermatome demonstrated distinct hydrophobic and antibacterial properties along with a considerable improvement of blade sharpness [84,85]. And the co sputtering of Zr–Cu and Al–Ag targets resulted in a kind of multicomponent TFMGs with ions such as Cu^{2+}, Al^{3+}, Ag^{+} [72], exhibiting good hydrophobicity and excellent antibacterial property. The excellent antibiosis of these TFMGs can be rationalized by that the combination of water-repellent surfaces and chemical ionization substantially reduce the bacterial adherence and lead to the bacterial cell membranes damage or enzyme function alteration [86,87]. A titanium (Ti)-based TFMGs with no cytotoxicity was sputtered on bio-implantable substrates, it was found that hydrophobic surface with lower surface energy of the films correlated to the higher electrochemical corrosion resistance [88]. The hydrophobicity of the contact interfaces also has an important influence on the adhesive capacity and tribological property between the biological tissues and TFMG biomaterials. Chu et al. [89,90] employed magnetron sputtering depositing the Zr-based TFMGs with thickness of 80 nm on the syringe needles, and the TFMGs coating reduced insertion and retraction forces by over 60%, which can be attributed to the smooth surface morphology and low surface free energy as well as water-repellency (CA over 100 degrees). The cells adhesion tests were subsequently conducted on the glass substrate sputtered with hydrophobic TFMGs [91], showing that the attachment of platelet and cancer cell was dramatically suppressed.

The sputtering process has also been adopted to deposit TFMGs into nanostructures to obtain water-repellent properties and other functions. Chen et al. [92–94] fabricated ordered nanotube arrays of Zr-based TFMGs by magnetron sputtering using a photoresist template as the mask with well-defined contact hole arrays, as shown in Fig. 1a and b. The air trapped in the nanochamber between water droplet and nanotubes formed the liquid–vapor–solid interfaces to support the water droplet, this contact states significantly improve the surface hydrophobicity with a higher contact angle (CA) than that of the flat thin film metallic glasses (TFMGs) according to the Cassie-Baxter model [32]. The 3D nanostructures also provide a new way to switch the surface wettability by various external stimuli. For instance, surface heating can produce air thermal expansion and positive pressure within the nanochambers of the TFMGs, lifting the droplets and preventing water intrusion into the nanotubes. Thus, the CA was sensitive to pressure change of the nanochambers, and the wettability of the nanotube arrays surface can be thermally regulated by the applied voltage positively correlated with surface temperature. The CA first increases as the applied voltage is increased, which can be rationalized on the premise that higher air fraction can be occupied in the contact interfaces, while the CA then decreases due to the air leakage in the nanochamber. The maximum CA was achieved as about 150 degrees on the TFMG surface with a nanotube diameter of 500 nm under a medium voltage as shown in Fig. 1c. The thermal-response behavior of the array TFMGs extends the potential applications in bionic instruments, such as biosensors [92] and nanosucker devices [93]. Chu et al. [95] used magnetron sputtering to coat Zr-based TFMGs on the polyacrylonitrile (PAN) nanofibers to gain high hydrophobicity for the oil/water separation membrane. The CA of the TFMG-coated membrane increased with

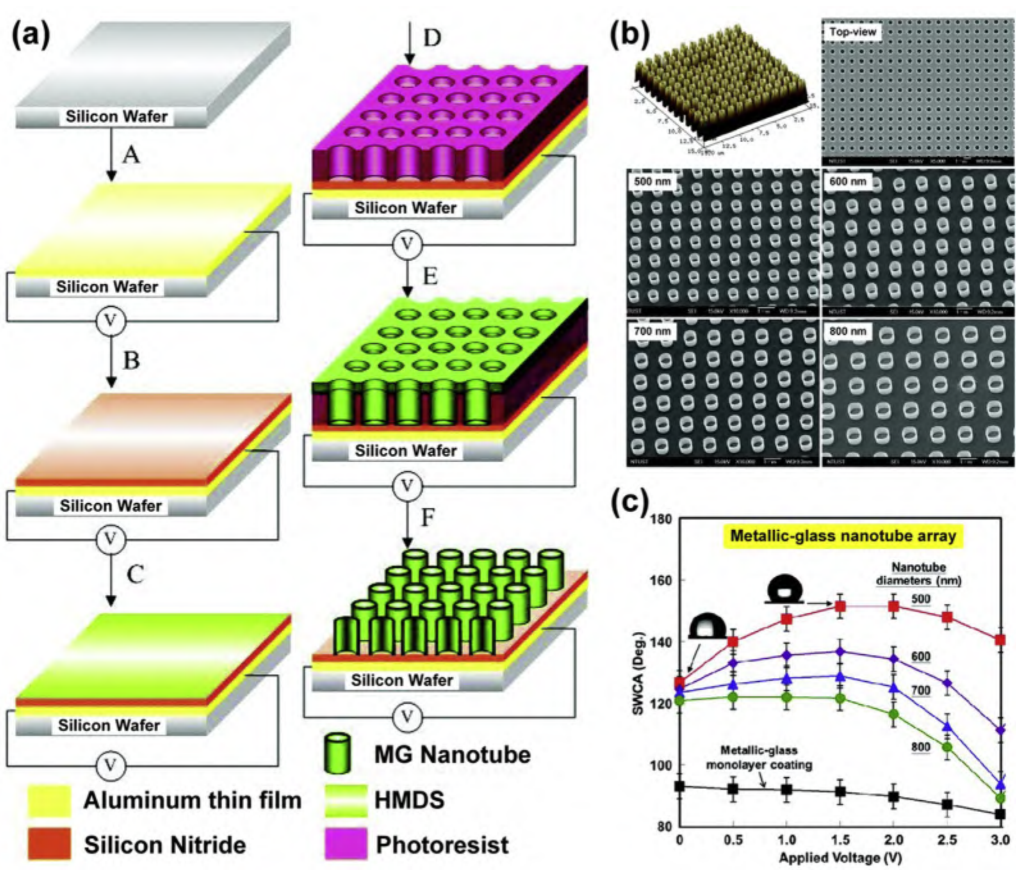

Fig. 1. (a) The fabrication process of the TFMG nanotube arrays. (b) AFM and SEM image nanotube arrays with different diameters. (c) Variation of the CA of the nanotube arrays and the plate TFMGs along with the heating voltages (Reproduced from ref. [93]).

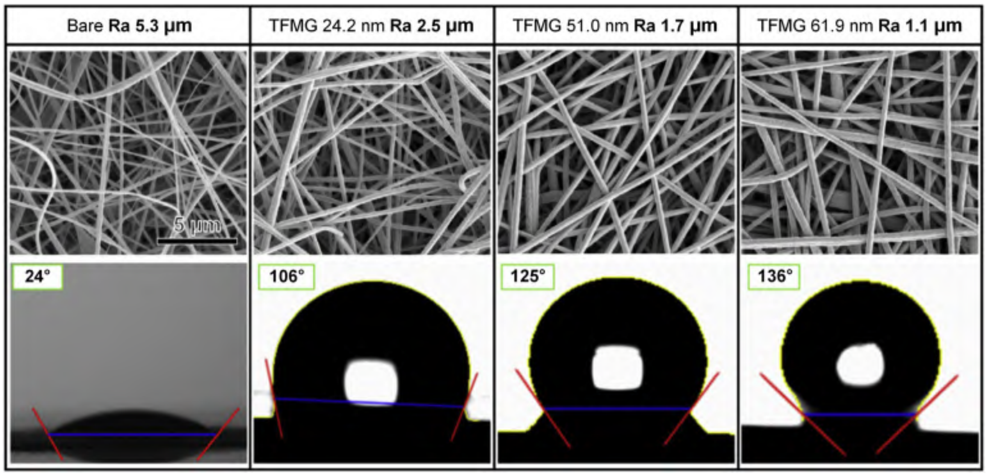

Fig. 2. Water contact angle of bare and coated membrane with various coating thickness of TFMGs (Reproduced from ref. [95]).

the coating thickness and smoothness due to the lower surface free energy, as shown in Fig. 2, by increasing the sputtering time from 10 to 35 min, the TFMG thickness increased to 61.9 nm, while the roughness decreased to Ra 1.1 μm, resulting to a high hydrophobic surface with a water contact angle of 136 degrees, so it is feasible to further improve the water-repellency of the fibers by optimizing the sputtering parameters.

A kind of flexible and stretchable TFMGs has been fabricated by utilizing the ductility of TFMGs [96,97]. The Cu-based amorphous coatings were deposited by ion beam sputtering on the polydimethylsiloxane (PDMS) substrates that had been stretched beforehand with a certain uniaxial or biaxial strain, as shown in Fig. 3a, after the TFMG layers were formed and bonded with the substrates, the stress of PDMS (before being subjected to tension) was then released to the initially unstrained state, resulting the compressive strain and the periodic wrinkles nanostructures on the TFMGs. Due to the structural flexibility, the film textures can be regulated reversibly by exerting different stretching stress along the directions of the substrates predisposed to straining (Fig. 3b), thus the corresponding surface wettability can be readily tuned in a quite wide range as shown in Fig. 3c, the hydrophobic and hydrophilic surface were switched along with the pre-applied strains,

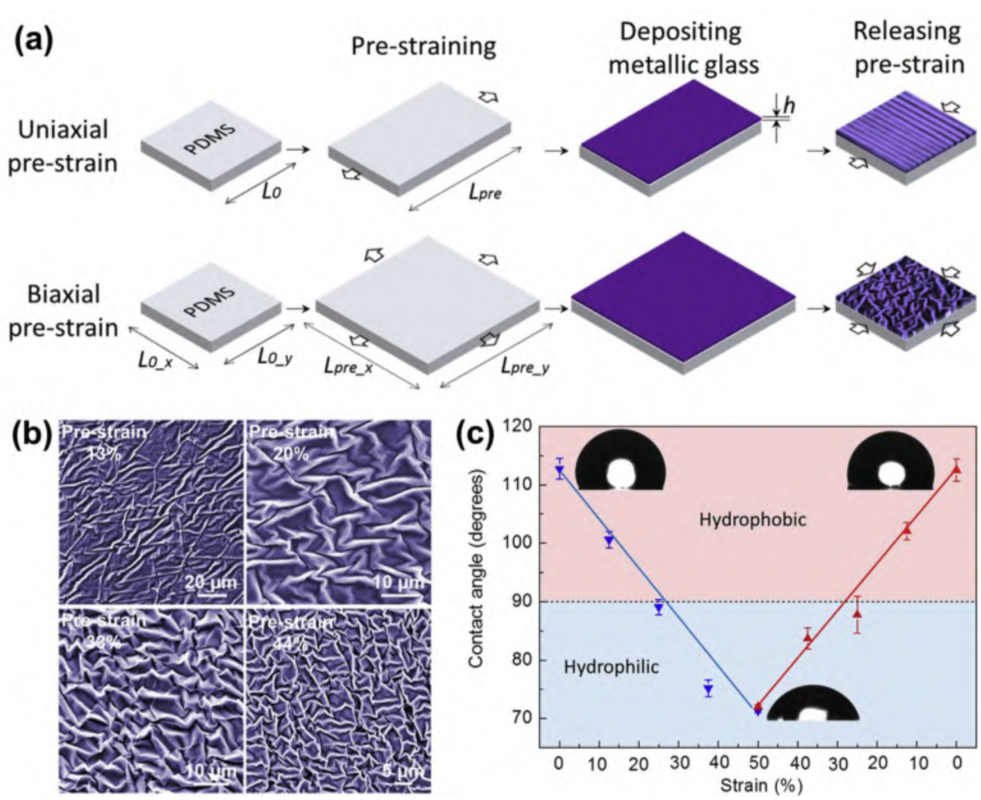

Fig. 3. (a) The folding approach for TFMGs structures fabrication. (b) Variation of the formed structures with different strains beforehand. (c) Water contact angle changes with biaxial stretching strain for the wrinkled films with initial thickness of 4 nm (Reproduced from ref. [97]).

which is very promising in the application of electronic skin. Another strategy to regulate the TFMGs structures during sputtering processes is to control the growth and evolution of films by adjusting different sputtering conditions. The nitrogen was generally introduced in the sputtering to enhance the mechanical and thermal properties of TFMGs [98,99]. The TFMGs structures exhibited a columnar morphology at low nitrogen contents, while the high nitrogen contents resulted in a compact and fully dense coating structure [100], which may change the surface wettability. The treatment of TFMGs after annealing in supercooled liquid region (SCLR) after sputtering has always been used to eliminate the columnar structures by increasing the atoms' mobility [101,102], achieving more uniform structures and smoother surfaces.

A novel coating approach combined co sputtering and oblique angle deposition was proposed to regulate the structures and compositions of TFMGs [103]. As shown in Fig. 4a, the gold nanoparticles arranged on substrate were used as seeds to tune the distribution of the deposited TFMGs, meanwhile the sputtering rate of multiple targets were independently regulated to adjust the TFMGs compositions. Therefore, it can realize the control of morphology, structure size and compositions of TFMGs at the nanoscale. The zigzag nanorods films with the hybrid compositions of Zr- and Ni-based MGs were fabricated by periodically changing the template orientation around its normal and altering glancing angle (Fig. 4b), and the nanoporous TFMGs with a mean pore size of ~100 nm (Fig. 4c) were fabricated using AAO template, respectively, demonstrating the versatility of this fabrication approach. A lot of experimental observations [104,105] shown that the TFMGs during sputtering generally exhibited dense columnar structures in the initial stages of film growth, while with the increase of deposition thickness, the film morphology evolved gradually to be rough surface with deeply grooved networks or nanogranular structures, inducing a hierarchical and fractal surface morphology. Though these studies have not concerned about the surface wettability, they provide potential approaches to fabricate structural water-repellent TFMGs by sputtering processes.

2.1.2. Spraying

The thermal spraying of TFMGs is to heat the MGs powders or wires to be melted or partly melted by oxy/air fuel flame, electric arc or plasma plume [106,107], and then the feedstocks are accelerated at high speed and propelled onto the substrate by compressed gas to obtain amorphous films. Miura et al. [108] firstly utilized the flame spraying approach to synthesize Fe–Ni based coatings with primarily amorphous structure. According to the thermal spraying principles and experiments, it has been found that the morphology and porosity of sprayed coatings are significantly influenced by melting state of powders and the heat radiation from the thermal resource [109–111]. In the high velocity oxy/air fuel spray (HVOF/HVAF), the porosity of the TFMGs was found decreased with increase of the spraying power referring to higher temperature flame [112–114], which can enhance the molten degree of MGs powders resulting in denser coatings with less pores. Meanwhile, the amorphous phase content in the sprayed films was remarkably influenced by the interaction between heat transfer and the melting state of powders. Under the low spraying power, the inadequately melted MGs powders tend to undergo the non-uniform heat distribution in the interfaces of the melted and unmelted zones, which may result in extensive crystallization. As spraying power increased, the melting degree of the powders will be improved, so the crystallization of the TFMGs can be suppressed.

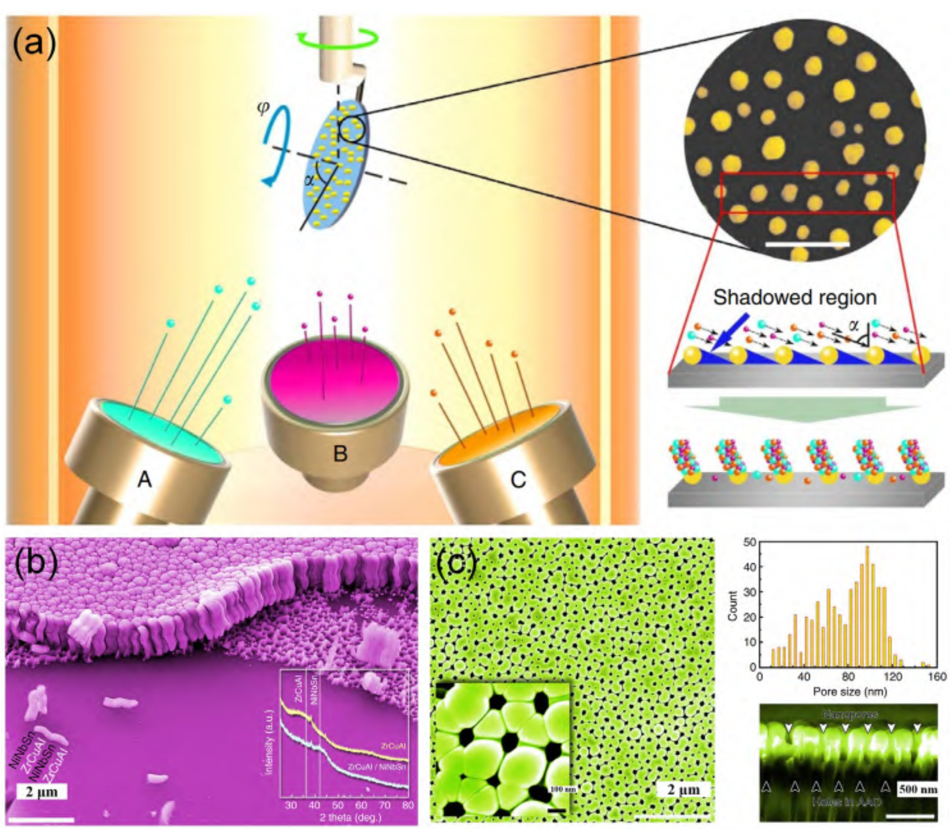

Fig. 4. (a) Multitarget carousel oblique angle deposition. (b) Hybrid nanostructures comprising two kinds of metallic glasses. (c) Nanoporous metallic glass membrane (Reproduced from ref. [103]).

However, when the spraying power or temperature is over high, the local reheating effect mentioned above and the oxidation may reduce the amorphous phase, therefore, the high proportion of amorphous phase can be obtained at a moderate temperature owing to the uniform heat distribution [115–117]. Due to the same formation mechanisms, similar experimental results have been obtained in other thermal spraying approaches for TFMGs including plasma spray [118,119], arc spray [120,121], and laser cladding [122,123].

In addition, the treatments before and after including high energy beam treatment [124,125], treatment after annealing [126,127], porosity sealing treatment [128,129], and adding compositions [130,131] were also carried out in spraying to improve the amorphous content and tune the properties of the TFMGs. These morphology and structure changes may influence the surface free energy and the wettability of the TFMGs. Zhang et al. conducted the HOVF spraying of Fe-based TFMGs with MGs powders in different sizes [117], finding that more porous TFMGs formed from coarser powders exhibited a better corrosion resistance rather than the compact films, due to the higher hydrophobicity of the porous surface. The surface roughness, which can be tailored by using various sizes of MG feedstock powders and different spraying energy, was also found to be critical in the transition between hydrophilicity and hydrophobicity of the TFMGs [132]. The CA of the sprayed films varied from 71 degrees to 136 degrees as the surface roughness increased in the range of Ra 5.4–9.4 μm, as shown in Fig. 5a–d, this indicates that the wettability of the TFMGs can be regulated by the surface roughness control. The superhydrophobicity then can be obtained by the low energy surface modification of the sprayed TFMGs with originally high hydrophobicity (Fig. 5e and f), resulting in a CA of 160 degrees and a sliding angle of around 9 degrees, thus the clearly self-cleaning effect of the modified TEMGs can be obtained (Fig. 5g and h).

The sealing treatment with different sealants was performed on the Al-based amorphous coating sprayed by HVAF, the stearic acid exhibited the best sealing effect due to its good impermeability and hydrophobicity, achieving a higher CA of 130 degrees for the treated coating compared to the as-sprayed coating with a CA of 70 degrees [133]. Qiao et al. [134] prepared a superhydrophobic Fe-based amorphous film by the combination processes of plasma spray and surface modification with fluoroalkylsilane (FAS) 17. By controlling the spraying power, a series of hierarchical features were obtained on the coating surface, as shown in Fig. 6a–f, the complexity of the surface monograph increased with the plasma power. A triple-level structure was observed at the spraying power of 30 kW consisting of no-flattening particles with tens microns, adherent splashing particles with several microns and oxides with nano size (Fig. 6c,f). As the spraying power increase, more small oxide structures were formed on the MG film, and this hierarchical surface with multi-scale structures can effectively trap air so that

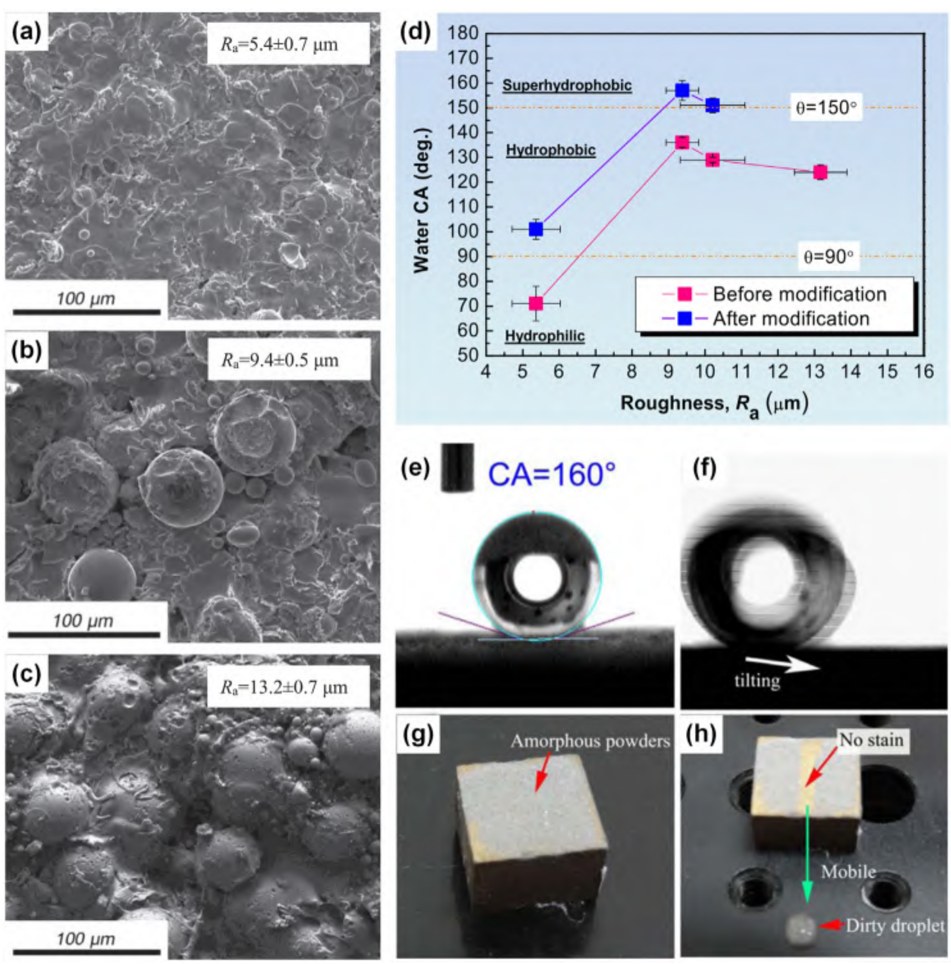

Fig. 5. (a), (b), (c) The typical morphology and surface roughness of the as-sprayed TFMGs. (d) The relation between surface roughness and water contact angle of the TFMGs with and without modification. (e), (f) The superhydrophobicity of the modified TFMGs with a contact angle of 160 degrees and a sliding angle of nearly 9 degrees. (g), (h) The self-cleaning ability of the modified TFMGs (Reproduced from ref. [132]).

the liquid-air contact interface replaces the liquid-solid contact area, leading the water contact conditions to transform from the Wenzel state to the Cassie-Baxter state, which will slightly increase the contact angle and significantly decrease the surface adhesion. Correspondingly, the highest water contact angle and lowest water sliding angle (WSA) was achieved on the triple-level features surface of TFMGs (Fig. 6g). The subsequently abrasion tests demonstrated the good durability of the water-repellent surfaces (Fig. 6h). Further research/investigations are essentially required for the correlation between surface wettability and chemical compositions as well as morphology of the sprayed TFMGs.

2.1.3. Deposition

Electrodeposition without vacuum requirements is a relatively low-cost technique to scale up TFMGs to large areas. The principle of amorphous films formation in electrodeposition is distinct with the fast-cooling processes in the sputtering and thermal spraying. The formation mechanisms of TFMGs from electrolyte is due to the higher nucleation rate than growth rate of the reduced ions under high potential, resulting in nanocrystalline or amorphous structure [135–138]. It was found that the size of the amorphous clusters was decreased with the increase of applied voltage/current density, this may be because the higher clusters formation rate suppressed the size growth. However, with the increasing of electroplating power, the elements segregation may occur inducing the proportional imbalance of the compositions in the deposited films, which may cause the crystallization of the TFMGs. Meanwhile, the specific ranges and proportions of chemical compositions that are reduced and co deposited during electrodeposition are also crucial for the formation of amorphous structure [139–147]. On the basis of these mechanisms, the surface micro-/nanostructures of the deposited TFMGs can be regulated by appropriate control of the formation and growth rates of clusters in short-range order.

The flexible manipulations of surface structures and compositions open a way to produce water-repellent TFMGs by electrodeposition. Wang et al. [148,149] prepared the amorphous Fe–W alloy films with good hydrophobicity by the combination of electroplating, post-annealing and surface modification. A kind of nubby clusters with cavities were observed on the as-deposited surface, and then evolved into hierarchical structures with micro-/nanowires and protuberances due to the slightly oxidization and crystallization after heat treatment, as shown in Fig. 7a–c, these surface morphologies are crucial to form a thin air cushion between the water and the TFMGs, as implied by the wettability theory. Through the annealing at 600 °C, the deposited TFMGs achieved highly water-repellency (CA = 134 degrees), due to the increase of surface roughness under high temperature (Fig. 7d–f). Other researchers fabricated metallic nanofiber networks [150] and nanowires [151,152] with flexible dimensions by the selective electrodeposition using pre-patterned templates. The crystalline and amorphous cobalt-nickel-rhenium-phosphorus [CoNi(Re)P] multicomponent nanowires with a diameter of about 100 nm and a thickness of 3 μm were electrodeposited on the surface through the porous anode aluminum oxide (AAO) templates [152], which is a potential approach to scale up TFMGs to large areas with regular surface structures, and also applicable to design and fabricate structural surface with different functions including water-repellency.

Some other deposition approaches have been also employed to form TFMGs with various surface structures, showing very promising availability for the water-repellent surface fabrication. Electroless plating were conducted to prepare uniform TFMGs with few voids and defects on conductive or non-conductive substrates

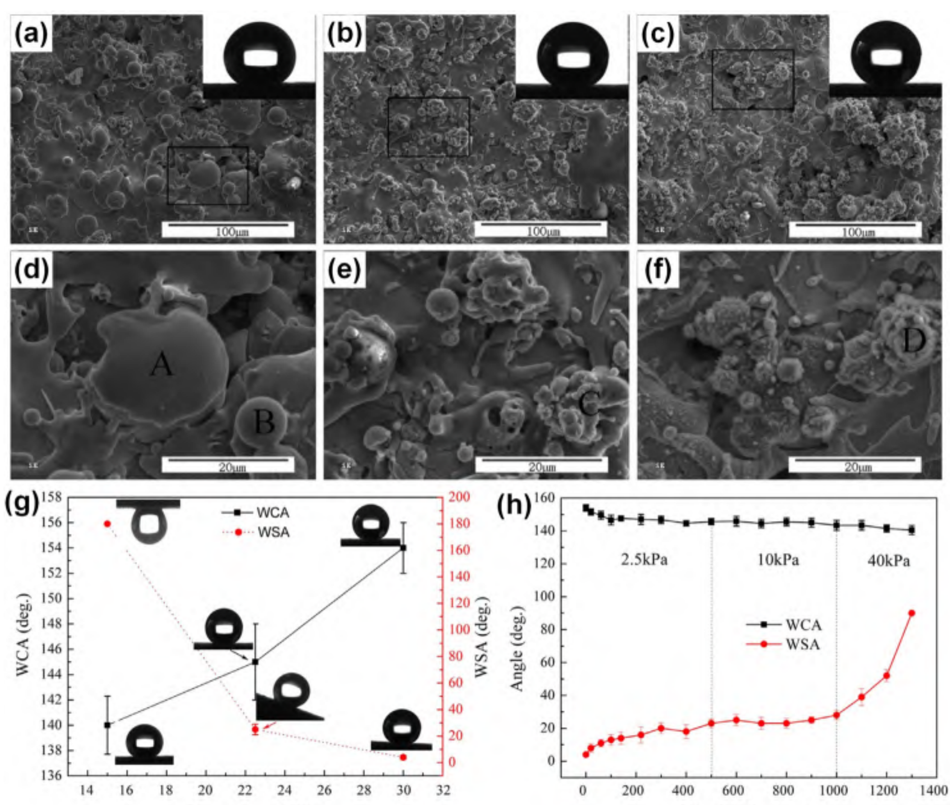

Fig. 6. Surface morphology of TFMGs (a, d), (b, e), and (c, f) at spraying power of 15, 22.5, and 30 kW respectively. (g) The wettability changes of TFMGs along with the spraying power. (h) The abrasion tests of the hydrophobic surface of TFMGs (Reproduced from ref. [134]).

[153–155]. By adjusting the mixture ratio of ionic solutions and the plating temperature as well as the resist masks or templates, a variety of amorphous films structures can be obtained including patterned surfaces [156] and hollow microlattices [157]. It is noted that a superhydrophobic nanosized copper films was fabricated by electroless plating [158], indicating that the water-repellent amorphous metal films may also be achieved by the regulation of reaction conditions. Pulsed laser deposition (PLD) of TFMGs is to induce plasma plume from the target surface by pulse laser due to the instant high temperature, and then the plasma deposited on substrate accompanied with rapid cooling. This approach, involving no additional elements during the process, can precisely keep the stoichiometric ratio of multicomponents in films consistent with that of the target materials [159,160], which is suitable for the fabrication of high purity TFMGs and can provide a potential solution for the fabrication of TFMGs with different wettability.

2.2. Surface patterning on bulk metallic glasses

Bulk metallic glasses (BMGs), as the 3D form of amorphous alloys beyond the 2D TFMGs, are commonly fabricated by rapid quenching techniques, such as liquid forging [161], fluxing melting [162] and mold casting [163], in which the BMGs are solidified from the molten state. The excellent glass forming ability (GFA) is crucial for the MGs with various compositions to be fabricated into the bulk size scale. It is considered that the structural disorder of MGs can be enhanced by the multiplicity of elements, which is conducive to the formation of amorphous alloys [164], thus most of the BMGs fabricated presently are multicomponent alloys. Due to the exceptional physical and chemical properties as mentioned in Section 1, BMGs have aroused wide interests to be utilized as a universal platform with patterned surfaces for structural and functional applications. Various surface patterning approaches for BMGs, including thermoplastic forming and subtractive process, have been developed to achieve water-repellent surfaces because of the intrinsic properties of BMGs and the formation principles of micro-/nanostructures.

2.2.1. Thermoplastic forming

BMGs generally tend to exhibit low plasticity at ambient temperature, owing to the formation of the localized sharp shear bands during deformation [165,166]. However, when the temperature is elevated to the range between the glass-transition point (Tg) and the crystallization point (Tx), they relax into the supercooled and metastable liquid with relatively low viscosity, and thus exhibiting superplastic flow behaviors, which fits the requirements of thermo-mechanically processes that generally conducted on glass and plastic, such as hot embossing [167], extrusion [168], rolling [169], injection [170], blow molding [171], and plastic bonding [172], etc. Meanwhile, BMGs are more homogeneous and isotropic compared to conventional metals due to the lack of grain structures, which can extend the net-shape forming limit to 10 nm scale [48]. Therefore, to achieve lower forming pressure and retain the amorphous properties [173], the key process of surface patterning for BMGs by thermoplastic forming (TPF) is to shape the micro-/nanostructures within the window of SCLR between Tg and Tx.

Since TPF of BMGs is a complex process involving micro-/nanostructures formation and material properties transition, a lot of studies have been conducted on some fundamental issues to give in-depth understanding on this top-down fabrication approach. One of the conspicuous concerns is the undesired crystallization kinetics of BMGs during TPF. However, the low viscosity induced by high temperature and the long processing time are always prompted to diminish capillary effect and enhance the filling ability of the supercooled MG liquid, when replicating the micro-/nanostructures from the mold [42,43], which may increase the risk of crystallization. A generally handling strategy for the contradiction between improving formability and avoiding crystallization is to construct a specific time-temperature-transformation (TTT) curve for the MGs with different thermodynamic properties [174,175],

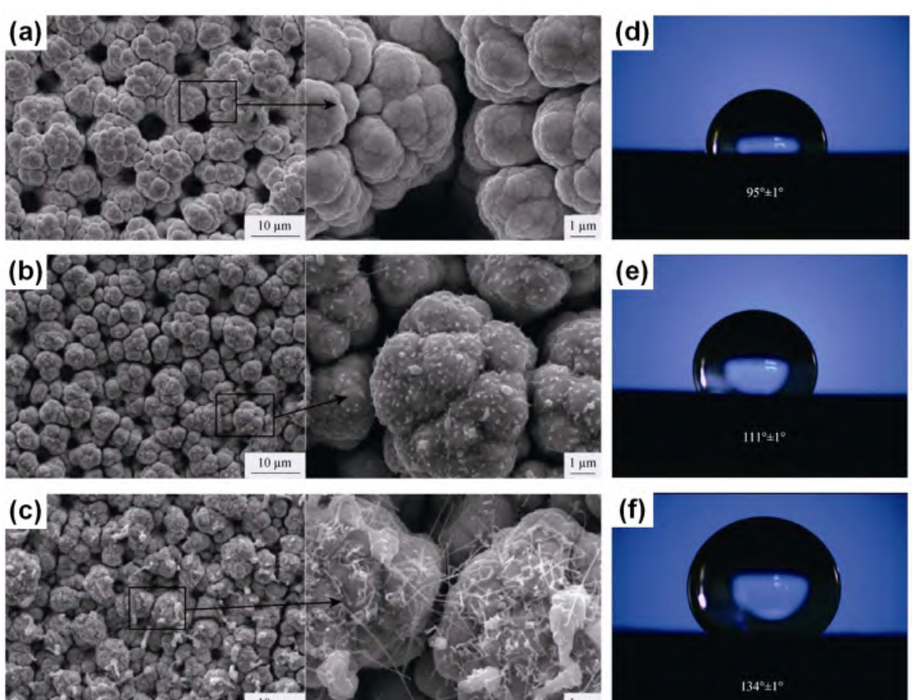

Fig. 7. Surface morphology of the TFMGs, (a) as-deposited surface, (b), (c) hierarchical surface annealed at 500 °C and 600 °C respectively. (d), (e), (f) The CA of the corresponding TFMGs (Reproduced from ref. [149]).

which can guide to select matched processing time and temperature for TPF in the SCLR and amorphous regime of the MGs. A TPF map of flow characteristics of MG supercooled liquid demonstrates that the high temperature and low processing strain rate tend to induce the Newtonian flow behavior of MGs [176], which can enhance the fully filling ability and guarantee the forming of complex microstructures with high fidelity. In addition, in the smaller scale TPF (e.g. structure size below 100 nm), the wettability of MGs flow on molds material will significantly influence the formability. For the antiwetting supercooled MGs liquid (CA > 90 degrees), the required forming pressure may dramatically increase to an infeasible level to overcome the significant capillary forces [45,47], thus, it is suggested that the supercooled MGs liquid should partially wet the molds to achieve controllable and precise forming of nanostructures. To facilitate the TPF processes, a various of factors have been proposed to evaluate the thermal formability of MGs, including the proportion of filled area in V-grooves (R_f) [42], fragility coefficient reflecting the intrinsic viscosity (m) [177], ranges of the supercooled liquid region (ΔT_x), and the maximum diameter of disc prepared by TPF (d) [178]. In addition, it has been found that high heating rate (e.g. 10^6 K/s) can dramatically decrease the viscosity of MGs and broaden the range of the SCLR [179,180], providing a wider processing window for TPF [181].

Based on these comprehensive studies on the fundamental mechanisms, a variety of geometries ranging from 10 nm to several centimeters were fabricated from BMGs by net-shaping TPF including nanowires [182,183], microchannels [184], microarrays [185], microgratings [186,187], cellular networks [188,189] and other 3D miniature parts [190]. The correlation between surface structures layout and wettability of BMGs have been generally explored. Li et al. fabricated the honeycomb structures consisting of different pitches between the adjacent cells on Pd-based BMGs by hot embossing [61,191], as shown in Fig. 8a–c, the patterned surface exhibited superhydrophobic behavior without any surface modification or post treatments when the pitch is greater than the critical size of 115.5 μm, and the corresponding CA reached up to 151.6 degrees (Fig. 8d), which is more consistent with the revised Cassie-Baxter model, this can be explained by the surface energy gradient effect in the horizontal direction caused by the tension of solid/liquid and liquid/vapor interfaces (Fig. 8e). The sealed air in the enclosed cellular structures can serve as a cushion layer buffering the diffusion and penetration of the water droplet, thus the CA only changed slightly after 30 min (Fig. 8f), achieving stable superhydrophobic surface of the patterned BMG.

However, the result may be disturbed by the undesired oxidation of MGs especially due to the chemical etching for demolding during the TPF process. To decouple the effects of surface textures and residual chemicals on the wettability of BMGs, the mechanical demolding method without introducing additional chemicals was developed to significantly reduce the oxidation and obtain pristine MG structures [192]. The plastic forming of the BMGs is performed in the Newtonian regime at a low strain rate, as shown in Fig. 9a, while the demolding is conducted at a high strain rate to achieve the non-Newtonian flow or even the shear-localized deformation of the supercooled MGs, thus the flow stress can increase to exceed the adhesive strength of the MG-mold interface, resulting in the effectively mechanical demolding. This process can avoid the exposure of the surface structures in etching solution such as KOH and retain the hydrophobicity of the patterned BMG surface (Fig. 9d and e). Taking this into account, the honeycomb, pillars and tubes structures in microscale were shaped on the surface of Pt- and Pd-based BMGs to study the textures influence on wettability [193]. It was revealed that oxides formation tended to increase the hydrophilicity regardless of surface topographies. By eliminating this interference, the larger aspect-ratio and pitch size of the micro-/nanofeatures were found critical to improve the hydrophobicity of BMGs surfaces, though the variation tendency may be not

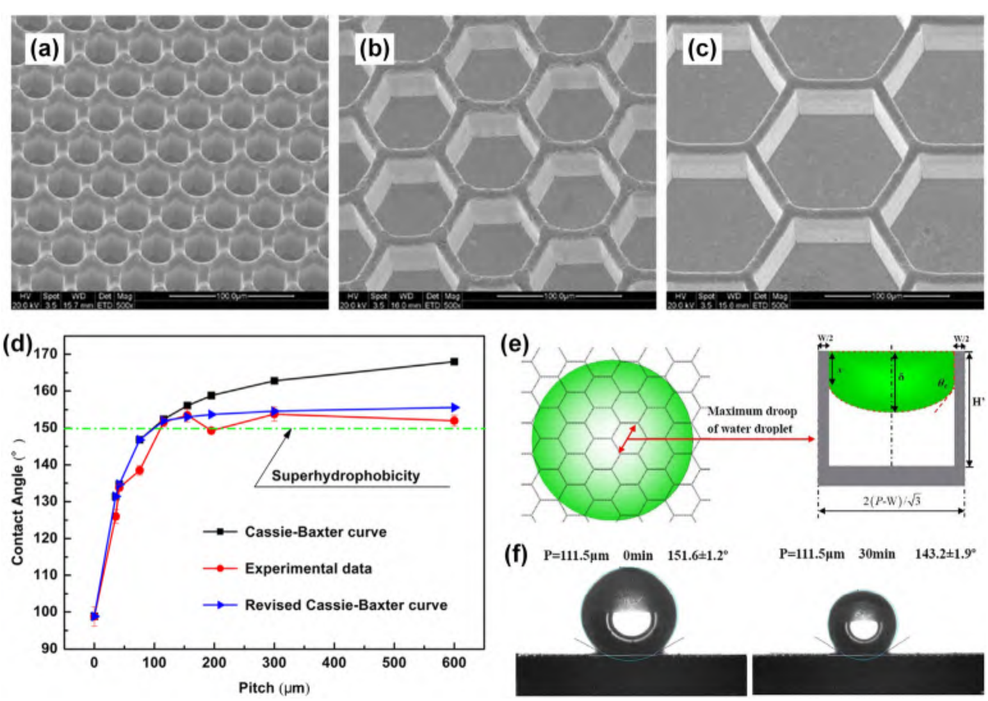

Fig. 8. The SEM images of honeycomb structures with different pitches hot-embossed on Pd-based BMG, (a) a pitch of 35.5 μm, (b) a pitch of 75.5 μm, and (c) a pitch of 115.5 μm. (d) Comparing of the measured CA-pitch data to the values calculated from the original Cassie-Baxter model and the improved model. (e) Schematics of a droplet with liquid-solid and liquid-vapor interfaces in closed cellular structures. (f) The shape and CA of the water droplet with a volume of 5 μl on the patterned surface of BMG after 0 min and 30 min (Reproduced from ref. [61]).

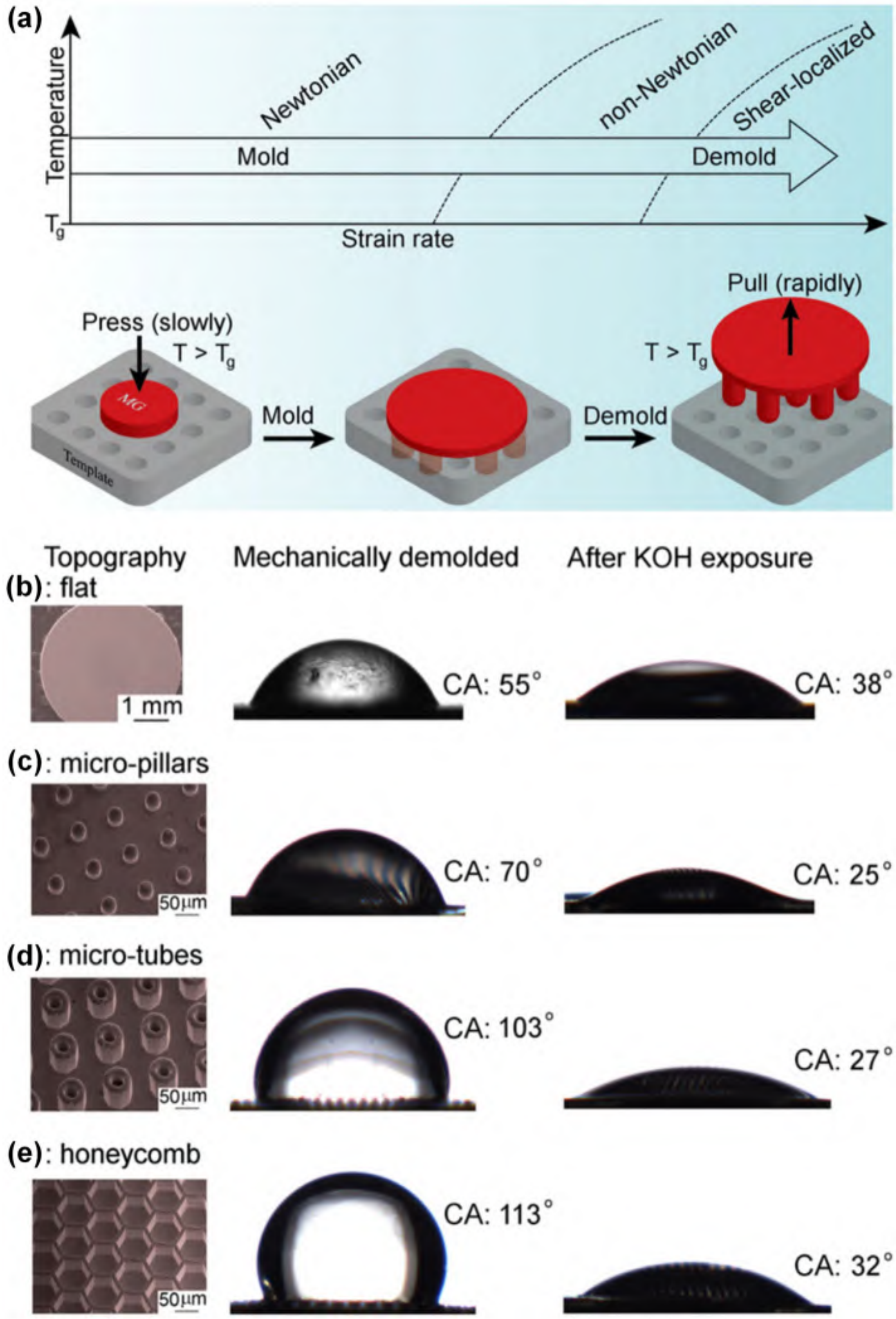

Fig. 9. (a) Forming and demolding of MG supercooled liquids at different strain rates corresponding to different flow regimes. (b), (c), (d), (e) Effect of surface structures and chemistry on the wetting behavior of the Pt-based MG, the wettability of the mechanically demolded surface evolves to hydrophobicity as the change of surface topography, while the KOH exposure obscures the topographic effects and induces hydrophilic surfaces (Reproduced from ref. [192]).

monotonic due to the wetting behaviors transition from Cassie to Wenzel state.

Micro-/nanowires or rods are extensively formed on the BMGs surfaces to achieve multiple functions recently. The smaller feature size, greater aspect ratio and controllable distribution of the micro-/nanowires patterned on the BMGs are the key factors to improve the functional surface performance. A main barrier of the wires formation into a fine scale is the high capillary resistance as well as the significantly increased forming pressure. Therefore, to facilitate the thermoplastic forming (TPF) process, the optimal contact angle of MGs in SCLR on mold materials should be slightly less than 90 degrees to achieve partially wetting behavior and precise replication of nanostructures [45,47] (Fig. 10a). A series of experiments have been conducted to determine the interface wetting angles between BMGs and potential mold materials to find the matched pairs such as Pt- and Au-based BMGs [194]. on the basis of these characteristics, the high-aspect-ratio (exceeding 50) wires with a diameter of 13 nm were prepared on the BMG surface, as shown in Fig. 10b–e, demonstrating that the nanowires with a broad range of forming sizes can be achieved by TPF. In addition, the surface patterned BMGs may also be utilized as molds to replicate surface structures on the identical materials or other BMGs with a lower Tg

(Fig. 10f–i), which can generally ensure the proper wetting behavior between the supercooled MGs and the molds. A more universal strategy to ameliorate the wetting behavior between BMGs and molds is to introduce an oil layer wetting well in the interface [195], which can effectively reduce the capillary force and flowing resistance in TPF and make it more readily to break the rigid oxide films. By these benefits, the nanowire structures with a diameter of 200 nm were firstly formed on a kind of Zr-BMGs. However, the high aspect ratio nanowires on BMGs fabricated by hot embossing tend to settle into bundles and form oblique array structures after released from molds, as shown in Fig. 10b and c, which will lose the structure fidelity and significantly influence the surface wettability. This phenomenon mainly results from the interaction of the Laplacian capillary force and the elastic restoring force of the nanowires during the demolding etching [196]. Thus, it was suggested to use the etching solvents with lower surface tension for demolding to reduce the capillary force and the size of bundles.

A co-embossing approach was developed for the synthesis of micro/nanorods with Janus compositions and functionalities [197], as shown in Fig. 11, two distinct thermoplastic materials including polymers and BMGs were simultaneously filled and bonded in the template cavities following by planarization to form the hybrid structures, such as core-shell structures (Fig. 11a) and microrod arrays (Fig. 11b), the obtained surface may exhibit to be both hydrophobicity and hydrophilicity due to the distinct material properties of BMGs. In addition, to bypass the filling challenges in embossing, the reversed process called thermoplastic drawing was conducted to fabricate the BMGs nanowires with high throughput in SCLR [198]. As shown in Fig. 12a, the wires were elongated and necked up to different degrees in distinct flow behaviors with varying pulling speed or stain rate. By regulating the supercooled MGs into the non-Newtonian flow at high pulling speed, the nanowires with extremely high aspect ratio up to 1,000 was obtained (Fig. 12b). A similar process was adopted to thermoplastic drawing MGs nanowires with spiral shapes by the combination of pulling and spinning [199], which is promising to tailor surface wettability of BMGs.

More sophisticated micro/nano structures have been thermoplastically formed on the BMGs to enhance various surface functions including water-repellent properties. Li et al. constructed the microscale honeycomb textures on the Zr-based BMGs by silicon thermo-molding, and subsequently roughen the surface by chemical etching to form nanoscale protrusions with a feature size varying from 10 to 30 nm [200] as shown in Fig. 13a. It was found that these micro-/nanohierarchical patterns can prominently increase the water contact angle (over 150 degrees) on the BMGs surfaces (Fig. 13b), exhibiting superhydrophobicity as well as high adhesion towards water droplet. It can be seen that the water droplet was tightly fixed on the hierarchically patterned surface

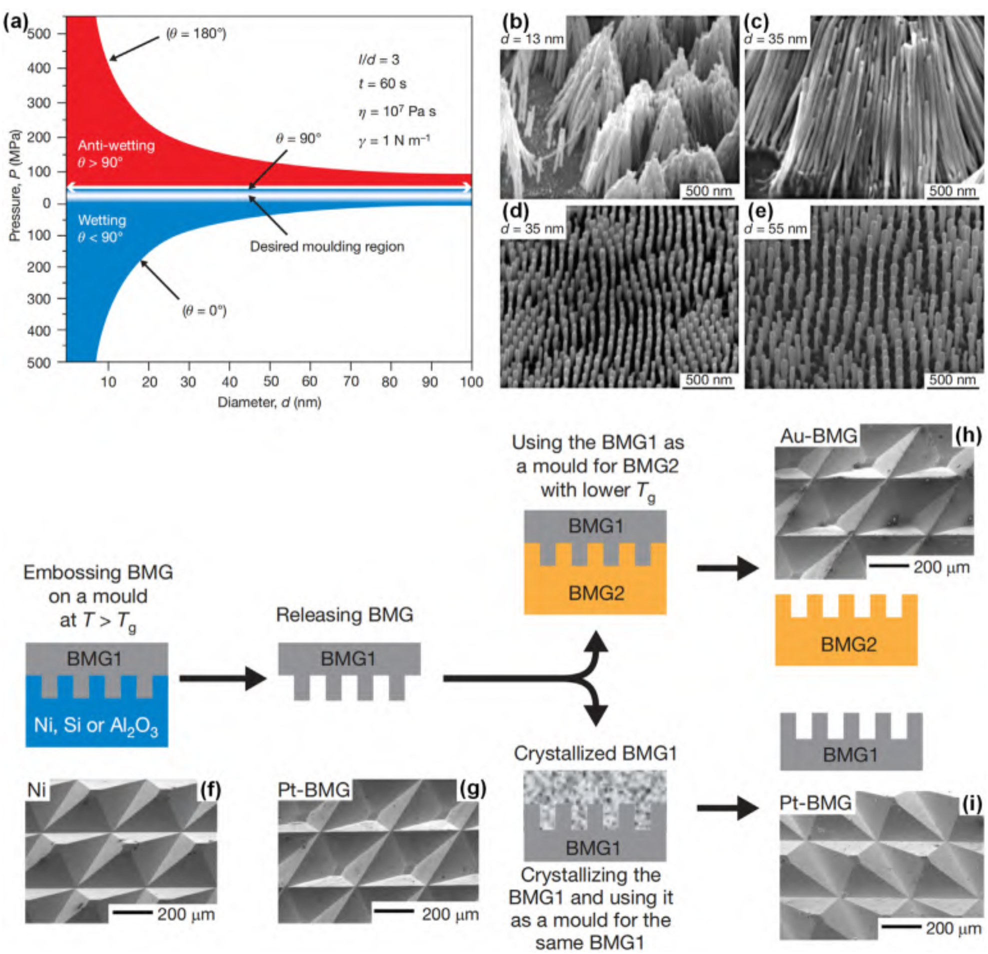

Fig. 10. (a) Forming pressure of the supercooled MGs that is required to fill the nano channels with a diameter d and an aspect ratio of 3 under both wetting ($\theta < 90$) and antiwetting ($\theta > 90$) behaviors. SEM images of nanorods formed on Pt-BMG by TPF, (b) and (c) are respectively the amorphous nanorods of diameters 13 nm and 35 nm with a high aspect ratio over 50, (d) and (e) are respectively the glassy rods of different diameters with an aspect ratio of 5. (f)–(i) The TPF process utilizing the patterned Pt-BMG as mold to fabricated surface textures on various BMGs (Reproduced from ref. [45]).

even when the BMG was turned upside down (Fig. 13c), and the adhesive force was also higher than that of the single scale patterned surfaces (Fig. 13g and h). This may be due to the improvement of sealed-air fraction in the contact interface and the capillary effect of the micro-/nanocavities. But the high adhesion of the surface may hinder the self-cleaning function. Inspired by the water-repellent lotus leaf with excellent self-cleaning properties, the micropillars with hemispherical top were shaped on the cerium (Ce)-based BMGs by TPF and then decorated by the deposited nano SiO_2/soot (Fig. 14a–d), mimicking the microscale papillae covered by branch-like nanostructures on the lotus leaf [201]. The original patterned surface exhibited superhydrophilicity (CA was about 0 degree) as shown in Fig. 14e, while, after deposition, the integration of the multiscale structures endowed the patterned BMGs surface with superhydrophobicity (CA was larger than 155 degrees) and self-cleaning behaviors with a sliding angle less than 5 degrees (Fig. 14f–h). However, the nanofeatures prepared by these foregoing approaches in the hierarchical structures on BMGs were randomly distributed, resulting in limited controllability of water-repellent properties.

Therefore, a more versatile synthesis approach for micro-/nanoscale integrated structures on BMGs were developed on the basis of multistage TPF processes. Ma et al. fabricated the hierarchical surface on Pd-BMGs by sequentially forming the nano and

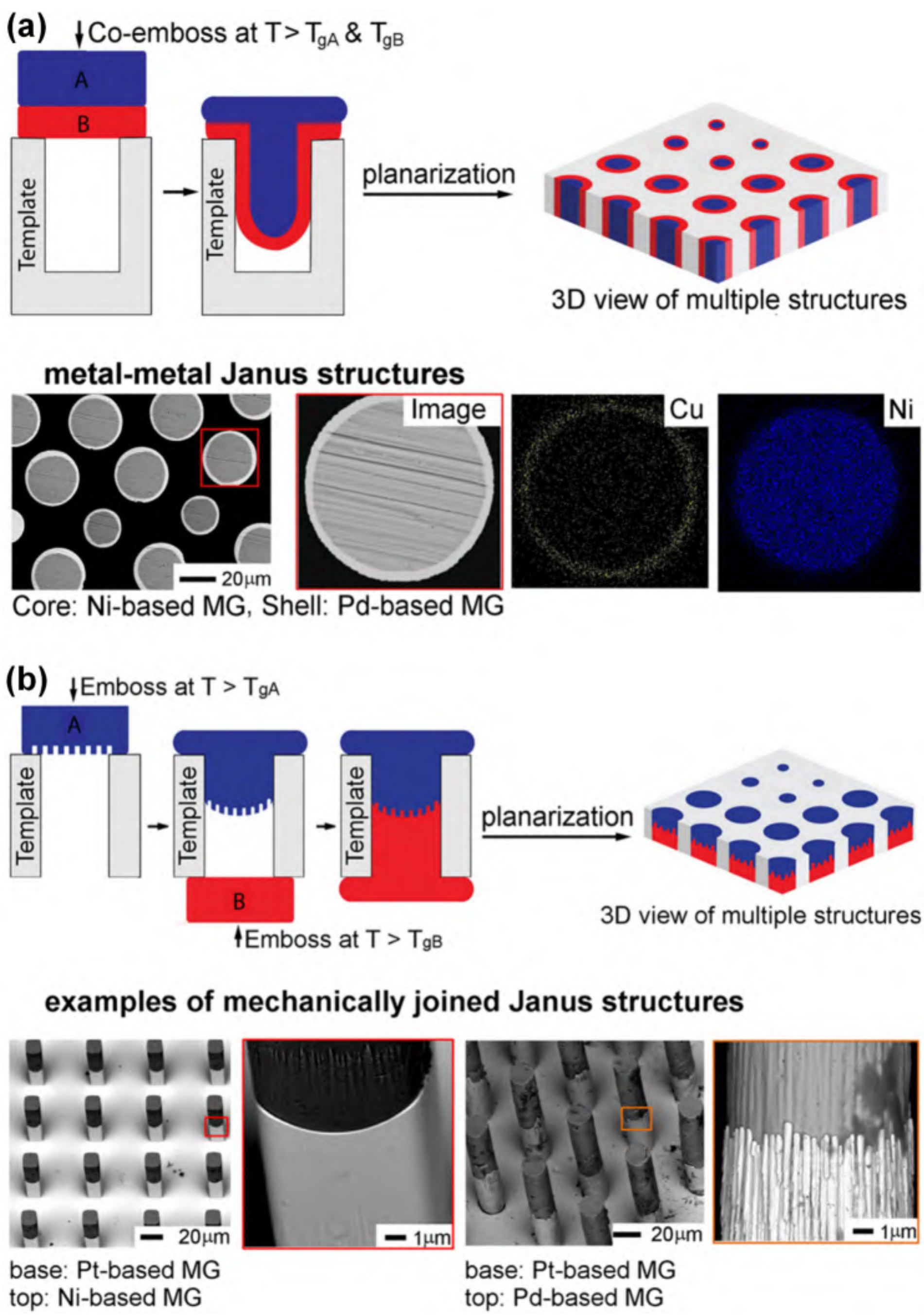

Fig. 11. (a) Fabrication of the core-shell Janus structures and interfaces through co-embossing of Ni- and Pd-based MGs. (b) Fabrication of the Janus rod arrays by thermal mechanical bonding and forming of two sets of MGs (Reproduced from ref. [197]).

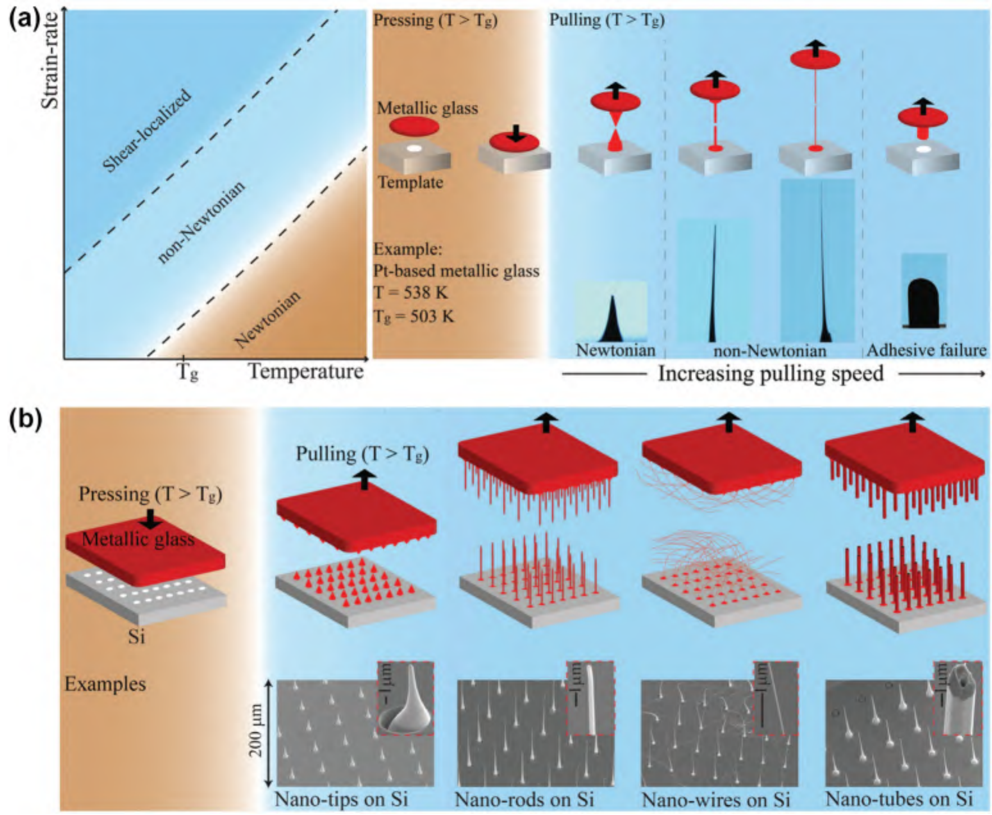

Fig. 12. (a) Regulation of the elongation behaviors of supercooled MG liquid in different flow regimes by changing the pulling speed. (b) Thermoplastic drawing processes of nanowires with various aspect ratios on BMGs (Reproduced from ref. [198]).

micropatterns respectively in two steps [202], as shown in Fig. 15a, the nanorods were firstly formed using the anodic aluminum oxide (AAO) template with nanopores array (a diameter of 80–100 nm), and a silicon mold with periodic micropores (a diameter of 12–14 μm) was then thermally printed on the nanopatterned surface. The hierarchical surface structures with well-defined geometries integrating the nanopillars on the micro-arrays exhibit superhydrophobicity and high adhesion (Fig. 15c), in contrast, the original polished BMG surface is hydrophilic (Fig. 15b). The secondary structures increased the fraction of air cushion between the liquid-solid interface, thus leading to obvious transition of the surface wettability. This hierarchical surface with controllable structures exhibited good mechanical stability, as shown in Fig. 15d and e, the patterned surface still retained the hydrophobic behavior after severe damage by abrasion. The multiscale features have also been built on the intrinsically hydrophilic Pt-based BMGs surfaces by the multistage TPF processes [203], as shown in Fig. 16a–d, the surface hydrophobicity was significantly decreased by the addition of single micro/nano patterns such as microholes and nanorods, while, a hybrid surface superposed with secondary nanostructures exhibited opposite wettability in different areas (Fig. 16g–f). This sequential TPF process of BMGs can be also combined with the blow molding and net-shaping to fabricate non-planar surface and 3D objects decorated with micro/nano hierarchical structures (Fig. 16h–n). The key requirement of this multi-embossing approach is to set the replication processes in the order from small to large in size, thus retaining the more sophisticated structures formed by the preceding operations, which can achieve an exquisite regulation of surface structures and wetting properties by the superposition of nano-, micro- as well as macrosized features on BMG surfaces.

To further improve the forming quality and extend the size limit, various of novel approaches for BMGs surface patterning have been carried out because of thermoplastic forming (TPF). A mechanical distortion method was employed to reduce the lateral size of BMGs' surface structures formed by TPF [48]. By adjusting the temperature and pulling velocity, the nanopillars can be elongated and necked from a diameter of 150 nm–40 nm during the demolding after TPF, while, exerting a uniaxial compression on the patterned BMGs, the nanopores can be shrunk to a diameter 10 times smaller than that of the original pores by regulating the pressure and MGs viscosity. This size-reduction method bypasses the high pressure needed in the conventional TPF, while maintaining the overall periodicity of surface patterns, which is applicable for smaller structures patterning of BMGs. In addition, an angstrom level smoothness for surface of Pt-BMG was achieved by controlling the metal flow to remove the rough surface oxides during TPF [204], and this process has been recently generalized to be atomic imprinting to replicate terrace flatness with a step height of 0.39 nm on platinum bulk metallic glasses (Pt-BMGs) [205], which opens up the possibilities to manipulate surface patterning of BMGs on the atomic scale.

Based on the intensive study of the forming mechanisms of BMGs, other effective thermal patterning approaches have also been proposed. To regulate the microfilling kinetics [206] and interfacial properties [207], the periodically vibrational loading was introduced in the in TPF to achieve a more homogeneous distribution of supercooled MG flow and facilitate the thermoplastic formability of higher aspect-ratio structures [208]. A series of amorphous metallic foams (AMFs) with high porosity (up to 80%) have been synthesized by liquid expansion combined with selective dissolution [209,210], and the as-prepared surface with

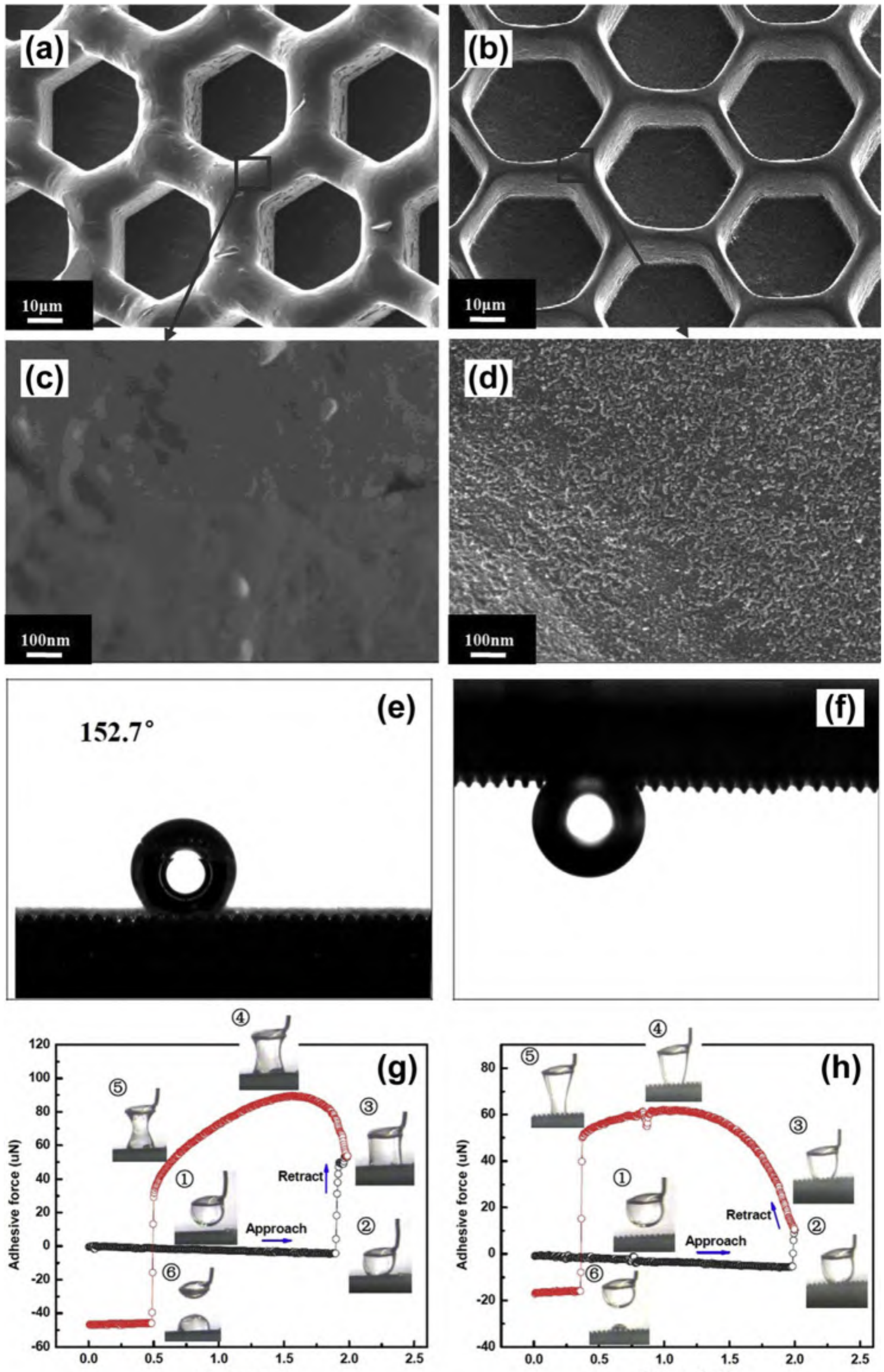

Fig. 13. SEM images of the Zr-MG surfaces with microhoneycomb structures, (a) before and (b) after etching, (c) and (d) are the corresponding images of magnified regions. (e) The CA of the hierarchically patterned MG surface. (f) The geometrical shape of water droplet on the fabricated surface at a tilt angle of 180°. (g), (h) The adhesion force of the micro/nano hierarchical surface and the surface with only microstructures, respectively (Reproduced from ref. [200]).

micropores or bubble structures may exhibit unique wettability, which can be a potential approach for the functional surface fabrication by manipulating the supercooled MGs. In spite of improving the formability, the avoidance of crystallization and oxidization of MGs is also crucial for the surface patterning with high fidelity. The solutions are generally to lower the forming temperature or reduce the processing time as much as possible. By performing a very low strain rate (1.5×10^{-5}/s) of uniaxial compression, the grids with a depth of 22 μm was patterned on hafnium (Hf)-based BMG at room temperature [211]. Although the

BMGs exhibits inherently brittle behavior, the features were transferred from a tungsten mold to the amorphous alloy without shear localization or fracture by controlling the homogenous flow. This cold plastic forming method extends new routes for the surface patterning of a variety of BMGs, despite the long loading cycles (21 h). A novel forming approach of MGs assisted by ultrasonic vibration under ambient temperature has been proposed [212–214], which is very promising to bypass the thermal effects that generally existed in the thermoplastic forming (TPF) of MGs [215,216]. Activated by the ultrasonic vibration, the liquid-like regions in bulk metallic glasses (BMGs) with low stiffness tend to absorb the input energy and increase the atoms' mobility, inducing the extension and connection of the liquid-like regions. Thus, the activated BMGs would exhibit viscous flow behavior and dramatical decrease in strength, due to the variation in the amorphous atomic structure, which facilitates the rapid forming of BMGs at room temperature [217]. Due to the softening and rejuvenation effect activated by high frequency vibration, various structures from nanoscale to macroscale can be formed on BMGs within 0.5 s [218], as shown in Fig. 17, demonstrating a facile method for the rapid forming of fine structures. These approaches offer a universal toolbox for the micro-/nanostructures fabrication to achieve various surface patterns and tunable wettability of BMGs.

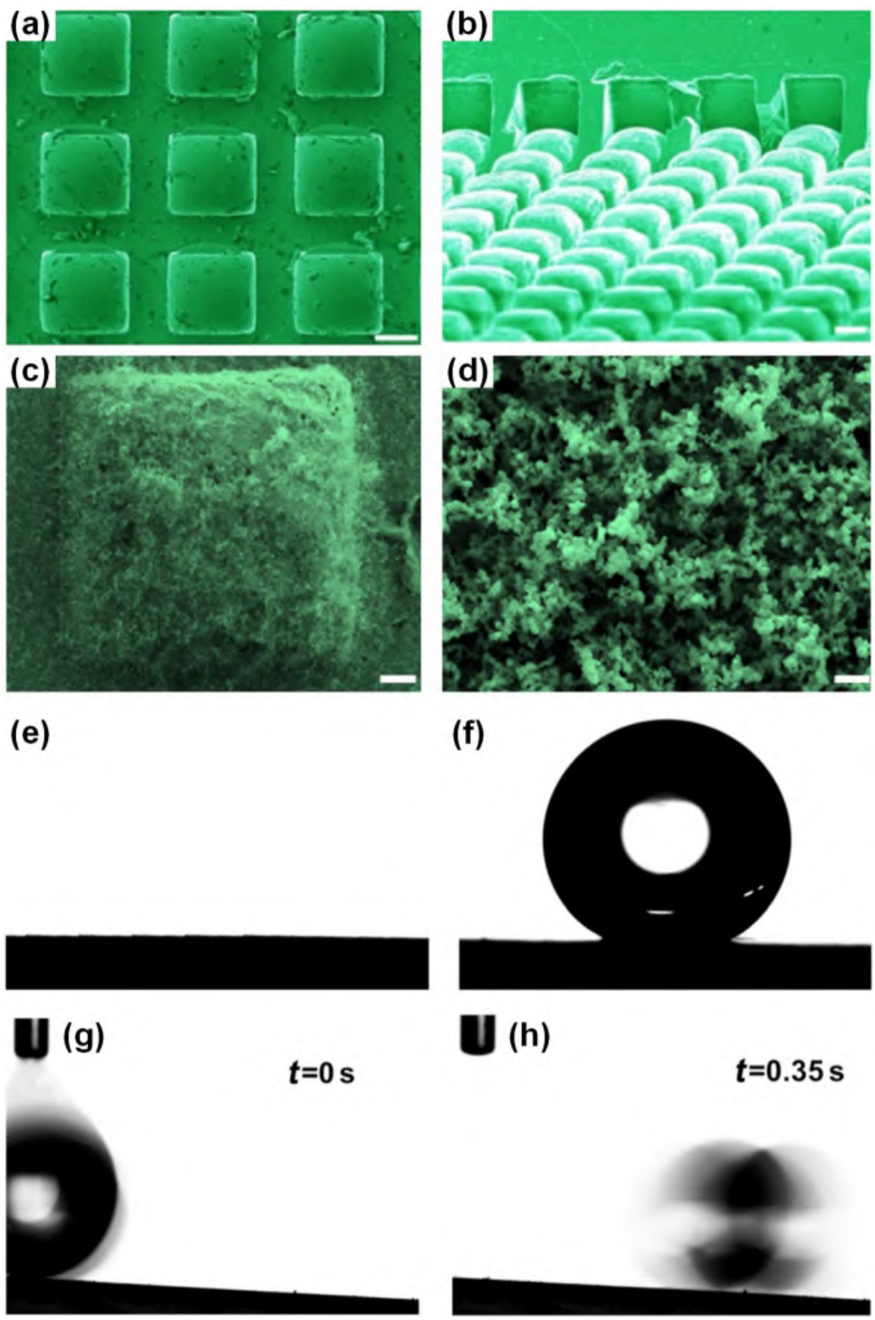

Fig. 14. (a) The top view of a regular array of square micropillars formed on the Ce-based BMGs. (b) The cross-sectional image of the patterned surface. (c), (d) ESEM images of the hierarchical surface structures after the SiO_2/soot deposit at different magnification. (e), (f) The CA of the as-patterned BMG surface and the hierarchical surface after deposition, respectively. (g), (h) The contact process of a water droplet on the hierarchical surface of BMGs with a small sliding angle (Reproduced from ref. [201]).

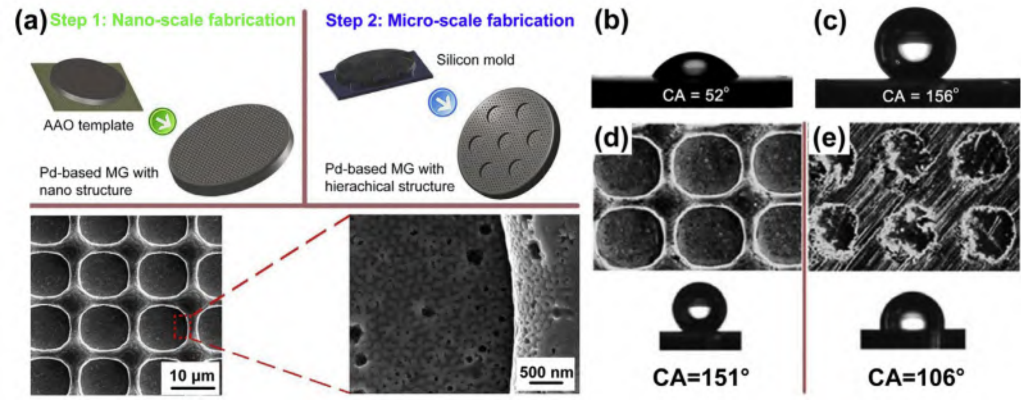

Fig. 15. (a) Formation of hierarchical features on Pd-BMG surface by the multistep TPF. (b), (c) The CA of the polished BMG surface and hierarchical BMG surface, respectively. (d), (e) The surface morphology and corresponding CA before and after sandpaper abrasion of the hierarchical structures (Reproduced from ref. [202]).

2.2.2. Subtractive machining

- **Microcutting**

The cutting processes are effective ways to generate microstructured surfaces on workpieces, for example, the fast tool servo (FTS) diamond turning [219] and elliptical vibration cutting approaches [220] have been generally employed to produce microlens arrays, gratings, sinusoidal grids and other complex structures on metal and brittle materials, achieving various functional surfaces for optical and biomedical applications. The principle of these processes is to selectively remove materials and form geometry

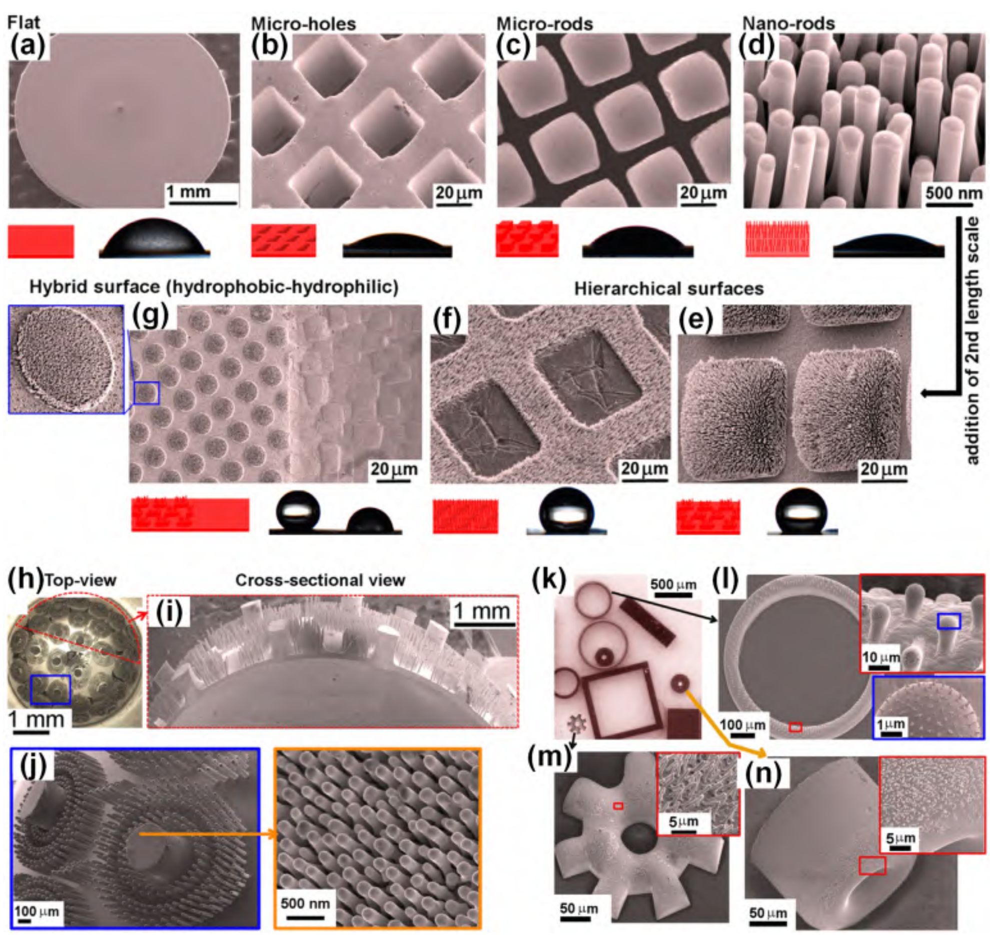

Fig. 16. Influence of the surface patterning on wetting behavior of Pt-BMG. (a) The flat sample is hydrophilic, CA = 58 degrees. (b)–(d) The patterned surfaces with single scale features remain the hydrophilicity. (g)–(e) Addition of a secondary nanostructure turn the surface to be hydrophobic with CA above 130 degrees. (h)–(j). Non-planar surface decorated with hierarchical structures fabricated by TPF and subsequent thermal blow molding. (k)–(n) 3D objects decorated with hierarchically patterned surface (Reproduced from ref. [203]).

structures by adjusting the cutting parameters and tool paths. And the regulation of material removal and chip formation mechanisms are crucial to obtain stable processes and controllable surface structures, which are quite mature processes for the crystalline metals. However, due to no grains and dislocations inside the amorphous structure, the ductile deformation of BMGs in the cutting area cannot be explained by the conventional metal cutting theory, especially the generation mechanisms of surface morphology and the control of MGs oxidation and crystallization still need be further studied. Therefore, the cutting processes have not been widely used for the surface structures fabrication of BMGs, and most of the studies focused on the cutting mechanisms. It has been found that the inhomogeneous deformation with the occurrence of localized shear bands during the cutting of BMGs induced the void formation and viscous flow of chips [221–223]. The scratching tests [224], theoretical modeling [225,226] and molecular dynamics simulations [227] were generally carried out to explore the cutting force and thermal characteristics in the machining of BMGs. On the basis of these fundamental studies, researchers recently attempted to fabricated microstructures on BMGs. The FTS diamond turning was firstly conducted on Zr-BMG to produce a typical sinusoidal grid surface [228], and a series of microgrooves with minimized burrs and chippings were fabricated on Ni–P BMG by ultra-precision cutting [229]. In addition, some non-conventional cutting methods were also introduced in the processes. Ultrasonic vibration cutting has been applied to drill microholes [230] and texture dimples array [231] on BMGs, which can improve the structures qualities. The direct laser assisted cutting were performed on Zr-BMG [232], achieving better surface finish than the conventional machining. Although the understanding of the deformation mechanism of BMGs in cutting area is still far from complete, the micro cutting processes are promising for the fabrication of structural BMG surfaces with different functions including the wettability properties.

- **High energy beam processing**

Laser ablation process has been used for micro- or nanoscale surface patterning on various materials to achieve hydrophobic and super-hydrophobic properties [233]. Recently, lasers texturing on BMGs surfaces received significant attention because the process is scalable and solvent-free [234]. Due to the amorphous structure without grain boundaries, the thermomechanical response of BMGs to laser ablation is distinct with the crystalline metals. The material removal by laser is generally lower for the crystallized sample than its amorphous counterpart, which can be attributed to the presence of grain boundaries resulting in energy loss from electron during the laser processing. The interactions between workpiece and laser are complex during the energy absorption, inducing a series of physical phenomena such as melting, vaporization, sublimation, splashing and re-solidification under different processing conditions, and correspondingly generating different surface structures. Therefore, the optimal parametric combination with a critical energy density is critical to retain the initial amorphous structure in the heat affected zone and producing a clear surface pattern at an acceptable removal rate. By adjusting the laser processing parameters, a variety of textures fabricated on BMGs

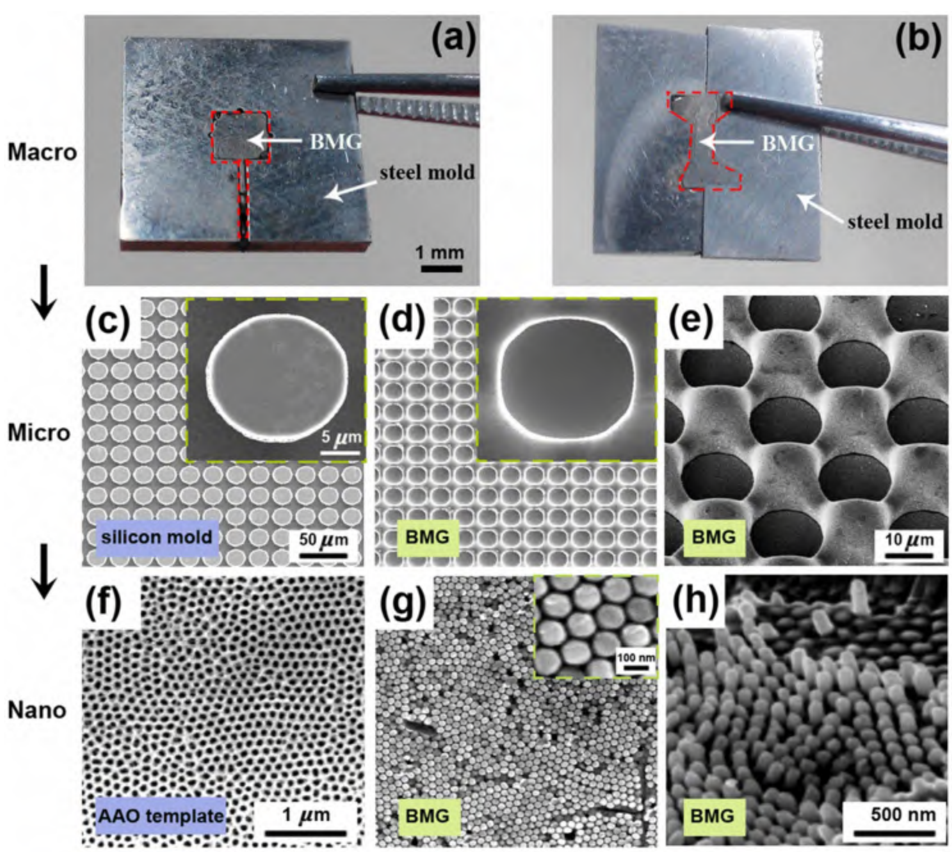

Fig. 17. Surface structures from nano- to macroscale on the Zr-based BMG fabricated by the ultrasonic assisted forming. (a), (b) BMGs fill into the rectangular hole and the dog-bone shaped hole. (c), (d), (e) scanning electron microscopy (SEM) images of the silicon molds and the microhole arrays patterned on the BMG surface. (f), (g), (h) SEM images of anode aluminum oxide (AAO) template and the formed surface with nanowires (Reproduced from ref. [218]).

like concentric rings [235], ripples [236,237], craters [238] and porous structures [239] by laser point shot as well as the periodic surface microstructures [240,241] by laser scanning. Though the underlying mechanism of laser ablation on BMGs still need further studies, some research efforts have been shown that the surface structures and the wettability of BMGs can be tuned by laser processing [242]. A pattern of hierarchical surface structures composed of nanoparticles, microgrooves, and cross-shaped protrusions, as shown in Fig. 18a, were generated on Zr-BMGs by nanosecond pulsed laser ablation in nitrogen gas [243,244], through regulating the specific laser scanning speeds, laser power intensities and pulse overlap rates. Thus, a highly hydrophobic BMG hierarchical surface with CA over 140° was obtained (Fig. 18b). In addition to the laser processing, the focused ion beam (FIB) [245,246] and abrasive waterjet (AWJ) [247,248] machining of BMGs have been also carried out. These high energy beam processes without tool wear are effective approaches to fabricated consistent structures with different wettability on BMGs.

- **Electromachining**

Utilizing the discharge corrosion or electrochemical effect, electromachining can remove workpiece materials in a microcosmic form and achieve various surface micro/nano structures with good water-repellency properties [249]. Surface patterns including microgrooves [250,251], holes [252], craters [253,254] and 3D structures [255] were fabricated on BMGs by micro-electrical discharge machining (EDM). The sizes and morphologies like burrs and debris of the structures can be regulated by selecting proper machining parameters such as discharge voltages and capacitances. However, since the target material was removed by sparking in the dielectric medium, the machined surfaces had undergone an electrothermal process [256], leading to the heat-affected zone and recast layer on the generated BMGs surface structures. In addition to oxidization and crystallization, the surface carbonization of BMGs due to the decomposition of dielectric oil is also a common issue in the electromachining process [257]. A hybrid process of micro-EDM and subsequently grinding has been proposed to remove the recast or carbonization layer and obtain an amorphous BMG surface [258]. Therefore, to achieve the effective surface patterning for BMGs, the understanding of electromachining mechanisms and parameter optimization are essential to retain the amorphous property and controllable surface structures. Besides, microwire electrochemical machining has been also conducted on Fe- [259] and Ni-BMG [260] to fabricate a series of complex structures, showing that electromachining can be one of the feasible ways for the BMGs functional surface fabrication.

2.2.3. Chemical etching and dealloying

Chemical etching and selective dealloying show very good feasibility to manipulate the wettability by the regulation of surface chemistry and morphology [261,262], and this approach has also been performed on BMGs in recent years. A rapid nanoscale surface patterning method is proposed on the Zr-BMG using FIB irradiation followed by wet etching [263]. By selectively removing oxide layer and implanting Ga^{+} ions, the irradiated area of the workpiece

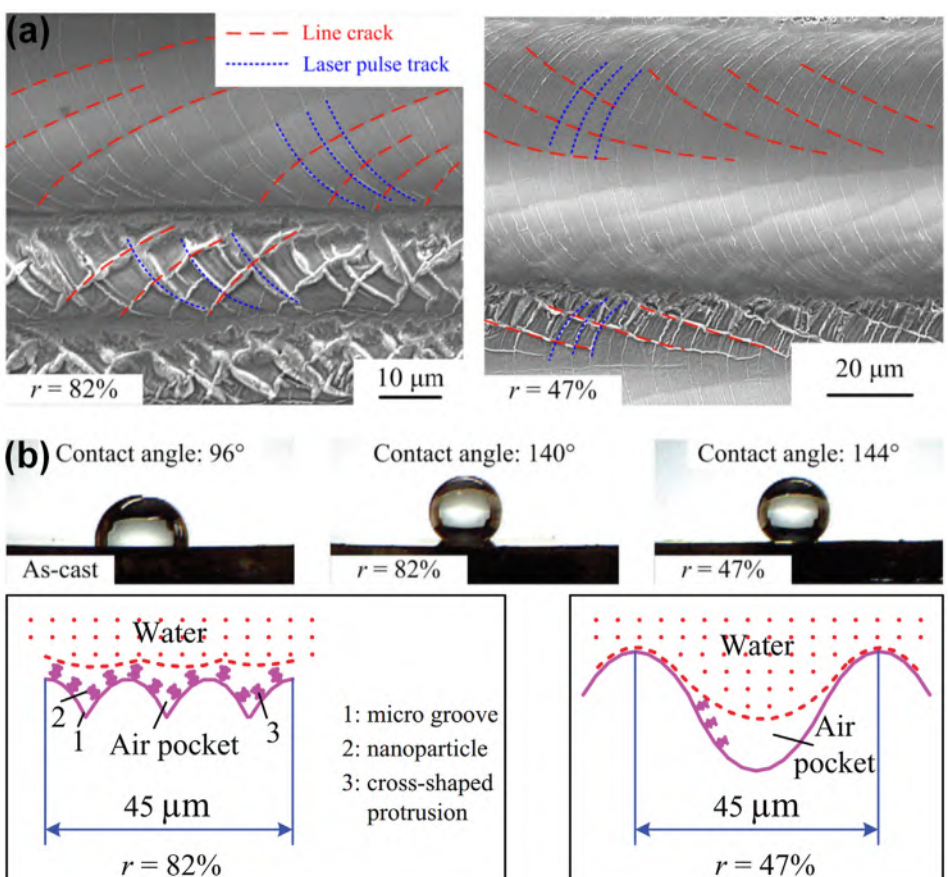

Fig. 18. (a) Surface morphology of the Zr-based BMG generated by laser processing with various pulse overlap rates r. (b) Corresponding wettability and contact status of hierarchical surfaces (Reproduced from ref. [244]).

surface was then preferentially dissolved in HN solution, and consequently the concave structures with a depth of several tens to hundreds of nanometers were formed on the surface, which is a very flexible fabrication method for various surface patterns on BMGs. Liu et al. constructed a superamphiphobic pattern on the CaLi-BMG by surface etching with water and the subsequent surface modification with fluoroalkylsilane (FAS) coating [264]. As shown in Fig. 19, the coral-like patterns composed of micro/nano hierarchical structures on the processed surface exhibited both superhydrophobic (CA = 162 degrees) and superoleophobic (CA = 156 degrees) properties with low adhesion to the liquids, resulting in excellent self-cleaning surface function. The water-repellent surface obtained by this method also showed a good stability after the exposure to air for 3 months (Fig. 19h). By selecting suitable etching solvents, the combination of chemical etching and surface modification processes can be further conducted on other BMGs. For example, the water contact angle of Ce-BMG surfaces was found changing from nearly 0 degree to about 157 degrees with different combinations of HCl treatment and FAS modification [265]. And the surface wettability of Ca-BMG was tuned from hydrophilic to hydrophobic by different water etching time and surface coatings [266], as shown in Fig. 20, the combination of Fe and FAS coating obtained the hydrophobic surface with a CA of 133 degrees. A superhydrophobic and superlipophilic surface has been fabricated on Zr-BMGs by electrochemical corrosion and surface modification with stearic acid, the water contact angle of the obtained micro-/nanohierarchical surface reached to near 170 degrees, while the contact angle of oil on the surface was 5 degrees [267], which is very promising in the application of nondestructive liquid transportation and oil–water separation, though the geometries of generated surface structures cannot be precisely controlled [268].

More intertwined surface structures with different elements enrichment were fabricated by the electrochemical dealloying process, synthesizing anisotropic nanostructures from homogeneous BMGs for various applications, especially in catalysis to facilitate the reaction kinetics [269,270]. The porous MGs can be obtained from the processes by selectively dissolving the target elements of the BMG sample using chemical or electrochemical treatments [271,272], for instance, the average size of the pores on Pd-BMG obtained by dealloying can reach to 10 nm [273]. To regulate the structures formed on the BMG surfaces in the dealloying process, the important factors need be controlled are the alloy compositions, electrolyte, and electrochemical potential. The evolutions of the surface morphology under different processing conditions were generally studied on the amorphous precursor structures like nanorods fabricated by TPF (Fig. 21a). It has been found that the enhanced diffusion of the more electrochemically active atoms at the alloy-electrolyte interface resulted in nanoporous networks when the dealloying potentials less than a critical value [274–276], as shown in Fig. 21b, while when the dealloying potentials increased to a certain extent, the dissolution and redeposition of metal atoms would induce highly branched dendrites with nanoscale substructures [277,278] (Fig. 21c). The nanorods surface subjected to dealloying process eventually turned to be palladium (Pd)-rich nanodendritic structures as the increase of potentials, and the surface wettability also changed accordingly [279] (Fig. 21d–g). The underlying mechanism of BMG morphology evolution during electrochemical dealloying still need further research, and this surface modification approach may extend to a wide range of BMGs possessing different compositions, achieving a desired wettability paired with catalysis functions.

2.3. Potential approaches on the basis of 1D metallic glasses

The fabrication approaches mentioned above for the water-repellent surfaces are mainly because of the 2D (TFMG) and 3D (BMG) forms of amorphous alloys respectively, which have been achieved great effectiveness in the integration of surface structures and functions for BMGs. However, the functional surface fabrication on the basis of one-dimensional (1D) MG structures, such as micro-/nanopowders, particles, wires or fibers, has not yet been largely applied in BMGs in the previous research efforts. The inert gas condensation [280], physical vapor deposition [281] and chemical reduction [282] processes are generally adopted to synthesize the micro/nano MG powders or particles as well as the metallic nanoglasses (NGMGs) assembled by MG nanogranules with a size ranging from a few to 100 nm [283], while the free standing micro/nanowires with a diameter from 70 nm to 300 μm are mainly produced by gas atomization [284] or superplastic

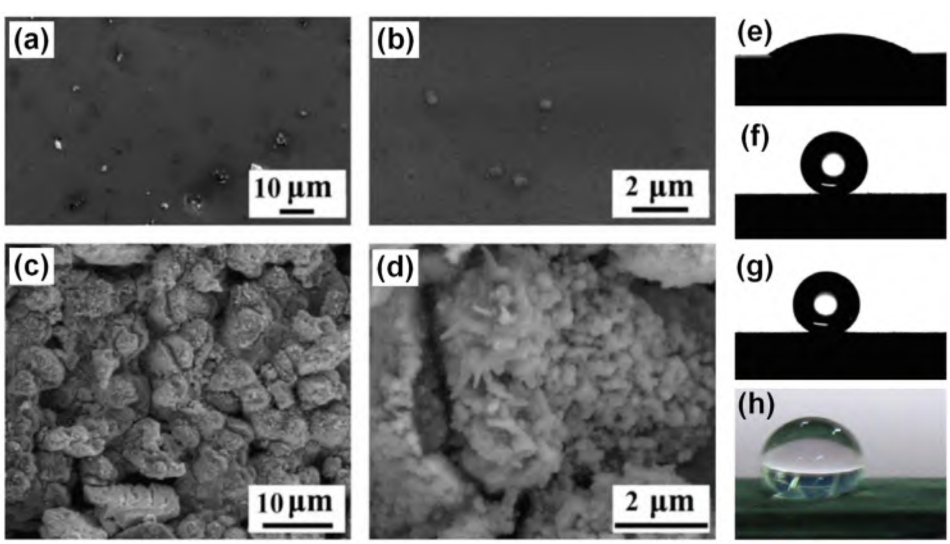

Fig. 19. (a), (b) The original surface of CaLi-based BMG surface. (c), (d) Hierarchical surface generated by the treatment of etching and FAS coating. (e) Water droplet on the original surface. (f) Water droplet on the etched and modified surface with a CA of 162 degrees. (g) Oil droplet on the treated surface with a CA of 156 degrees. (h) A water droplet on the treated BMG surface after exposure to air for three months (Reproduced from ref. [264]).

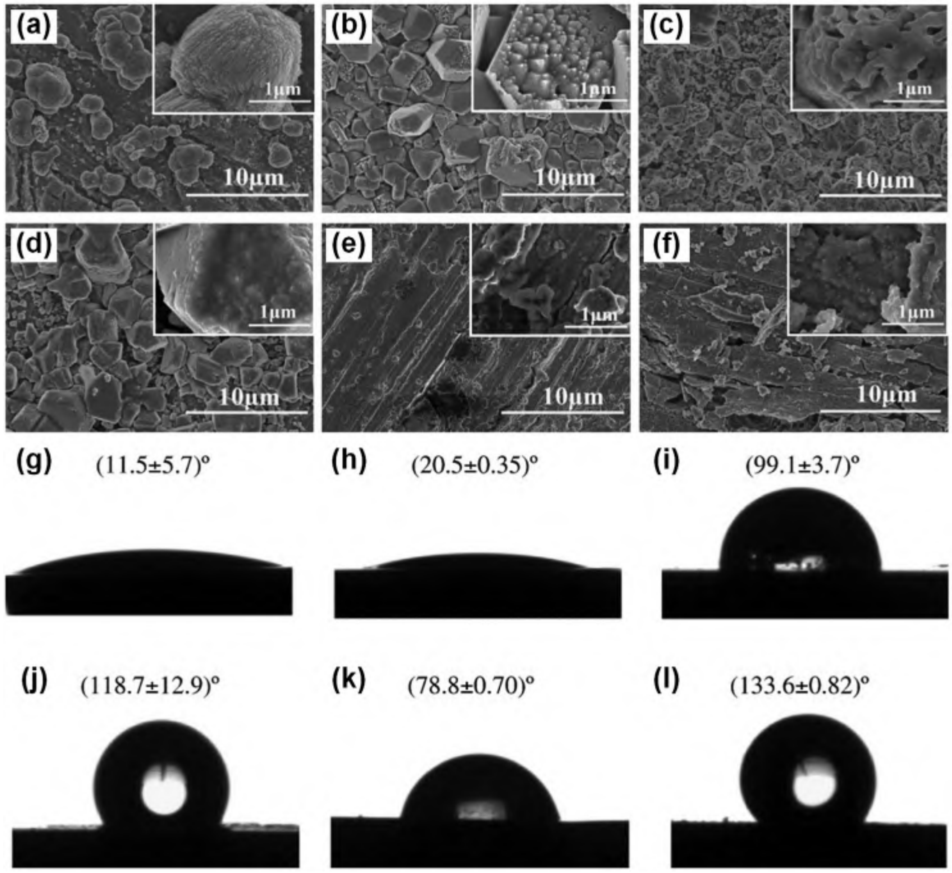

Fig. 20. Surface topography of the Ca-based BMG after different surface treatment: (a) 15 min water etching; (b) 30 min water etching; (c) 15 min water etching+ FAS; (d) 30 min water etching+ FAS; (e) Fe coating; (f) Fe+ FAS coating. (g)–(l) The corresponding CA of the BMG surface after different treatments (Reproduced from ref. [266]).

deformation of MGs in the SCLR [285,286]. One of the emerging manipulation methods of these 1D MGs is additive manufacturing, typically the 3D printing by selective laser melting (SLM), in which the glassy powders were used as feedstocks to fabricate the complex surface patterns or 3D shapes of MGs, like lattice structures [287], porous scaffold [288], micro-arrays [289,290], etc. As shown in Fig. 22, a lattice sample with the amorphous phase fraction of 81% was fabricated from the Zr-based glassy powders by 3D printing, and then subjected to chemical dealloying to achieve the milli-nanohierarchical poriferous structures in the surface areas with a thickness of 10 μm, which is very promising in the synthesis of complex geometries of MGs with functional surfaces.

Inspired by the synthesis of water-repellent colloidal surfaces [291,292], self-assembly, driven by a variety of interactions such as capillary, microgravity, magnetic, electrostatic, and van der Waals force [49,293], can also be an effective approach for the

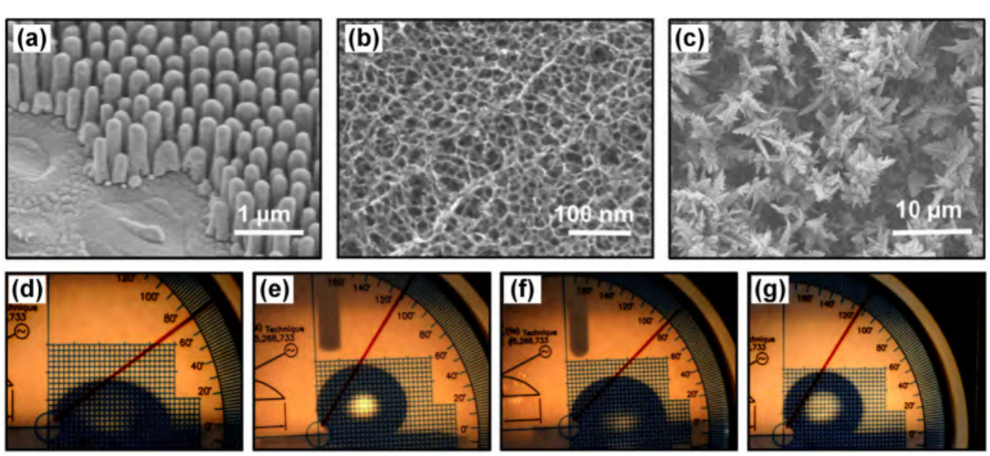

Fig. 21. Pd-based BMG surface: (a) the nanorod structure patterned by TPF, (b) the nanoporous morphology after low potential dealloying, (c) the nanodendrites formed by high potential dealloying. Water contact angle on different surfaces: (d) a flat BMG surface, (e) a nanorod patterned surface, (f) a nanoporous surface and (g) a nanodendritic surface (Reproduced from ref. [279]).

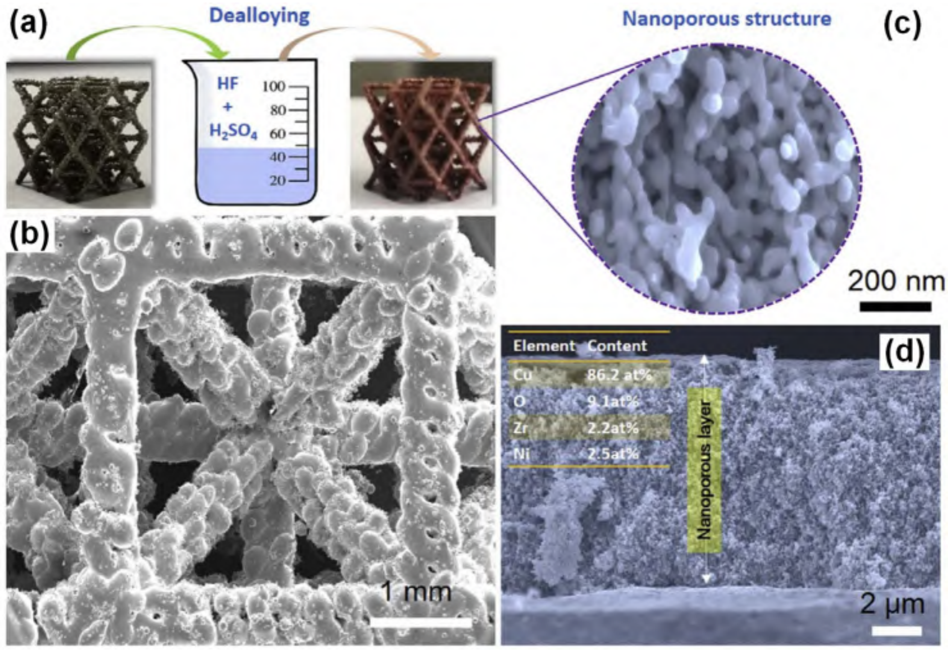

Fig. 22. (a) The Zr-based MG lattice fabricated by 3D printing before and after chemical dealloying for 60 h in the acid solution. (b) SEM morphology of the as-prepared lattice structures. (c) Fabrication of the nanoporous structures on the as-prepared MG lattice by dealloying. (d) Cross-section morphology of the uniform nanoporous layer around 10 μm-thick (Reproduced from ref. [287]).

reconfiguration of 1D MGs. An attempt to realize the self-assembly of MG nanorods on the surfaces has been done [48], as shown in Fig. 23a, the free nanorods was detached from the surface of TPF patterned BMGs by sonication, then the nanostructures were dispersed in a solvent and settled on a partially crystallized MG substrate that of the same compositions with the nanorods. It is interesting to note that the nanorods tended to preferentially decorate the crystallized regions, which may be due to the crystal-

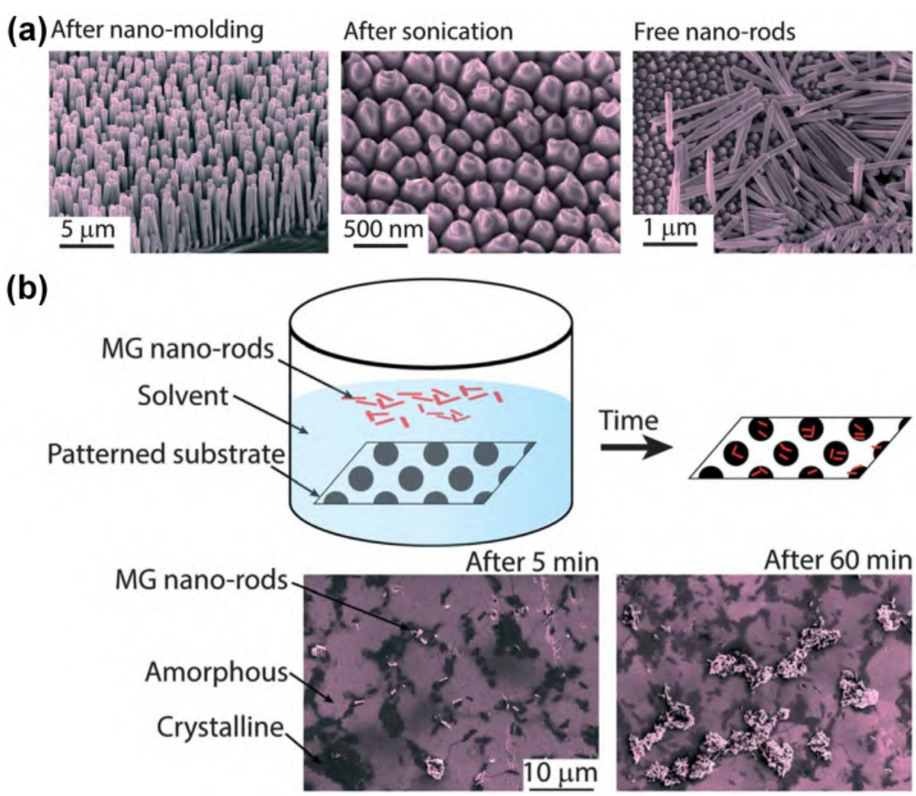

Fig. 23. (a) Fabrication of free nanorods by the sonication processing of patterned MGs. (b) Self-assembly of the free nanorods of MGs that may be driven by the effect of crystal-field, and the nanorods tend to gather in the crystalline regions (dark) rather than the amorphous region (light) (Reproduced from ref. [48]).

field interactions between the crystalline regions of MGs and the surface layers of nanorods. A variety of free Janus structures consist of polymer and MGs have been synthesized by TPF with sequential planarization process and etching of template, as shown in Fig. 24a and b. These structures comprising of distinct materials generally exhibit dual properties, for instance, the water contact angle of the Pt-MG and polypropylene are 58 degrees and 104 degrees respectively, leading to the hybrid surface wettability of their Janus structures. These anisotropic properties can also be employed to achieve the self-assembly of surface structures, as shown in Fig. 24c, the ferromagnetic particles preferentially concentrated in the crystallized Ni-MG in the upper side of the Janus pillars, and the selective dealloying of the Zr-MG in Janus pillars by KOH solution resulted in the nucleation of Cu dendrites on the Ni-MG (Fig. 24d). In addition, it has been demonstrated that the focused ion beam (FIB) nanomanipulator [294] and centrifuge technique [295] can be utilized to pick up or collect MG nanostructures in the mechanical and thermal property tests, which is also possible to be applied in the flexible arrangement of 1D MGs. More potential approaches need to be developed for the fabrication of structural and functional surfaces on the basis of MGs including the extensively required water-repellent surfaces. The surface wetting behaviors of MGs with different compositions and surface structures processed by various approaches are presented in Table 1.

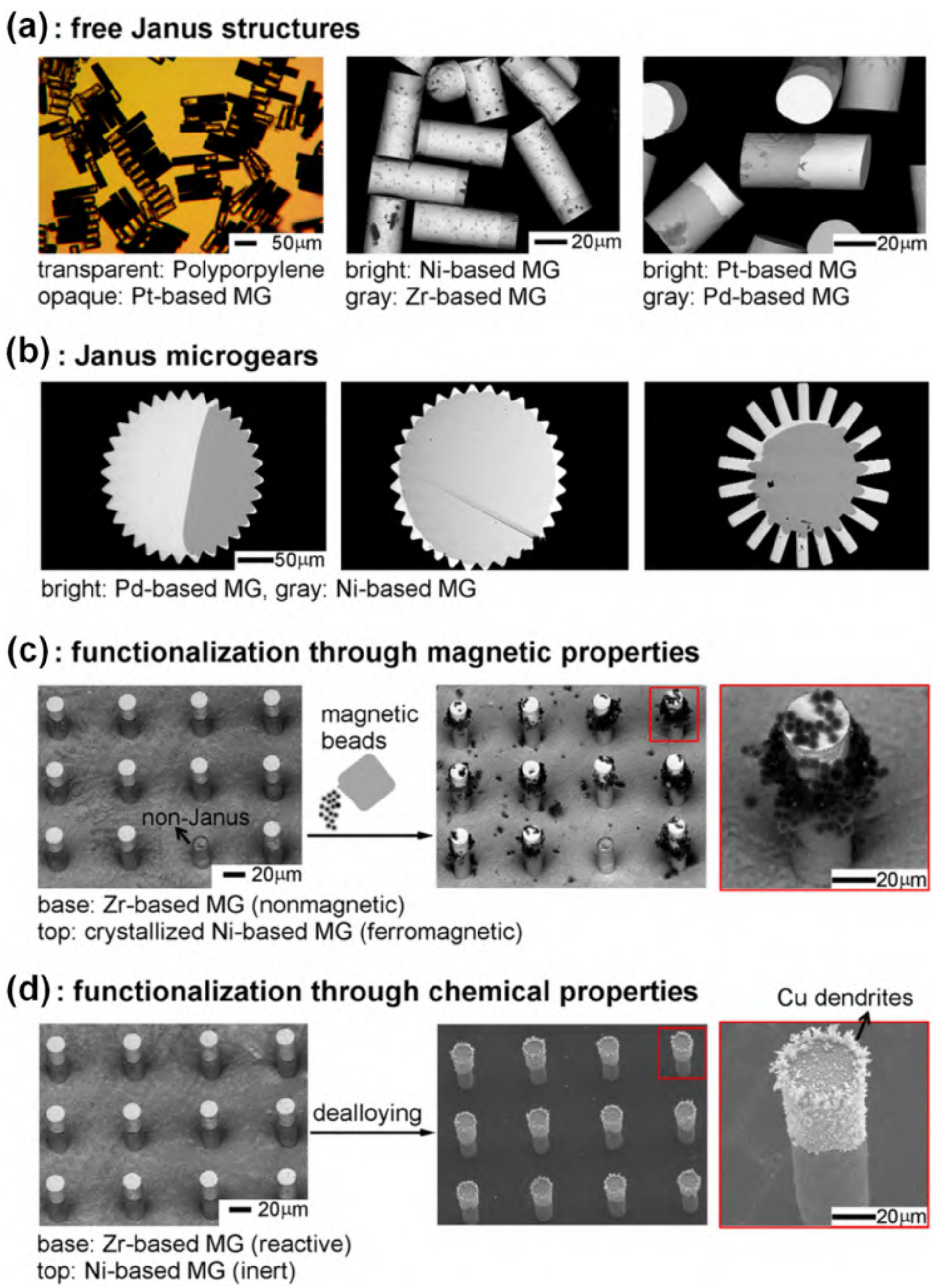

Fig. 24. Free Janus structures comprising of distinct materials such as polymer-MG and MG-MG, (a) Janus microrods, (b) Janus microgears. Utilizing the anisotropic properties of Janus arrays to generate various surface structures, (c) arrangement of ferromagnetic beads by magnetic effect, (d) formation of dendrite structures by dealloying of Janus MG rods (Reproduced from ref. [197]).

Table 1
Surface wettability of MGs with different structures fabricated by various methods.

MG Compositions	Surface structure	Feature size	Surface wettability (WCA)	Processing methods
$Zr_{61}Al_{7.5}Ni_{10}Cu_{17.5}Si_4$	Smooth surface	Surface roughness: R_{max} ~ 1.0 nm	~90.85 degrees	Magnetron sputtering [78]
$Zr_{38.79}Cu_{30.98}Ni_{17.47}Al_{25.1}V_{1.54}$	Smooth surface	Surface roughness: R_{max} ~ 1.3 nm	~90.85 degrees	Magnetron sputtering [79]
Zr–Cu	Smooth surface	Surface roughness: Ra < 1 nm	98 degrees–108 degrees	Magnetron sputtering [80]
Zr-Hf-Cu	Smooth surface	Surface roughness: Ra ~0.2 nm	~109 degrees	Magnetron sputtering [81]
Zr-Hf-Al/Si–Cu	Smooth surface	Surface roughness: Ra 0.3–1.2 nm	97 degrees–100 degrees	Magnetron sputtering [82]
$Zr_{61}Al_{7.5}Ni_{10}Cu_{17.5}Si_4$	Smooth surface	Surface roughness: Ra ~1 nm	~87.9 degrees	Magnetron sputtering [83]
$Zr_{53}Cu_{33}Al_9Ta_5$	Smooth surface	Surface roughness: Rq ~ 0.12 nm	~119.5 degrees	Magnetron sputtering [84]
$Cu_{48}Zr_{42}Ti_4Al_6$	Smooth surface	Surface roughness: Rq ~ 0.14 nm	~106.6 degrees	
$Zr_{51.4}Cu_{29.5}Ni_{12.3}Al_{6.8}$	Smooth surface	Surface roughness: Ra 0.8–1.5 nm	99.5 degrees–104 degrees	Magnetron sputtering [85]
$Ti_{40}Cu_{36}Pd_{14}Zr_{10}$	Smooth surface	Surface roughness: Ra 0.3 nm	~116.9 degrees	Magnetron sputtering [88]
$Zr_{53}Cu_{33}Al_9Ta_5$	Smooth surface	Surface roughness: Rq ~ 10 nm	~104 degrees	Magnetron sputtering [89]
$Zr_{53}Cu_{33}Al_9Ta_5$	Smooth surface	Surface roughness: Rq ~ 0.19 nm	~97.7 degrees	Magnetron sputtering [91]
$Zr_{55}Cu_{30}Al_{10}Ni_5$	Nanotube array	Nanotube diameter: 500–800 nm	117 degrees–151 degrees	Magnetron sputtering on photoresist template [93]
$Zr_{53}Cu_{26}Al_{16}Ni_5$	Fiber membrane	Fiber diameter: 284.2–359.8 nm	106 degrees–136 degrees	Magnetron sputtering [95]
$Zr_{53}Cu_{26}Al_{16}Ni_5$	Smooth surface	/	~96.2 degrees	
$Ti_{40}Zr_{10}Cu_{36}Nb_7Co_7$	Smooth surface	/	~91 degrees	
$W_{50}Ni_{25}B_{25}$	Smooth surface	/	~64.3 degrees	
$Pd_{71.5}Cu_{12}Si_{6.5}$	Smooth surface	/	~67.5 degrees	
$Cu_{47}Zr_{42}Al_7Ti_4$	Smooth surface	/	~83 degrees	
$Zr_{55}Cu_{30}Ni_5Al_{10}$	Smooth surface	Surface roughness: RMS ~ 0.358 nm	~90 degrees	Ion beam sputtering [96]
$Cu_{50}Zr_{50}$	Wrinkle surface	Wrinkle amplitude: 250–750 nm	72.3 degrees–112.8 degrees	Magnetron sputtering [97]
$Fe_{48}Mo_{14}Cr_{15}Y_2C_{15}B_6$	Original surface of BMG	/	~78 degrees	Polishing [132]
	Rough surface	Surface roughness: Ra 5.4–13.2 nm	71 degrees–140 degrees	HVOF spray [132]
			101 degrees–150 degrees	HVOF spray and surface modification [132]
$Al_{86}Ni_6Y_{4.5}Co_2La_{1.5}$	Rough surface	/	~70 degrees	HVAF spray [133]
			~130 degrees	HVAF spray and surface modification [133]
$Fe_{67.19}Cr_{21}Mo_{8.84}C_{2.56}Si_{0.22}Co_{0.15}Al_{0.02}Y_{0.01}$	Hierarchical surface	Surface roughness: Rsa 8.7–12.8 μm	~154 degrees	Plasma spray and FAS17 modification [134]
Fe–W	Hierarchical surface	Roughness factor: R_f 82.2–117.5	95 degrees–134 degrees	Electroplating, post-annealing and surface modification [149]
$Pd_{40}Cu_{30}Ni_{10}P_{20}$	Honeycomb patterns	Pitch size: 0–600 μm	98.8 degrees–152 degrees	Hot-embossing [61]
$La_{55}Al_{25}Ni_5Cu_{10}Co_5$	Smooth surface	/	~82 degree°	Polishing [183]
	Nanowire surface	Nanowire diameter: 170–330 nm		[183]
$Pt_{57.3}Cu_{14.6}Ni_{5.3}P_{22.8}$	Flat surface	/	~55 degrees	/
	Micropillars array	Pillars diameter: ~27 μm	~70 degrees	Hot-embossing [192]
	Microtubes array	Tube diameter:~ 50 μm	~103 degrees	
	Honeycomb	Pitch size:~ 50 μm	~113°	
$Zr_{35}Ti_{30}Be_{26.75}Cu_{8.25}$	Honeycomb	Pitch size: 0–600 μm	82.5 degrees–133.8 degrees	Hot embossing [200]
	Honeycomb with nanostructure	Pitch size: 0–600 μm Nanoprotrusion size: 10–30 nm	94.7 degrees–151.4 degrees	Hot embossing and chemical etching [200]
$Ce_{65}Al_{10}Cu_{20}Co_5$	Flat surface	/	~40 degrees	/[201]
	Flat surface	/	~110 degrees	FAS modification [201]
	Micropillars array	Pillars size: 20 μm, spacing: 9 μm	~0 degrees	Hot embossing [201]
	Micropillars with nanostructure	Pillars size: 20 μm, spacing: 9 μm Soot particle: nanoscale	~150 degrees	Hot embossing and SiO_2/soot deposition [201]

(*continued on next page*)

Table 1 (*continued*)

MG Compositions	Surface structure	Feature size	Surface wettability (WCA)	Processing methods
$Pd_{40}Ni_{10}Cu_{30}P_{20}$	Smooth surface	/	~52 degrees	Polishing [202]
	Micropore array with nanostructure	Pore diameter: 12–14 μm Nanostructure diameter: 80–100 nm	~156 degrees	Multistage thermoplastic forming [202]
$Zr_{41.2}Ti_{13.8}Cu_{12.5}Ni_{10}Be_{22.5}$	Smooth surface	/	~96°	Polishing [244]
	Hierarchical surface	Microscale ~ Nanoscale	140 degrees–144°	Laser ablation [244]
$Ca_{65}Li_{10}Mg_{8.5}Zn_{16.5}$	Hierarchical surface with coral patterns	Average diameter of: 100 nm	<90 degrees	Chemical etching [264]
	Hierarchical surface with coral patterns	Average diameter of: 100 nm	~162 degrees	Chemical etching and FAS modification [264]
$Ce_{65}Al_{10}Cu_{20}Co_5$	Smooth surface	Surface roughness: RMS ~ 15 nm	~37 degrees	/[265]
	Smooth surface	Surface roughness: RMS ~ 15 nm	~105 degrees	FAS modification [265]
	Hierarchical surface	Surface roughness: RMS ~ 85 nm	~0 degree	Chemical etching [265]
	Hierarchical surface	Surface roughness: RMS ~ 85 nm	~157 degrees°	Chemical etching and FAS modification [265]
$Ca_{60}Mg_{15}Zn_{25}$	Hierarchical surface	Microscale ~ Nanoscale	11.5 degrees–20.5 degrees	Chemical etching [266]
	Hierarchical surface	Microscale ~ Nanoscale	99.1 degrees–118.7 degrees	Chemical etching and FAS modification [266]
	Rough surface	Microscale ~ Nanoscale	~78.8 degrees	Fe coating [266]
	Rough surface	Microscale ~ Nanoscale	~133.6 degrees	Fe+FAS coating [266]
$Zr_{55}Cu_{30}Ni_5Al_{10}$	Flat surface	Surface roughness: Ra ~0.07 μm	~67.5 degrees	Polishing [267]
	Flat surface	Surface roughness: Ra ~0.07 μm	~99.5 degrees	Polishing and surface modification [267]
	Rough surface	Surface roughness: Ra 2.54–8.21 μm	131.6 degrees–169.6 degrees	Electrochemical corrosion and surface modification [267]
$Pd_{43}Ni_{10}Cu_{27}P_{20}$	Flat surface	Surface roughness: Ra ~2 nm	~70 degrees	Polishing [279]
	Nanorod surface	Nanorod diameter: 200 nm	~110 degrees	Thermoplastic forming [279]
$Ni_{60}Pd_{20}P_{17}B_3$	Nanoporous surface	Surface roughness: Ra ~7.05 nm	~84 degrees	Electrochemical dealloying [279]
	Nanodendritic surface	Nanoscale	~112 degrees	Electrochemical dealloying [279]

3. Properties evaluation and applications

These MG surfaces synthesized in lab generally exhibit excellent hydrophobic or superhydrophobic behavior under the well-controlled conditions. However, the functional stability and mechanical robustness in a real environment have not been sufficiently evaluated [296], which are essential for the practical applications of functional surfaces. In view of this, the critical evaluation that needed to be concerned for the MG water-repellent surfaces are proposed in this section, aiming to further the process of practicality. Considering the metastable sate of MGs and the involved surface micro/nanostructures, some special properties of the MG structural surfaces are emphatically elucidated, such as the wetting kinetics responding to the physical or chemical factors in the ambient environment as well as the size effect influencing the amorphous structures and mechanical properties. On the basis of these systematic evaluations, the cutting-edge applications of MG water-repellent surfaces are then discussed.

3.1. Critical evaluation of MG water-repellent surfaces

3.1.1. Wetting kinetics

The general factors to characterize the water-repellency of surfaces are the static water contact angle (WCA) and the advancing or receding contact angles measured by the specific instruments [297], which have been developed to be a relatively standard method and can reflect the surface wetting behavior from macroscopic aspect. However, more sophisticated surface structures of MGs as shown in the previous Section have been fabricated by various approaches to enhance the surface functions, thus the contact states on microscopic level between liquid and surface are more complex beyond the equilibrium conditions including Wenzel state and Cassie-Baxter state [298]. On this account, the responses of surface wetting behaviors to the physical or chemical stimuli in a real environment may be distinct, though the static contact angle of the surfaces are similar. It has been found that the contact geometrical shape of the liquid droplet generally exhibits as a downward curve with air trapped between the liquid droplet and surface structures because of the Laplace pressure [299,300]. The liquid bridge formed on low aspect-ratio pillars tend to more likely to collapse under the inertia forces [193], such as the acceleration of the workpiece and the impingement or bouncing of liquid droplet [301], which will change the surface wetting behavior during the dynamic movement in real environment. While the high aspect-ratio structures comprising of hierarchical features can help pin the liquid bridge on the surface and retain a more stable contact state. The wettability of the side surface of surface structures also has significant influence on the wetting kinetics, a hydrophobic side surface is capable of preventing the water infiltration into the surface structures and retain a stable wetting behavior [193]. In addition, due to the thermal induced pressure changes and air tightness, the wetting behavior of MG surface structures with a closed air trapping space is more sensitive to the temperature variation than the that of the semiclosed space [92–94].

Another kind of common stimuli from the external environment is the chemicals introduced on the surface structures during the fabrication or utilization period, which may change the surface free energy and structure morphology. Due to the patterned micro-/nanostructures, the superficial area of the MG surface exposed to the air or solutions will be dramatically increased, resulting in a high surface chemical activity. It was found that the nanotextured Pd-MG adsorbed more carbon than the flat surface, and thus turning from hydrophilic to superhydrophobic surface after 10 days in air [193], which may be caused by the decrease of the surface energy. While the CaLi-BMG surface without FAS modification were found severely oxygenated after exposure to ambient atmospheric conditions within 1–2 weeks [264], leading to the loss of the original wetting behaviors. Besides, the change of surface chemical compositions may incur a chain effect on the distribution of surface micro/nanostructures. The BMG nanowires with high aspect-ratio synthesized by TPF generally appeared tilted and bundling to varying degree after dissolving the template in different solvents [45,196], due to the bending and clustering of the nanowires by the capillary forces caused by the surface tension of solvents, which will significantly change the surface wetting behaviors. Therefore, on the basis of the foregoing discussions, to effectively characterize the wetting kinetics of MG surfaces, it is essential to decouple the effects of surface textures and chemistries on the wetting behaviors. In addition to the macroscopic contact angle of patterned surface, the surface free energy of the original smooth MGs [61,302] as well as the microcosmic contact geometries between the liquid and surface structures need to be analyzed, providing a foundation for the systematic testing of the dynamic responses of surface wettability to the physical or chemical stimuli that are pervasive in nature and practical applications.

3.1.2. Amorphous structure evolutions

The amorphous atomic structure with short-range order and long-range disorder contributes to the unique performance of MG functional surfaces. However, due to the metastable state of MGs, the crystallization, relaxation or rejuvenation may appear on the MG surfaces spontaneously along the time or incurred by the inducements in the real environments such as thermal variation, strain exertion, ion radiation and chemical reaction, which may change the original material properties and structures as well as surface wettability. It is found that the MGs with less free volume and relatively compact atomic packing possessed lower surface energy and higher water-repellency [302]. Because of the size effect, the crystallization kinetics of micro-/nanostructures on the MG surfaces are quite different with that of the bulk counterpart. The crystallization temperature of the Pt-MG nanorods with a diameter of 100 and 200 nm was found lower 6 °C and 24 °C respectively than the nominal value of BMGs [295]. This non-monotonic crystallization behavior may be due to the competition of size-dependent apparent viscosity, nucleation probability and heterogeneous nucleation [303,304]. In addition to the thermal stability, the plastic deformation and ion radiation of MGs also have a significant effect on the evolution of amorphous atomic structures [305,306]. The plastic strain facilitates the free volume annihilation and provides excess driving force for atoms diffusion, which may cause the atomic-scale damage and mechanical relaxation of MGs [307,308]. While the rejuvenation of MGs can be effectively stimulated under special conditions by increasing the free volume or liquid-like structure content, such as the severe plastic deformation [309,310], local heat treatment (re-rising temperature above Tg followed by rapid quenching) [311,312], alkaline solutions soaking [313], ion irradiation [314], etc. Therefore, to assess the stability of MG water-repellent surface in a practical context, the atomistic structural evolution of the surface features along with the time and external stimuli should be taken into consideration in the verification of amorphous structure. The kinetics of crystallization, relaxation and rejuvenation of MGs in a micro-/nanoscale need be further studied focusing on the size effect and their influence on the surface wetting behaviors.

3.1.3. Mechanical properties

The functional surfaces may be subjected to various loadings like tensile and compressive stresses in the applications, thus the mechanical properties of the structured MGs are generally concerned in the designing and building robust water-repellent surfaces. For the TFMGs, several standard mechanical tests have been conducted including the tensile [315], bending [316] and nanoindentation tests [317], which are also widely adopted for the other materials. However, the mechanical properties evaluation for the BMG surface structures have not yet been amenable for formulation of a ripe theory and method comparing with that of their crystalline counterparts, mainly due to the insufficient understanding of the effect of amorphous atomic structure variation on mechanical properties. Most of the relevant researches focused on the MG micro-/nanowires to analyze the deformation behavior by molecular dynamics simulations [318,319] and mechanical tests to obtain the tensile [320] and compression strength [321,322] as well as the elastic modulus [323]. It has been found that the unique size effect exists in the MGs due to the size constraints on shear band formation and propagation, inducing the transition of deformation mechanisms along with the dimension changes [46,324]. The ductility of MG structures tends to be significantly enhanced due to the homogeneous deformation behavior as the dimension decrease, due to the suppression of shear bands formation [325,326]. These mechanisms also rationalize the phenomenon that the tensile strength of MG microwires is nearly twice as high as that of the bulk counterpart [327].

It should be noted that the processing history [48] and structural relaxation [328] of the MG micro-/nanostructures have a remarkable effect on the mechanical properties. For instance, the chemical segregation was found near the surface zone of MG nanowires [329], due to the element diffusion driven by both thermal activation and internal stress during different fabrication processes. Further studies found that the nanowires also exhibited a near-surface (~1 nm thick) layer with substantially faster dynamics than the bulk [330]. These gradient effects of MG structures result in distinct mechanical responses to the external stimuli. The nanowires synthesized by casting exhibit excellent ductility with homogeneous deformation but relatively low strength, while those fabricated via FIB and TPF show higher strength but localized plastic deformation [331], which is closely correlated to the distinct atomic structure and packing density of MGs induced by various fabrication processes. It has been also demonstrated that the plasticity of MG micro/nano structures can be regulated by different intensity of ion irradiation [332,333], due to the irradiation-induced structural disorder that may increase the free volume fraction [294,334] and incur the transition of deformation mechanism from localized shear banding to homogeneous shear flow [335]. Therefore, in the evaluation of mechanical properties for MG functional surfaces, the size effect and element segregation as well as the atomic structure variation induced by the external stimuli and processing history should be taken into consideration, and the underlying mechanisms of plastic deformation in amorphous structure also need further investigations.

3.1.4. Wear and corrosion resistance

The durability of MG water-repellent surfaces is crucial for the practical applications in various harsh environments, and commonly characterized by the comprehensive indices such as wear and corrosion resistance. To assess the contact friction behavior of MG surfaces in the real environments, the sliding or reciprocating wear tests have been generally carried out for TFMGs and BMGs in the air and solutions [336,337], especially to simulate the wearing in physiological environment for the biomedical implants [338,339], which can obtain the macroscopic wear behaviors of MG surfaces. However, for most of the contact conditions, the loads sustained by functional surface structures mainly concentrated in the micro-/nano areas, thus the analysis of micro-/nanoscale tribological behavior of MGs is essential in the wear resistance evaluation of the functional surfaces. The wear resistance of MGs has been found dominated by the synergistic effects of strength factors including the hardness, plasticity, etc. [340] Therefore, the size effect existing in mechanical properties also have a significant influence on the wearing behaviors in different scales. The typical abrasion morphology containing shear bands without noticeable ductile features was found in the macrosliding wear track of BMGs, while the wear tracks became ductile as the sliding size decreased, resulting in higher wear resistance and friction for smaller structures [341]. To get more detailed wear behaviors, the micro-/nanoscratching tests and theoretical analysis [342] have been conducted on MGs under different normal loads and scratching velocities, focusing on the tangential force [343], frictional coefficient [344], scratching morphology [224], acoustic emission [345] as well as the effect of oxidation layer [346]. On the basis of these evaluations, the surface patterns of MGs can be tailored to enhance the wear resistance of MG surfaces and retain the same wetting behavior [191,347].

For the corrosion resistance evaluation of MG surfaces, the oxidation in air, corrosion soaking in solutions or electrochemical corrosion as well as their influences on surface wetting behaviors have been commonly concerned in different application environments. The corrosion test methods of MGs such as anodic polarization and *in vivo* experiments [348] were quite mature referencing to the test processes performed on other materials. It was found that corrosion behaviors are closely correlated to the internal atomic structure of MGs. The corrosion resistance tends to be enhanced in the relaxed MGs due to the decrease of free volume reducing chemical potentials, while the chemical order and clusters formation caused by relaxation may promote the pit nucleation on the MG surfaces during electrochemical corrosion [349]. And the crystallization of the MGs resulting in the grain boundary and dislocation defects will also undermine the surface corrosion resistance [350]. Therefore, the thermal stimuli in the real environments transforming the internal structure of MGs will further alter the corrosion behavior of MG surfaces. Annealing near the glass transition temperature (Tg) was found shifting the corrosion potential of MGs to the cathodic values, which is conducive to enhance the pitting corrosion resistance of MGs in the simulated body fluid [351,352]. This indicating that the corrosion resistance of MG surfaces can be tuned through regulating the free volume concentration by thermal or other treatments that affect the atomic structure, while the detailed relations between atomic structure and corrosion behavior still need further studies. In addition, the evaluation for the synergy behaviors of wear and corrosion of MG surfaces also important under the tribocorrosion conditions [353], especially in the biomedical applications [354,355], such as the movable joint implants in the body fluid.

3.2. Cutting-edge applications of MG water-repellent surfaces

MG materials have been exploited as structural and functional materials, due to its unique amorphous structure and excellent micro/nano forming ability. As a basic surface function, water-repellency may greatly extend the engineering applications of MG surfaces in the real environments by the multifunctional integration with catalysis, biocompatibility, optical features, etc. In addition to the superficial functions, the variation of internal atomic structure of MGs combined with desired surface wetting behavior may also create new possibilities in cutting-edge applications. For instance, inspired by the conventional semiconductor circuit, the metastable state of MG amorphous structure under phase transition stimuli has been studied for the design of data storage systems, which may also have a demand of water-repellent surface to enhance the durability in practical use. Therefore, some advanced and potential applications of MG surfaces with multifunction including water-repellency were discussed as follows on the basis of the critical evaluations outlined previously.

3.2.1. Micro-/nano-electromechanical system

It has been well known that MGs generally exhibit superplastic behavior in SCLR and can be formed into net-shaping 3D components with versatile geometries [356] as well as various 2D surface patterns [357,358] on the micro-/nanoscales. Due to the amorphous structure without crystalline grains, the high precision MG parts can be fabricated by TPF with negligible volume shrinkage and extremely good surface finish even reaching to atomic scale [204,205], which is very suitable for micro-/nano-electromechanical systems (MEMS/NEMS). Meanwhile, utilizing the properties of high strength and high elastic limit, a series of mechanical-energy-dissipation structures [359] and compliant mechanisms [360] can be synthesized based on MGs. However, as the ratio of the surface area to volume increases with the decrease of part dimensions, the stictions of micro-/nanostructures with the ambient medium, such as capillary, electrostatic, van der Waals and Casimir forces, tend to be increasingly apparent [361], causing the failure of MEMS/NEMS. Water-repellent surface patterns with low surface energy for the parts have been found effective to reduce the micro-adhesion and friction [191], especially can be exploited for reducing drag and increasing buoyancy in liquid [362], which can significantly enhance the reliability of MEMS/NEMS. Therefore, the hierarchical structures of MGs are highly required to achieve the desired surface wetting behavior while retaining the geometries and functions of the micro/nano parts in the electromechanical systems. These special MG parts for MEMS/NEMS can be fabricated by multistage TPF processes as discussed in Section 2 [202,203].

In addition to the rigid micro-electromechanical system (MEMS)/ nano-electromechanical system (NEMS), the flexible electronics on the basis of TFMGs have also received high attentions in recent years, particularly for stretchable and wearable electronic systems. The TFMG parts were generally deposited on substrate and subsequently patterned by etching or imprint lithography, which can be integrated with silicon integrated circuit [363]. On the basis of this process, the Zr-TFMGs have been made as conical springs and moving torsion bars for the new type electrostatic micro-actuator [364] and microscanner [365] respectively. Similarly, a kind of stretchable and transparent electrodes as wearable heaters using copper-zirconium thin film metallic glasses (CuZr-TFMGs) in the form of nanotrough networks have been fabricated by co sputtering process [366]. Inspired by the kirigami, the straight and curved patterns were formed on Fe-MG ribbon by photochemical machining [367], obtaining highly stretchable film with ultra-small strain energy loss during cyclic loading. However, the flexible electronic systems with high requirement of safety, such as the emerging electronic skin and human body sensors, need keep good electrical conductivity and corrosion resistance even under wet and humid conditions [368]. Thus, the water-repellent surfaces are especially desired in the TFMGs electronics. By controlling the periodic and crumpled surface morphology, TFMGs with tunable

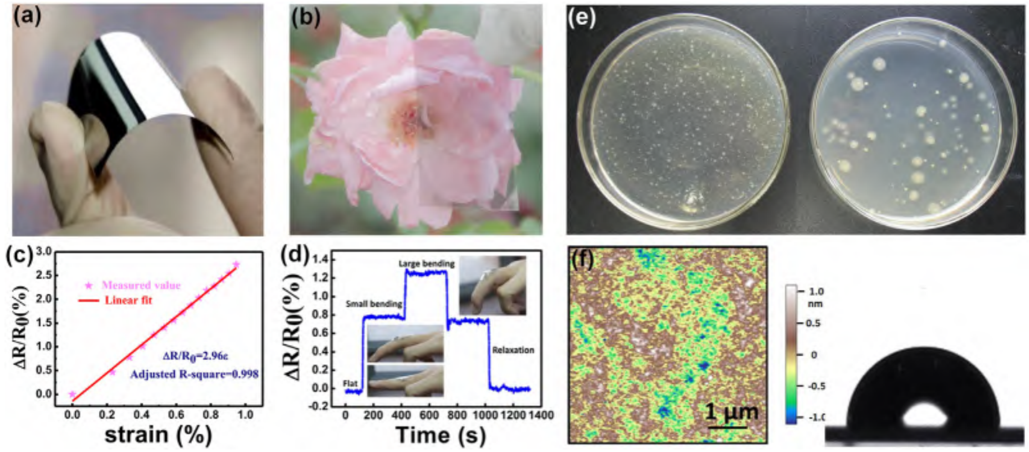

Fig. 25. (a) (b) TFMG skin can be transparent with the decrease of thickness. (c) Relative change of resistance vs. strain after bending 1000 times. (d) TFMG skin for monitoring hand movements with different bending degrees. (e) *E. coli* on different surface after antibacterial test. Left: PE control plate. Right: Zr-TFMG skin. (f) The morphology of TFMG (RMS 0.36 nm) and water contact angle (90°) (Reproduced from ref. [96]).

wetting behaviors were fabricated for strain sensing in wearable devices [96,97], as shown in Fig. 25a–d, the piezoresistance of the film is sensitive to the applied strains, and the transmittance spectra of the TFMGs in the wavelength range of 380–760 nm can be also tuned by different deposition thicknesses. Meanwhile, the hydrophobic TFMG skin is obtained with good antibacterial property (Fig. 25e and f). It is no doubt that MGs in 3D or 2D forms will further broaden the applications in novel electronics systems, while the wetting kinetics, thermal stability and mechanical durability in use environment of the MG parts also should be taken into account during the design of MEMS/NEMS.

3.2.2. Biomedical engineering

MGs have attracted extensive research interests as promising biomedical materials with excellent mechanical properties and corrosion resistance especially in the physiological environment. Moreover, due to the flexibility in the choice of combinations with respect to compositions of MGs, the stable or biodegradable materials [369] can be designed without toxic elements for complete biocompatibility, such as the biocompatible Ni-free Zr-BMGs [370], significantly eliminating the potential local immune responses. A variety of soft or hard tissue implants on the basis of MGs have been emerging such as the vascular stents [371], orthopedics implants [372] and *in vivo* biosensors [373]. However, a common issue in these biomedical applications involving the contact with blood is the platelet adhesion on artificial implants, which may cause blood coagulation and thrombosis. It has been supposed that the water-repellent surfaces exhibit good anti-adhesion to platelets and blood compatibility [374], which has been proved in the clinical testing for platelet and cancer cells adhesion on a hydrophobic Zr-TFMG surface [91]. Without introducing extra chemical elements, MGs surface patterning is an effective route to generate functional surface with desired wetting behaviors. A kind of Pt-BMG electrode with nanowire patterns for the glucose biosensor has been fabricated to enhance the sensing signal and sensitivity, and the wetting behavior of the BMG surface has significant influence on the biosensor performance in the enzyme functionalization process [375].

Besides, the surface patterns and the corresponding wettability have been also found directly influencing the cellular interactions with substrate surfaces, several studies demonstrate that cell spreading is dramatically enhanced on water-repellent surfaces [376], through affecting the protein layer adsorption and formation [377]. Various cellular behaviors on the micro/nanopatterned MG surfaces and TFMGs have been studied including macrophage polarization [378], bone cell forming [379], vascular cell response [380], osteoblast [381] and mesenchymal stem cell differentiation [382]. As shown in Fig. 26, the micropatterned surface induced greater macrophage fusion and bigger cell areas, while the addition of nanoscale topography tended to effectively reduce the cell proliferation. Thus, the macrophage growth is significantly affected by the synergy of surface patterns and wettability, indicating a potential way to modulate different types of cells behaviors [182,383]. In addition to the *in vivo* applications, the high-performance MG biomedical devices *in vitro* like surgical tools [384] and non-stick syringe needles [89,90] with water-repellent surfaces have also been produced and tested, showing the improved sharpness and antimicrobial property. A series of nanowire arrays were patterned on Pd-BMG for surface enhanced Raman scattering (SERS) [385], which can be used for trace amounts of biomarker and antigen detections, and the superhydrophobic surface can concentrate molecules by several million-fold significantly augmenting the SERS sensitivity [386]. Therefore, it is promising to integrate the water-repellent behavior with SERS substrate on the basis of MGs, opening new avenue for ultrasensitive biosensing and environmental pollution monitoring.

3.2.3. Solar and fuel cell

MGs can be readily tailored into micro/nanostructures possessing the desired surface wettability accompanying with the unique optical property and catalytic performance, especially suitable for the application in energy conversion and storage cells. Antireflection is crucial in increasing the efficiency of solar devices by enhancing light coupling into the photoelectric active region, which is significantly affected by the surface textures. A nanowire patterned surface based on Pt-BMG has been fabricated by TPF, demonstrating a low diffuse reflectance (1.6%) with small angular and wavelength dependence [387], and the reflectivity can be tuned in wide range by controlling the surface topography such as nanowire size, spacing and aspect-ratio. Meanwhile, the nanostructures of MGs have been verified to increase the absorption and retention of thermal energy, due to the effective restriction of heat pathways [388], inducing a rise of the photoinduced temperature for concentrated solar thermoelectric generators [389]. Besides, MG films also has been explored to enhance the performance of solar cells. By forming Al-MG frits into an interlayer between the

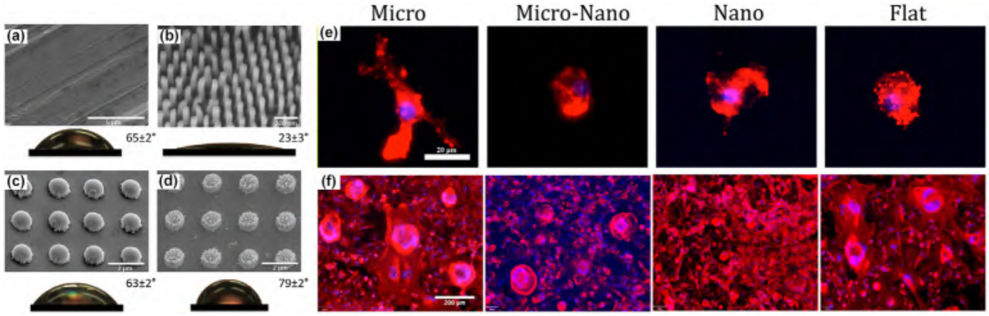

Fig. 26. Influence of surface patterns on the water contact angles for Pt-BMG, (a) flat surface, (b) nanopatterned surface, (c) micropatterned surface, (d) micro-/nanohierarchical surface. The cell responses and immunofluorescence images of macrophage fused on different MG surfaces, (e) low magnification images, (f) high magnification images (Reproduced from ref. [383]).

electrodes and Si layers, a large contact area working as tunneling barrier can be achieved with low specific contact resistance, obtaining a conversion efficiency of 19.6% in solar cells [390]. A 70 nm thick Zr-TFMG was used as a barrier for copper indium gallium selenide (CIGS) solar cells to effectively hindered the detrimental diffusion from the stainless substrate, obtaining a higher solar cell efficiency (5.25%) nearly twice as that of the bare substrate [391]. However, the solar devices, such as solar panels and perovskite solar cells [392] are generally exposed in ambient air, thus it is highly desired the water-repellent and self-cleaning [393] MG surfaces to reduce the liquid or atmospheric dust adhesion that will undermine the efficiency of solar cells [29].

Electrocatalysis plays a fundamental role in the energy conversion and storage processes of fuel cells. By employing the remarkable catalytic properties, particularly the high activities for methanol/ethanol oxidation [394] and hydrogen evolution [269] of Pt- and Pd-MGs, amorphous alloys have been used for the critical parts including the catalyst layers, diffusion layers and flow fields in fuel cells [371]. To enhance the durability and maintain the reactivity, the MGs as a versatile platform for electrocatalytic surfaces design were generally patterned into hierarchical structures by TFP or dealloying [274]. A kind of Pt-BMG electrode comprising of nano and microsized features has been synthesized by multistage TPF [55], as shown in Fig. 27, the nanowires uniformly decorated on the

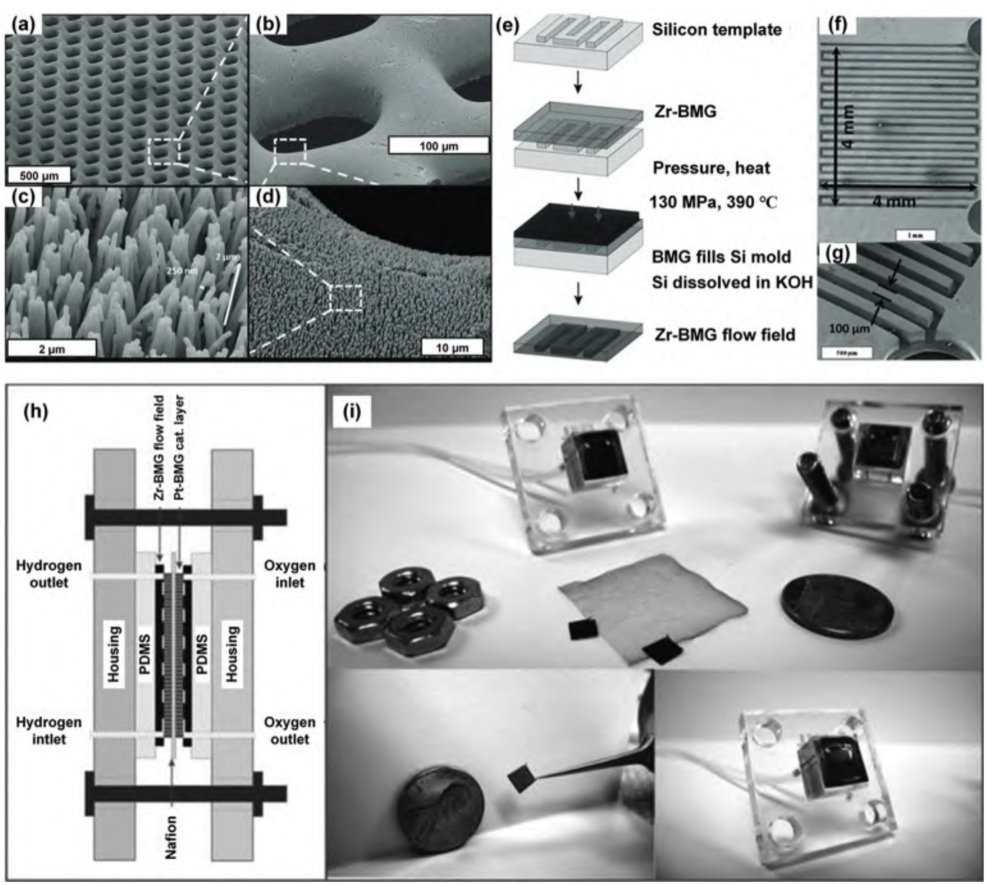

Fig. 27. (a)–(d) The nanowire electrode of Pt-BMG with gas feeding holes formed by multistage TPF. (e)–(g) Zr-BMG flow fields formed by TPF. (h) (i) Microfuel cell using the catalytic layers of porous Pt-BMG nanowires, and the flow field/current collector plates of Zr-BMG (Reproduced from ref. [55]).

surface ensure the high electrochemical activities, while the micro-through-holes facilitate the reactive gas reaching to the catalytic interfaces. By assembling the porous nanowires of Pt-BMG as electrode layers with the Zr-BMG flow fields, a microfuel cell (MFC) was produced with a peak power density of 9.4 mW/cm^2 at room temperature, providing an economical approach to develop novel MFCs. To further improve the performance of fuel cells, the influence of surface patterns and wetting behavior on electrolyte dispersion in conjunction with catalytic reactions need systematic studies to integrate the optimized wettability and catalytic property on the MG surfaces.

3.2.4. Microfluidic chip and data memory

Microfluidic chip, receiving intensive attentions and researches in recent years, has been identified as an ideal platform for biochemical sample processing with high throughput and low consumption [395], which is especially required in the tests and analysis of genomics and proteomics [396]. Utilizing droplet as microreactor and sample carrier, the key issues of the lab on a chip is how to flexibly manipulate the microdroplets to desired positions. Generally, the electrowetting on dielectric (EWOD) and dielectrophoresis (DEP) force have been adopted [397], inducing the variation of contact angle and pressure differential on the liquid-solid and air-liquid interfaces, to actuate the droplets in the electric field. Thus, the hydrophobic surface as a barrier to confine small volumes of sample within test zones and the hydrophilic microchannels to transport droplets are commonly involved in the microfluidic chip [398]. On the basis of this principle, MG surfaces have great potentials to be designed as a substrate with desired micro/nanostructures and wettability as well as bio/chemical compatibility for microfluidic chip. By analogizing to CPU of computer, a concept of central fluid processing unit (CFPU) on the basis of microfluidic chip has been proposed for the sophisticated and large-scale chemical/biological analysis, which is promising in biomedical diagnosis and drug development. In addition, MGs such as ternary compound of germanium, antimony, and tellurium ($Ge2Sb_2Te_5$) [399] and $Ge_{15}Sb_{85}$ [400] have been used to fabricate phase-change random-access memory (PCRAM), as shown in Fig. 28, the memory cells can be rapidly switched between logic states '0' (glassy) and '1' (crystalline) with different electrical resistance, which are programmed through the reversible ultrafast phase transformation, even in 700 ps using the $Sc_{0.2}Sb_2Te_3$ MGs [401]. Therefore, the PCRAM is regarded as a leading candidate for the next generation non-volatile electronic hierarchy memory that may be employed for the neuron computing of artificial intelligence beyond the standard Von Neumann architecture. In view of this, MGs multifunctional surfaces with tailored wetting behaviors are expected to be applied in these cutting-edge fields to enhance effectiveness and durability of the advanced systems.

4. Summary and future outlook

MGs have been taken as the excellent structural and functional materials, providing a versatile toolbox for synthesis of multi-functional surfaces. In the past few years, various fabrication approaches have been developed for the MG water-repellent surfaces including TFMG coating and BMG surface patterning as well as the emerging routes because of the manipulation of 1D MGs. However, there is still a gap between the MG functional surfaces synthesized in lab and the practical use in real environments, especially the stability of the amorphous structures and micro-/nanosurface patterns may be susceptible to the external stimuli during practical applications, leading to a decline or even complete loss of their unique properties and wettability. The prerequisite for the practical application is to effectively characterize the MG surface properties for the specific application scenarios. The future research works are addressed as follows:

(1) A systematic scheme with the feedback and iterative optimization mechanism needs to be built up, covering from the design stage to fabrication and application of MG water-repellent surfaces. As shown in the graphical abstract, in the upper reaches of the scheme, material screening [402] still needs to be conducted to develop new MGs with higher

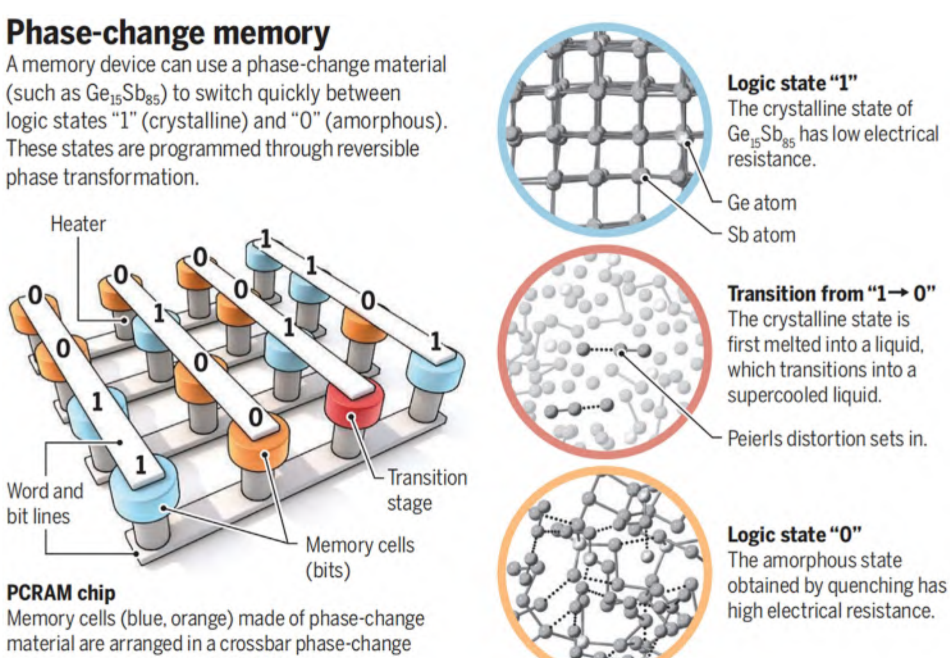

Fig. 28. The principle of PCRAM because of the amorphous phase transformation of memory arrays (Reproduced from ref. [400]).

glass forming ability (GFA) and better formability for the functional surface fabrication and application, particularly, the coupling effect of the intrinsic surface free energy and micro-/nanosurface patterns of MGs should be further studied in the design of water-repellent surfaces. On the basis of this, the high throughput and precision fabrication approaches need be developed, synthesizing more sophisticated surface structures in a large scale to enhance the surface functions and practicability by utilizing the unique properties of MGs such as the superplasticity in SCLR. Then, more detailed and standard evaluation system should be proposed for the MG functional surfaces fabricated from distinct routes to give critical instructions, so that the fabrication approaches can be selected to match the specific applications in different service environments. Meanwhile, a feedback loop from the evaluation and application of MG functional surfaces is crucial to iteratively improve the fabrication processes as well as the materials screening and surface structures designing.

(2) The fundamental mechanisms in the design and fabrication of MG water-repellent surfaces still need in-depth studies. For the wetting behavior of MG surfaces, the contact states of the liquid droplet on the hierarchical surface need be analyzed according to the specific surface structures, and then subdivided into more detailed conditions beyond the equilibrium contact states such as the classic Wenzel and Cassie-Baxter types, providing basic theories to predict the wetting kinetics under the external stimuli such as thermal effect, impact and inertia force in real environments. Moreover, the amphiphobic/omniphobic property [403] or switchable wettability [404] are highly desired to be explored on MG surfaces to further extend the potential applications. For the amorphous structure of MG surfaces, the evolution of atomic structure such as crystallization, relaxation and rejuvenation induced by the factors in real service environment, like thermal variation, strain exertion, ion radiation and chemical reaction, need to be systematically studied, especially focusing on the free volume changing mechanisms and the corresponding influences on the surface properties.

(3) Novel synthesis strategies of MG water-repellent surfaces suitable for industrial scale production are required to obtain robust functional surfaces and extend the size limit of the controllable surface patterns to sub-10 nm. Ultrasonic assisted forming has been recently proven a rapid forming route to achieve fast rejuvenation and high plasticity of MGs at ambient temperature [405,406], which can significantly reduce thermal defects when fabricating functional surfaces [407–409]. In addition to developing completely new technologies, the hybridization/integration of the existing techniques may be an effective strategy to synthesize more sophisticated surface structures and further enhance the performance of MG functional surfaces. It is very attractive to generate functional surface patterns combining with the strengthening effect because of the improved wear and corrosion resistance, such as the hydrophobic fractal MG surface fabricated by bending fracture [410] and textured MG surfaces by plastic deformation induced by electropulsing [411] or the laser shock peening [412]. The fabrication processes of the ultrastable MGs are also desired to upgrade from TFMGs to the bulk counterpart [66,413,414], which can significantly improve the stability of MG functional surfaces, though this process will be very challenging. Recently, the machine learning approach has been employed in the property prediction and composition screening of MGs [52,69,415], and a new strategy of armored superhydrophobic surface has been proposed by the arrangement of micro-/nanostructures [416], these novel concepts can be adopted in the design and fabrication of MG water-repellent surfaces. This comprehensive review is aiming to provide some inspirations to the interdisciplinary research/ investigations of surface engineering, materials science and other frontier fields on the basis of the MG functional surfaces.

Author contributions

Zhen Li: Formal analysis; Investigation; Writing - Original Draft; Writing - Review & Editing; Visualization. **Jiang Ma:** Conceptualization; Methodology; Validation; Writing - Review & Editing; Supervision; Project administration.

Data availability

The raw/processed data required to reproduce these findings cannot be shared at this time due to technical or time limitations. All data needed to make the conclusions in the paper are present in the paper. Additional data related to this paper can be requested from the authors.

Declaration of competing interest

The authors declare that they have no known competing financial interests or personal relationships that could have appeared to influence the work reported in this paper.

Acknowledgments

The work was supported by the Natural Science Foundation of Guangdong Province [grant number 2019B030302010], the NSF of China [grant number 51871157], the Science and Technology Innovation Commission Shenzhen [grant number JCYJ20170412111216258], the National Key Research and Development Program of China [grant number 2018YFA0703605], and the Guangdong Basic and Applied Basic Research Foundation [grant number 2020A1515110390].

References

[1] L. Feng, S. Li, Y. Li, H. Li, L. Zhang, J. Zhai, et al., Super-hydrophobic surfaces: from natural to artificial, Adv. Mater. 14 (2002) 1857–1860.
[2] K. Koch, B. Bhushan, W. Barthlott, Multifunctional surface structures of plants: an inspiration for biomimetics, Prog. Mater. Sci. 54 (2009) 137–178.
[3] L. Feng, Y. Zhang, J. Xi, Y. Zhu, N. Wang, F. Xia, et al., Petal effect: a superhydrophobic state with high adhesive force, Langmuir 24 (2008) 4114–4119.
[4] J. Xi, L. Jiang, Biomimic superhydrophobic surface with high adhesive forces, Ind. Eng. Chem. Res. 47 (2008) 6354–6357.
[5] C.P. Hsu, Y.M. Lin, P.Y. Chen, Hierarchical structure and multifunctional surface properties of carnivorous pitcher plants nepenthes, JOM 67 (2015) 744–753.
[6] H. Chen, P. Zhang, L. Zhang, H. Liu, Y. Jiang, D. Zhang, et al., Continuous directional water transport on the peristome surface of Nepenthes alata, Nature 532 (2016) 85–89.
[7] Y. Zheng, X. Gao, L. Jiang, Directional adhesion of superhydrophobic butterfly wings, Soft Matter 3 (2007) 178–182.
[8] D. Byun, J. Hong, Saputra, J.H. Ko, Y.J. Lee, H.C. Park, et al., Wetting characteristics of insect wing surfaces, J. Bionic Eng. 6 (2009) 63–70.
[9] X. Gao, X. Yan, X. Yao, L. Xu, K. Zhang, J. Zhang, et al., The dry-style antifogging properties of mosquito compound eyes and artificial analogues prepared by soft lithography, Adv. Mater. 19 (2007) 2213–2217.
[10] W.K. Kuo, J.J. Hsu, C.K. Nien, H.H. Yu, Moth-eye-inspired biophotonic surfaces with antireflective and hydrophobic characteristics, ACS Appl. Mater. Interfaces 8 (2016) 32021–32030.
[11] X. Gao, L. Jiang, Water-repellent legs of water striders, Nature 432 (2004) 36.

[12] X.Q. Feng, X. Gao, Z. Wu, L. Jiang, Q.S. Zheng, Superior water repellency of water strider legs with hierarchical structures: experiments and analysis, Langmuir 23 (2007) 4892−4896.
[13] S. Farhadi, M. Farzaneh, S.A. Kulinich, Anti-icing performance of superhydrophobic surfaces, Appl. Surf. Sci. 257 (2011) 6264−6269.
[14] A.J. Meuler, G.H. McKinley, R.E. Cohen, Exploiting topographical texture to impart icephobicity, ACS Nano 4 (2010) 7048−7052.
[15] B. Bhushan, Y.C. Jung, Natural and biomimetic artificial surfaces for superhydrophobicity, self-cleaning, low adhesion, and drag reduction, Prog. Mater. Sci. 56 (2011) 1−108.
[16] A. Rastegari, R. Akhavan, On the mechanism of turbulent drag reduction with super-hydrophobic surfaces, J. Fluid Mech. 773 (2015) R4.1−R4.14.
[17] S. Nishimoto, B. Bhushan, Bioinspired self-cleaning surfaces with superhydrophobicity, superoleophobicity, and superhydrophilicity, RSC Adv. 3 (2013) 671−690.
[18] L. Yao, J. He, Recent progress in antireflection and self-cleaning technology - from surface engineering to functional surfaces, Prog. Mater. Sci. 61 (2014) 94−143.
[19] X. Hong, X. Gao, L. Jiang, Application of superhydrophobic surface with high adhesive force in no lost transport of superparamagnetic microdroplet, J. Am. Chem. Soc. 129 (2007) 1478−1479.
[20] C. Lv, P. Hao, Driving droplet by scale effect on microstructured hydrophobic surfaces, Langmuir 28 (2012) 16958−16965.
[21] V.A. Lifton, S. Simon, R.E. Frahm, Reserve battery architecture based on superhydrophobic nanostructured surfaces, Bell Syst. Tech. J. 10 (2005) 81−85.
[22] E. Shawat, I. Perelshtein, A. Westover, C.L. Pint, G.D. Nessim, Ultra high-yield one-step synthesis of conductive and superhydrophobic three-dimensional mats of carbon nanofibers via full catalysis of unconstrained thin films, J. Mater. Chem. 2 (2014) 15118−15123.
[23] F. Su, K. Yao, Facile fabrication of superhydrophobic surface with excellent mechanical abrasion and corrosion resistance on copper substrate by a novel method, ACS Appl. Mater. Interfaces 6 (2014) 8762−8770.
[24] R. Kaur, S. Liu, Antibacterial surface design–contact kill, Prog. Surf. Sci. 91 (2016) 136−153.
[25] P. Hao, D.K. Schwartz, J.W. Medlin, Effect of surface hydrophobicity of Pd/Al_2O_3 on vanillin hydrodeoxygenation in a water/oil system, ACS Catal. 8 (2018) 11165−11173.
[26] A. Ranella, M. Barberoglou, S. Bakogianni, C. Fotakis, E. Stratakis, Tuning cell adhesion by controlling the roughness and wettability of 3D micro/nano silicon structures, Acta Biomater. 6 (2010) 2711−2720.
[27] K. Liu, X. Yao, L. Jiang, Recent developments in bio-inspired special wettability, Chem. Soc. Rev. 39 (2010) 3240−3255.
[28] S. Wang, K. Liu, X. Yao, L. Jiang, Bioinspired surfaces with superwettability: new insight on theory, design, and applications, Chem. Rev. 115 (2015) 8230−8293.
[29] U. Mehmood, F.A. Al-Sulaiman, B.S. Yilbas, B. Salhi, S.H.A. Ahmed, M.K. Hossain, Superhydrophobic surfaces with antireflection properties for solar applications: a critical review, Sol. Energy Mater. Sol. Cells 157 (2016) 604−623.
[30] A.W. Adamson, A.P. Gast, Physical Chemistry of Surfaces, vol. 150, Interscience publishers, New York, 1967.
[31] R.N. Wenzel, Resistance of solid surfaces to wetting by water, Ind. Eng. Chem. 28 (1936) 988−994.
[32] A.B.D. Cassie, S. Baxter, Wettability of porous surfaces, Trans. Faraday Soc. 40 (1944) 546−551.
[33] Y.Y. Yan, N. Gao, W. Barthlott, Mimicking natural superhydrophobic surfaces and grasping the wetting process: a review on recent progress in preparing superhydrophobic surfaces, Adv. Colloid Interface Sci. 169 (2011) 80−105.
[34] W. Klement, R.H. Willens, P. Duwez, Non-crystalline structure in solidified Gold-Silicon alloys, Nature 187 (1960) 869−870.
[35] H.S. Chen, Thermodynamic considerations on the formation and stability of metallic glasses, Acta Metall. 22 (1974) 1505−1511.
[36] A. Inoue, T. Zhang, T. Masumoto, Glass-forming ability of alloys, J. Non-Cryst. Solids 156−158 (1993) 473−480.
[37] P.G. Debenedetti, F.H. Stillinger, Supercooled liquids and the glass transition, Nature 410 (2001) 259−267.
[38] M. Telford, The case for bulk metallic glass, Mater. Today 7 (2004) 36−43.
[39] J. Das, M.B. Tang, K.B. Kim, R. Theissmann, F. Baier, W.H. Wang, et al., "Work-Hardenable" ductile bulk metallic glass, Phys. Rev. Lett. 94 (2005) 205501.
[40] W.H. Wang, Bulk metallic glasses with functional physical properties, Adv. Mater. 21 (2009) 4524−4544.
[41] W. Xu, W. Li, S. Chen, X. Wang, F. Li, Superplastic diffusion bonding of metallic glasses by rapid heating, Intermetallics 98 (2018) 143−147.
[42] Y. Saotome, K. Itoh, T. Zhang, A. Inoue, Superplastic nanoforming of Pd-based amorphous alloy, Scripta Mater. 44 (2001) 1541−1545.
[43] Y.H. Liu, G. Wang, R.J. Wang, D.Q. Zhao, M.X. Pan, W.H. Wang, Super plastic bulk metallic glasses at room temperature, Science 315 (2007) 1385−1388.
[44] Z. Li, Z. Huang, F. Sun, X. Li, J. Ma, Forming of metallic glasses: mechanisms and processes, Mater. Today Adv. 7 (2020) 100077.
[45] G. Kumar, H.X. Tang, J. Schroers, Nanomoulding with amorphous metals, Nature 457 (2009) 868−872.
[46] G. Kumar, A. Desai, J. Schroers, Bulk metallic glass: the smaller the better, Adv. Mater. 23 (2011) 461−476.
[47] J. Schroers, Processing of bulk metallic glass, Adv. Mater. 22 (2010) 1566−1597.
[48] L. Liu, M. Hasan, G. Kumar, Metallic glass nanostructures: fabrication, properties, and applications, Nanoscale 6 (2014) 2027−2036.
[49] W. Yao, Q.P. Cao, S.Y. Liu, X.D. Wang, H.J. Fecht, A. Caron, et al., Tailoring nanostructured Ni-Nb metallic glassy thin films by substrate temperature, Acta Mater. 194 (2020) 13−26.
[50] H.Z. Li, Z. Li, J. Yang, H.B. Ke, B.A. Sun, C.C. Yuan, et al., Interface design enabled manufacture of giant metallic glasses, Sci. China Mater. 64 (2021) 964−972.
[51] M.H. Cohen, D. Turnbull, Composition requirements for glass formation in metallic and ionic systems, Nature 189 (1961) 131−132.
[52] X. Liu, X. Li, Q. He, D. Liang, Z. Zhou, J. Ma, et al., Machine learning-based glass formation prediction in multicomponent alloys, Acta Mater. 201 (2020) 182−190.
[53] L. Huang, E.M. Fozo, T. Zhang, P.K. Liaw, W. He, Antimicrobial behavior of Cu-bearing Zr-based bulk metallic glasses, Mater. Sci. Eng. C 39 (2014) 325−329.
[54] X. Wang, R. Li, Z. Li, R. Xiao, X.-B. Chen, T. Zhang, Design and preparation of nanoporous Ag-Cu alloys by dealloying Mg-(Ag,Cu)-Y metallic glasses for antibacterial applications, J. Mater. Chem. B 7 (2019) 4169−4176.
[55] R.C. Sekol, G. Kumar, M. Carmo, F. Gittleson, N. Hardesty-Dyck, S. Mukherjee, et al., Bulk metallic glass micro fuel cell, Small 9 (2013) 2081−2085.
[56] Y.C. Hu, Y.Z. Wang, R. Su, C.R. Cao, F. Li, C.W. Sun, et al., A highly efficient and self-stabilizing metallic-glass catalyst for electrochemical hydrogen generation, Adv. Mater. 28 (2016) 10293−10297.
[57] Z. Lv, Y. Yan, C. Yuan, B. Huang, C. Yang, J. Ma, et al., Making Fe-Si-B amorphous powders as an effective catalyst for dye degradation by high-energy ultrasonic vibration, Mater. Des. (2020) 108876.
[58] F. Chu, B. Han, K. Edalati, J. Ma, Y.Y. Meng, C. Wang, et al., Severe plastic deformed Pd-based metallic glass for superior hydrogen evolution in both acidic and alkaline media, Scripta Mater. 204 (2021) 114145.
[59] L.B. Zhang, L.X. Qiu, Q.Y. Zhu, X. Liang, J.X. Huang, M.T. Yang, et al., Insight into efficient degradation of 3,5-dichlorosalicylic acid by Fe-Si-B amorphous ribbon under neutral condition, Appl. Catal. B Environ. 294 (2021) 120258.
[60] Y.Q. Yan, C. Wang, Z.Y. Huang, J.N. Fu, Z.Z. Lin, X. Zhang, et al., Highly efficient and robust catalysts for hydrogen evolution reaction by surface nano engineering of metallic glass, J. Mater. Chem. 9 (2021) 5415−5424.
[61] T. Xia, N. Li, Y. Wu, L. Liu, Patterned superhydrophobic surface based on Pd-based metallic glass, Appl. Phys. Lett. 101 (2012) 81601.
[62] P.-G. De Gennes, F. Brochard-Wyart, D. Quéré, Capillarity and Wetting Phenomena: Drops, Bubbles, Pearls, Waves, Springer Science & Business Media, 2013.
[63] J. Kramer, Produced the first amorphous metals through vapor deposition, Ann. Phys. 19 (1934) 37.
[64] A. Brenner, D.E. Couch, E.K. Williams, Electrodeposition of alloys of phosphorus with nickel or cobalt, J. Res. Natl. Bur. Stand. 44 (1950) 109.
[65] Y.-C. Hu, H. Tanaka, W.-H. Wang, Impact of spatial dimension on structural ordering in metallic glass, Phys. Rev. E 96 (2017) 22613.
[66] H.B. Yu, Y. Luo, K. Samwer, Ultrastable metallic glass, Adv. Mater. 25 (2013) 5904−5908.
[67] J.P. Chu, J.E. Greene, J.S.C. Jang, J.C. Huang, Y.L. Shen, P.K. Liaw, et al., Bendable bulk metallic glass: effects of a thin, adhesive, strong, and ductile coating, Acta Mater. 60 (2012) 3226−3238.
[68] R. Liontas, M. Jafary-Zadeh, Q. Zeng, Y.W. Zhang, W.L. Mao, J.R. Greer, Substantial tensile ductility in sputtered Zr-Ni-Al nano-sized metallic glass, Acta Mater. 118 (2016) 270−285.
[69] L. Ward, S.C. O'Keeffe, J. Stevick, G.R. Jelbert, M. Aykol, C. Wolverton, A machine learning approach for engineering bulk metallic glass alloys, Acta Mater. 159 (2018) 102−111.
[70] O. Glushko, M. Mühlbacher, C. Gammer, M.J. Cordill, C. Mitterer, J. Eckert, Exceptional fracture resistance of ultrathin metallic glass films due to an intrinsic size effect, Sci. Rep. 9 (2019) 1−9.
[71] B.S. Lou, Y.C. Yang, J.W. Lee, L.T. Chen, Biocompatibility and mechanical property evaluation of Zr-Ti-Fe based ternary thin film metallic glasses, Surf. Coating. Technol. 320 (2017) 512−519.
[72] J. Lee, M.L. Liou, J.G. Duh, The development of a Zr-Cu-Al-Ag-N thin film metallic glass coating in pursuit of improved mechanical, corrosion, and antimicrobial property for bio-medical application, Surf. Coating. Technol. 310 (2017) 214−222.
[73] W.H. Wang, J.H. Hsu, J.C. Huang, Optical reflectivity improvement by upgrading metallic glass film quality, Appl. Phys. Lett. 103 (2013) 161906.
[74] C.L. Chiang, J.P. Chu, F.X. Liu, P.K. Liaw, R.A. Buchanan, A 200 nm thick glass-forming metallic film for fatigue-property enhancements, Appl. Phys. Lett. 88 (2006) 131902.
[75] Q.K. Jiang, P. Liu, Y. Ma, Q.P. Cao, X.D. Wang, D.X. Zhang, et al., Super elastic strain limit in metallic glass films, Sci. Rep. 2 (2012) 852.
[76] Y. Liu, S. Hata, K. Wada, A. Shimokohbe, Thermal, mechanical and electrical properties of Pd-based thin-film metallic glass, Jpn. J. Appl. Phys. 40 (2001) 5382.
[77] Y.H. Liu, T. Fujita, D.P.B. Aji, M. Matsuura, M.W. Chen, Structural origins of Johari-Goldstein relaxation in a metallic glass, Nat. Commun. 5 (2014) 1−7.
[78] C.W. Chu, J.S.C. Jang, G.J. Chen, S.M. Chiu, Characteristic studies on the Zr-based metallic glass thin film fabricated by magnetron sputtering process, Surf. Coating. Technol. 202 (2008) 5564−5566.

[79] C.W. Chu, J.S.C. Jang, S.M. Chiu, J.P. Chu, Study of the characteristics and corrosion behavior for the Zr-based metallic glass thin film fabricated by pulse magnetron sputtering process, Thin Solid Films 517 (2009) 4930–4933.
[80] P. Zeman, M. Zítek, Š. Zuzjaková, R. Čerstvý, Amorphous Zr-Cu thin-film alloys with metallic glass behavior, J. Alloys Compd. 696 (2017) 1298–1306.
[81] M. Zítek, P. Zeman, Š. Zuzjaková, M. Kotrlová, R. Čerstvý, Tuning properties and behavior of magnetron sputtered Zr-Hf-Cu metallic glasses, J. Alloys Compd. 739 (2018) 848–855.
[82] M. Zítek, P. Zeman, M. Kotrlová, R. Čerstvý, Impact of Al or Si addition on properties and oxidation resistance of magnetron sputtered Zr–Hf–Al/Si–Cu metallic glasses, J. Alloys Compd. 772 (2019) 409–417.
[83] P.T. Chiang, G.J. Chen, S.R. Jian, Y.H. Shih, J.S.C. Jang, C.H. Lai, Surface antimicrobial effects of Zr61Al7.5Ni10Cu17.5Si4 thin film metallic glasses on Escherichia coli, Staphylococcus aureus, Pseudomonas aeruginosa, Acinetobacter baumannii and Candida albicans, Fooyin J. Health Sci. 2 (2010) 12–20.
[84] J.P. Chu, T.Y. Liu, C.L. Li, C.H. Wang, J.S.C. Jang, M.J. Chen, et al., Fabrication and characterizations of thin film metallic glasses: antibacterial property and durability study for medical application, Thin Solid Films 561 (2014) 102–107.
[85] J.H. Chu, J. Lee, C.C. Chang, Y.C. Chan, M.L. Liou, J.W. Lee, et al., Antimicrobial characteristics in Cu-containing Zr-based thin film metallic glass, Surf. Coating. Technol. 259 (2014) 87–93.
[86] Z.G. Dan, H.W. Ni, B.F. Xu, J. Xiong, P.Y. Xiong, Microstructure and antibacterial properties of AISI 420 stainless steel implanted by copper ions, Thin Solid Films 492 (2005) 93–100.
[87] X. Zhang, X. Huang, L. Jiang, Y. Ma, A. Fan, B. Tang, Surface microstructures and antimicrobial properties of copper plasma alloyed stainless steel, Appl. Surf. Sci. 258 (2011) 1399–1404.
[88] B. Subramanian, In vitro corrosion and biocompatibility screening of sputtered $Ti_{40}Cu_{36}Pd_{14}Zr_{10}$ thin film metallic glasses on steels, Mater. Sci. Eng. C 47 (2015) 48–56.
[89] J.P. Chu, C.C. Yu, Y. Tanatsugu, M. Yasuzawa, Y.L. Shen, Non-stick syringe needles: beneficial effects of thin film metallic glass coating, Sci. Rep. 6 (2016) 31847.
[90] J.P. Chu, N. Bonninghoff, C.C. Yu, Y.K. Liu, G.H. Chiang, Coating needles with metallic glass to overcome fracture toughness and trauma: analysis on porcine tissue and polyurethane rubber, Thin Solid Films 688 (2019) 137320.1–137320.7.
[91] C.H. Chang, C.L. Li, C.C. Yu, Y.L. Chen, S. Chyntara, J.P. Chu, et al., Beneficial effects of thin film metallic glass coating in reducing adhesion of platelet and cancer cells: clinical testing, Surf. Coating. Technol. 344 (2018) 312–321.
[92] W.T. Chen, S.S. Li, J.P. Chu, K.C. Feng, J.K. Chen, Fabrication of ordered metallic glass nanotube arrays for label-free biosensing with diffractive reflectance, Biosens. Bioelectron. 102 (2018) 129–135.
[93] W.T. Chen, K. Manivannan, C.C. Yu, J.P. Chu, J.K. Chen, Fabrication of an artificial nanosucker device with a large area nanotube array of metallic glass, Nanoscale 10 (2018) 1366–1375.
[94] J.K. Chen, W.T. Chen, C.C. Cheng, C.C. Yu, J.P. Chu, Metallic glass nanotube arrays: preparation and surface characterizations, Mater. Today 21 (2018) 178–185.
[95] S.T. Kassa, C.C. Hu, Y.C. Liao, J.K. Chen, J.P. Chu, Thin film metallic glass as an effective coating for enhancing oil/water separation of electrospun polyacrylonitrile membrane, Surf. Coating. Technol. 368 (2019) 33–41.
[96] H.J. Xian, C.R. Cao, J.A. Shi, X.S. Zhu, Y.C. Hu, Y.F. Huang, et al., Flexible strain sensors with high performance based on metallic glass thin film, Appl. Phys. Lett. 111 (2017) 121906.
[97] H. Xian, M. Liu, X. Wang, F. Ye, P. Wen, H. Bai, et al., Flexible and stretchable metallic glass micro-and nano-structures of tunable properties, Nanotechnology 30 (2018) 85705.
[98] C.Y. Chuang, J.W. Lee, C.L. Li, J.P. Chu, Mechanical properties study of a magnetron-sputtered Zr-based thin film metallic glass, Surf. Coating. Technol. 215 (2013) 312–321.
[99] J. Lee, H.C. Tung, J.G. Duh, Enhancement of mechanical and thermal properties in Zr-Cu-Ni-Al-N thin film metallic glass by compositional control of nitrogen, Mater. Lett. 159 (2015) 369–372.
[100] O. Jimenez, M. Audronis, M.A. Baker, A. Matthews, A. Leyland, Structure and mechanical properties of nitrogen-containing Zr-Cu based thin films deposited by pulsed magnetron sputtering, J. Phys. D Appl. Phys. 41 (2008) 155301.
[101] M. Apreutesei, C. Esnouf, A. Billard, P. Steyer, Impact of local nanocrystallization on mechanical properties in the Zr-59 at.% Cu metallic glass thin film, Mater. Des. 108 (2016) 8–12.
[102] J.P. Chu, C.M. Lee, R.T. Huang, P.K. Liaw, Zr-based glass-forming film for fatigue-property improvements of 316L stainless steel: annealing effects, Surf. Coating. Technol. 205 (2011) 4030–4034.
[103] Y. Liu, J. Liu, S. Sohn, Y. Li, J.J. Cha, J. Schroers, Metallic glass nanostructures of tunable shape and composition, Nat. Commun. 6 (2015) 7043.
[104] J. Liu, Y. Fu, Y. Tang, X.D. Wang, Q.P. Cao, D.X. Zhang, et al., Thickness dependent structural evolution in Mg-Zn-Ca thin film metallic glasses, J. Alloys Compd. 742 (2018) 524–535.
[105] A. Rauf, Y. Fang, H. Zhang, G. Peng, T. Feng, Thickness effects on microstructure, mechanical and soft magnetic properties of sputtered FeZr thin film metallic glass, J. Non-Cryst. Solids 521 (2019) 119500.
[106] J.R. Davis, Handbook of Thermal Spray Technology, ASM international, 2004.
[107] S.S. Joshi, S. Katakam, H. Singh Arora, S. Mukherjee, N.B. Dahotre, Amorphous coatings and surfaces on structural materials, Crit. Rev. Solid State Mater. Sci. 41 (2016) 1–46.
[108] H. Miura, S. Isa, K. Omuro, Production of amorphous iron-nickel based alloys by flame-spray quenching and coatings on metal substrates, Trans. Japan Inst. Met. 25 (1984) 284–291.
[109] F. Otsubo, H. Era, K. Kishitake, Formation of amorphous Fe-Cr-Mo-8P-2C coatings by the high velocity oxy-fuel process, J. Therm. Spray Technol. 9 (2000) 494–498.
[110] W. Guo, Y. Wu, J. Zhang, S. Hong, G. Li, G. Ying, et al., Fabrication and characterization of thermal-sprayed Fe-based amorphous/nanocrystalline composite coatings: an overview, J. Therm. Spray Technol. 23 (2014) 1157–1180.
[111] L. Liu, C. Zhang, Fe-based amorphous coatings: structures and properties, Thin Solid Films 561 (2014) 70–86.
[112] R.Q. Guo, C. Zhang, Q. Chen, Y. Yang, N. Li, L. Liu, Study of structure and corrosion resistance of Fe-based amorphous coatings prepared by HVAF and HVOF, Corrosion Sci. 53 (2011) 2351–2356.
[113] J. Zhang, M. Liu, J. Song, C. Deng, C. Deng, Microstructure and corrosion behavior of Fe-based amorphous coating prepared by HVOF, J. Alloys Compd. 721 (2017) 506–511.
[114] G.Y. Koga, R. Schulz, S. Savoie, A.R.C. Nascimento, Y. Drolet, C. Bolfarini, et al., Microstructure and wear behavior of Fe-based amorphous HVOF coatings produced from commercial precursors, Surf. Coating. Technol. 309 (2017) 938–944.
[115] H. Zhang, Y. Hu, G. Hou, Y. An, G. Liu, The effect of high-velocity oxy-fuel spraying parameters on microstructure, corrosion and wear resistance of Fe-based metallic glass coatings, J. Non-Cryst. Solids 406 (2014) 37–44.
[116] M. Jalali Azizpour, M. Tolouei-Rad, The effect of spraying temperature on the corrosion and wear behavior of HVOF thermal sprayed WC-Co coatings, Ceram. Int. 45 (2019) 13934–13941.
[117] C. Zhang, R.Q. Guo, Y. Yang, Y. Wu, L. Liu, Influence of the size of spraying powders on the microstructure and corrosion resistance of Fe-based amorphous coating, Electrochim. Acta 56 (2011) 6380–6388.
[118] G. Liu, Y. An, Z. Guo, J. Chen, G. Hou, J. Chen, Structure and corrosion behavior of iron-based metallic glass coatings prepared by LPPS, Appl. Surf. Sci. 258 (2012) 5380–5386.
[119] P. Bijalwan, A. Kumar, S.K. Nayak, A. Banerjee, M. Dutta, T. Laha, Microstructure and corrosion behavior of Fe-based amorphous composite coatings developed by atmospheric plasma spraying, J. Alloys Compd. 796 (2019) 47–54.
[120] Y. Li, T. Liang, R. Ao, H. Zhao, X. Chen, J. Zeng, Oxidation resistance of iron-based coatings by supersonic arc spraying at high temperature, Surf. Coating. Technol. 347 (2018) 99–112.
[121] J. Lin, Z. Wang, P. Lin, J. Cheng, J. Zhang, X. Zhang, Microstructure and corrosion resistance of Fe-based coatings prepared by twin wires arc spraying process, J. Therm. Spray Technol. 23 (2014) 333–339.
[122] X. Wul, Y. Hong, Fe-based thick amorphous-alloy coating by laser cladding, Surf. Coating. Technol. 141 (2001) 141–144.
[123] D. Zhang, D. Kong, Microstructures and immersion corrosion behavior of laser thermal sprayed amorphous Al-Ni coatings in 3.5 % NaCl solution, J. Alloys Compd. 735 (2018) 1–12.
[124] Q.Y. Wang, Y.C. Xi, Y.H. Zhao, S. Liu, S.L. Bai, Z.D. Liu, Effects of laser remelting and annealing on microstructure, mechanical property and corrosion resistance of Fe-based amorphous/crystalline composite coating, Mater. Charact. 127 (2017) 239–247.
[125] H. Chen, D. Kong, Effects of laser remelting speeds on microstructure, immersion corrosion, and electrochemical corrosion of arc–sprayed amorphous Al–Ti–Ni coatings, J. Alloys Compd. 771 (2019) 584–594.
[126] J.B. Cheng, X.B. Liang, B.S. Xu, Devitrification of arc-sprayed FeBSiNb amorphous coatings: effects on wear resistance and mechanical behavior, Surf. Coating. Technol. 235 (2013) 720–726.
[127] J. Lin, Z. Wang, P. Lin, J. Cheng, X. Zhang, S. Hong, Effects of post annealing on the microstructure, mechanical properties and cavitation erosion behavior of arc-sprayed FeNiCrBSiNbW coatings, Mater. Des. 65 (2015) 1035–1040.
[128] Y. Wang, S.L. Jiang, Y.G. Zheng, W. Ke, W.H. Sun, J.Q. Wang, Effect of porosity sealing treatments on the corrosion resistance of high-velocity oxy-fuel (HVOF)-sprayed Fe-based amorphous metallic coatings, Surf. Coating. Technol. 206 (2011) 1307–1318.
[129] M.M. Liu, H.X. Hu, Y.G. Zheng, Effects of three sealing methods of aluminum phosphate sealant on corrosion resistance of the Fe-based amorphous coating, Surf. Coating. Technol. 309 (2017) 579–589.
[130] W.H. Liu, F.S. Shieu, W.T. Hsiao, Enhancement of wear and corrosion resistance of iron-based hard coatings deposited by high-velocity oxygen fuel (HVOF) thermal spraying, Surf. Coating. Technol. 249 (2014) 24–41.
[131] Z. Chu, X. Zheng, C. Zhang, J. Xu, L. Gao, Study the effect of AT13 addition on the properties of AT13/Fe-based amorphous composite coatings, Surf. Coating. Technol. 379 (2019) 125053.
[132] C. Zhang, Y. Wu, L. Liu, Robust hydrophobic Fe-based amorphous coating by thermal spraying, Appl. Phys. Lett. 101 (2012) 121603.
[133] L.M. Zhang, S.D. Zhang, A.L. Ma, H.X. Hu, Y.G. Zheng, B.J. Yang, et al., Influence of sealing treatment on the corrosion behavior of HVAF sprayed Al-based amorphous/nanocrystalline coating, Surf. Coating. Technol. 353 (2018) 263–273.

[134] J.H. Qiao, X. Jin, J.H. Qin, H.T. Liu, Y. Luo, D.K. Zhang, A super-hard super-hydrophobic Fe-based amorphous alloy coating, Surf. Coating. Technol. 334 (2018) 286–291.
[135] T.P. Moffat, Electrodeposition of Al-Cr metallic glass, J. Electrochem. Soc. 141 (1994) L115–L117.
[136] S. Yao, S. Zhao, H. Guo, M. Kowaka, A new amorphous alloy deposit with high corrosion resistance, Corrosion 52 (1996) 183–186.
[137] M. Saitou, Y. Okudaira, W. Oshikawa, Amorphous structures and kinetics of phosphorous incorporation in electrodeposited Ni-P thin films, J. Electrochem. Soc. 150 (2003) C140.
[138] C. Yao, B. Wei, P. Zhang, X. Lu, P. Liu, Y. Tong, Facile preparation and magnetic study of amorphous Tm-Fe-Co-Ni-Mn multicomponent alloy nanofilm, J. Rare Earths 29 (2011) 133–137.
[139] B.P. Daly, F.J. Barry, Electrochemical nickel-phosphorus alloy formation, Int. Mater. Rev. 48 (2003) 326–338.
[140] S. Wang, C. Zeng, Y. Ling, J. Wang, G. Xu, Phase transformations and electrochemical characterizations of electrodeposited amorphous Fe–W coatings, Surf. Coating. Technol. 286 (2016) 36–41.
[141] C. Guo, Y. Fang, B. Wu, S. Lan, G. Peng, X.L. Wang, et al., Ni-P nanoglass prepared by multi-phase pulsed electrodeposition, Mater. Res. Lett. 5 (2017) 293–299.
[142] F. Wang, T. Watanabe, Preparation and characterization of the electrodeposited Fe-Cr alloy film, Mater. Sci. Eng., A 349 (2003) 183–190.
[143] N. Yamachika, Y. Musha, J. Sasano, K. Senda, M. Kato, Y. Okinaka, et al., Electrodeposition of amorphous Au-Ni alloy film, Electrochim. Acta 53 (2008) 4520–4527.
[144] F. Bahrami, R. Amini, A.H. Taghvaei, Microstructure and corrosion behavior of electrodeposited Ni-based nanocomposite coatings reinforced with $Ni_{60}Cr_{10}Ta_{10}P_{16}B_4$ metallic glass particles, J. Alloys Compd. 714 (2017) 530–536.
[145] M. Maril, P. Tobosque, J. Núñez, C.A. Rodriguez, M.P. Delplancke, J.L. Delplancke, et al., Synthesis and structural analysis of electrodeposited Pb-Co films for oxygen evolution applications, Mater. Charact. 148 (2019) 323–329.
[146] G. Yar-Mukhamedova, M. Ved', N. Sakhnenko, T. Nenastina, Composition electrolytic coatings with given functional properties, Appl. Surf. Sci. (2019) 1–17.
[147] H. Li, H. Sun, C. Wang, B. Wei, C. Yao, Y. Tong, et al., Controllable electrochemical synthesis and magnetic behaviors of Mg-Mn-Fe-Co-Ni-Gd alloy films, J. Alloys Compd. 598 (2014) 161–165.
[148] S. Wang, Y. Ling, P. Zhao, N. Zang, J. Wang, S. Guo, et al., Bonding tungsten, W-Cu-alloy and copper with amorphous Fe-W alloy transition, Fusion Eng. Des. 88 (2013) 248–252.
[149] S. Wang, Y.H. Ling, J. Zhang, J.J. Wang, G.Y. Xu, Microstructure and properties of hydrophobic films derived from Fe-W amorphous alloy, Int. J. Miner. Metall. Mater. 21 (2014) 395–400.
[150] C. Zhang, J. Cai, C. Liang, A. Khan, W.-D. Li, Scalable fabrication of metallic nanofiber network via templated electrodeposition for flexible electronics, Adv. Funct. Mater. 29 (2019) 1903123.
[151] G. Ali, M. Maqbool, Fabrication of cobalt-nickel binary nanowires in a highly ordered alumina template via AC electrodeposition, Nanoscale Res. Lett. 8 (2013) 1–8.
[152] M.A. Zeeshan, D. Esqué-De Los Ojos, P. Castro-Hartmann, M. Guerrero, J. Nogués, S. Suriñach, et al., Electrochemically synthesized amorphous and crystalline nanowires: dissimilar nanomechanical behavior in comparison with homologous flat films, Nanoscale 8 (2016) 1344–1351.
[153] A. Shibata, Y. Imamura, M. Sone, C. Ishiyama, Y. Higo, Pd-Ni-P metallic glass film fabricated by electroless alloy plating, Thin Solid Films 517 (2009) 1935–1938.
[154] B. Zhang, Amorphous and Nano Alloys Electroless Depositions: Technology, Composition, Structure and Theory, Elsevier, 2015.
[155] L.W. Ren, Z. Wang, M.M. Meng, H. Tian, H.J. Yang, J.W. Qiao, Plasticity enhancement in bulk metallic glasses by electroless plating with Ni-P amorphous films, J. Non-Cryst. Solids 430 (2015) 115–119.
[156] N. Yoshida, T. Tasaki, T.F.M. Chang, A. Shibata, C. Ishiyama, M. Sone, Pd-Ni-P metallic glass pattern with controllable microstructure fabricated by electroless alloy plating, Microelectron. Eng. 88 (2011) 2401–2404.
[157] J. Rys, L. Valdevit, T.A. Schaedler, A.J. Jacobsen, W.B. Carter, J.R. Greer, Fabrication and deformation of metallic glass micro-lattices, Adv. Eng. Mater. 16 (2014) 889–896.
[158] X. Liu, Z. Jiang, Y. Guo, Z. Zhang, L. Ren, Fabrication of super-hydrophobic nano-sized copper films by electroless plating, Thin Solid Films 518 (2010) 3731–3734.
[159] P.I. Nikitin, A.A. Beloglazov, A.Y. Toporov, M.V. Valeiko, V.I. Konov, A. Perrone, et al., Amorphous magnetic films produced by pulsed laser deposition, J. Appl. Phys. 82 (1997) 1408–1415.
[160] T. Orui, J. Herms, Y. Hanyu, S. Ueda, K. Watanabe, I. Sakaguchi, et al., Charge compensation by excess oxygen in amorphous In-Ga-Zn-O films deposited by pulsed laser deposition, IEEE/OSA, J Disp Technol 11 (2015) 518–522.
[161] N. Nishiyama, K. Amiya, A. Inoue, Novel applications of bulk metallic glass for industrial products, J. Non-Cryst. Solids 353 (2007) 3615–3621.
[162] A. Inoue, N. Nishiyama, H. Kimura, Preparation and thermal stability of bulk amorphous $Pd_{40}Cu_{30}Ni_{10}P_{20}$ alloy cylinder of 72 mm in diameter, Mater. Trans., JIM 38 (1997) 179–183.
[163] A. Inoue, A. Takeuchi, Recent development and application products of bulk glassy alloys, Acta Mater. 59 (2011) 2243–2267.
[164] P. Lucas, C. Conseil, Z. Yang, Q. Hao, S. Cui, C. Boussard-Pledel, et al., Thermoelectric bulk glasses based on the Cu-As-Te-Se system, J. Mater. Chem. 1 (2013) 8917–8925.
[165] S.X. Song, H. Bei, J. Wadsworth, T.G. Nieh, Flow serration in a Zr-based bulk metallic glass in compression at low strain rates, Intermetallics 16 (2008) 813–818.
[166] Y.Q. Cheng, E. Ma, Atomic-level structure and structure-property relationship in metallic glasses, Prog. Mater. Sci. 56 (2011) 379–473.
[167] X. Liu, R. Mo, K. Li, J. Shen, J. Ma, F. Gong, Manufacturing of 3D microlens array mold on bulk metallic glass by self-aligned multi-ball hot embossing, Int. J. Precis. Eng. Manuf. Green Technol. (2020) 1–15.
[168] Y. Kawamura, T. Shibata, A. Inoue, T. Masumoto, Workability of the supercooled liquid in the $Zr_{65}Al_{10}Ni_{10}Cu_{15}$ bulk metallic glass, Acta Mater. 46 (1998) 253–263.
[169] X. Xiao, S.S. Fang, Q. Wang, G.M. Wang, Q. Hua, Y.D. Dong, Effect of hot rolling on thermal stability and microstructure of $Zr_{52.5}Al_{10}Ni_{10}Cu_{15}Be_{12.5}$ bulk metallic glass, Mater. Lett. 58 (2004) 2357–2360.
[170] A. Wiest, J.S. Harmon, M.D. Demetriou, R. Dale Conner, W.L. Johnson, Injection molding metallic glass, Scripta Mater. 60 (2009) 160–163.
[171] J. Schroers, T.M. Hodges, G. Kumar, H. Raman, A.J. Barnes, Q. Pham, et al., Thermoplastic blow molding of metals, Mater. Today 14 (2011) 14–19.
[172] J.N. Fu, J. Yang, K. Wu, H.J. Lin, W.X. Wen, W.Q. Ruan, et al., Metallic glue for designing composite materials with tailorable properties, Mater. Horiz. 8 (2021) 1690–1699.
[173] J. Ma, K.C. Chan, L. Xia, S.H. Chen, F.F. Wu, W.H. Li, et al., Multi-layer laminated Pd-based metallic glass with enhanced plasticity, Mater. Sci. Eng., A 587 (2013) 240–243.
[174] N. Li, W. Chen, L. Liu, Thermoplastic micro-forming of bulk metallic glasses: a review, JOM 68 (2016) 1246–1261.
[175] N. Li, L. Liu, K.C. Chan, Q. Chen, J. Pan, Deformation behavior and indentation size effect of $Au_{49}Ag_{5.5}Pd_{2.3}Cu_{26.9}Si_{16.3}$ bulk metallic glass at elevated temperatures, Intermetallics 17 (2009) 227–230.
[176] N. Li, Y. Chen, M.Q. Jiang, D.J. Li, J.J. He, Y. Wu, et al., A thermoplastic forming map of a Zr-based bulk metallic glass, Acta Mater. 61 (2013) 1921–1931.
[177] H. Kato, T. Wada, M. Hasegawa, J. Saida, A. Inoue, H.S. Chen, Fragility and thermal stability of Pt- and Pd-based bulk glass forming liquids and their correlation with deformability, Scripta Mater. 54 (2006) 2023–2027.
[178] J. Schroers, On the formability of bulk metallic glass in its supercooled liquid state, Acta Mater. 56 (2008) 471–478.
[179] W.L. Johnson, G. Kaltenboeck, M.D. Demetriou, J.P. Schramm, X. Liu, K. Samwer, et al., Beating crystallization in glass-forming metals by millisecond heating and processing, Science 332 (2011) 828–833.
[180] G. Kaltenboeck, T. Harris, K. Sun, T. Tran, G. Chang, J.P. Schramm, et al., Accessing thermoplastic processing windows in metallic glasses using rapid capacitive discharge, Sci. Rep. 4 (2014) 6441.
[181] J. Ma, Z. Huang, H. Zheng, F. Gong, X. Liang, Controllable thermoplastic forming of bulk metallic glasses in milliseconds by resistance welding forming, Mater. Res. Express 6 (2019) 75210.
[182] J. Padmanabhan, E.R. Kinser, M.A. Stalter, C. Duncan-Lewis, J.L. Balestrini, A.J. Sawyer, et al., Engineering cellular response using nanopatterned bulk metallic glass, ACS Nano 8 (2014) 4366–4375.
[183] J.N. Fu, Z.Y. Huang, J. Yang, J. Ma, J. Shen, Nano-forming of the rare earth La-based metallic glass, J. Non-Cryst. Solids 558 (2021) 120682.
[184] J.J. He, N. Li, N. Tang, X.Y. Wang, C. Zhang, L. Liu, The precision replication of a microchannel mould by hot-embossing a Zr-based bulk metallic glass, Intermetallics 21 (2012) 50–55.
[185] S. Bera, B. Sarac, S. Balakin, P. Ramasamy, M. Stoica, M. Calin, et al., Micro-patterning by thermoplastic forming of Ni-free Ti-based bulk metallic glasses, Mater. Des. 120 (2017) 204–211.
[186] J.P. Chu, H. Wijaya, C.W. Wu, T.R. Tsai, C.S. Wei, T.G. Nieh, et al., Nanoimprint of gratings on a bulk metallic glass, Appl. Phys. Lett. 90 (2007) 34101.
[187] J. Ma, J. Yi, D.Q. Zhao, M.X. Pan, W.H. Wang, Large size metallic glass gratings by embossing, J. Appl. Phys. 112 (2012) 64505.
[188] B. Sarac, J. Ketkaew, D.O. Popnoe, J. Schroers, Honeycomb structures of bulk metallic glasses, Adv. Funct. Mater. 22 (2012) 3161–3169.
[189] Z. Liu, W. Chen, J. Carstensen, J. Ketkaew, R.M.O. Mota, J.K. Guest, et al., 3D metallic glass cellular structures, Acta Mater. 105 (2016) 35–43.
[190] Y. Saotome, K. Imai, S. Shioda, S. Shimizu, T. Zhang, A. Inoue, The micro-nanoformability of Pt-based metallic glass and the nanoforming of three-dimensional structures, Intermetallics 10 (2002) 1241–1247.
[191] N. Li, E. Xu, Z. Liu, X. Wang, L. Liu, Tuning apparent friction coefficient by controlled patterning bulk metallic glasses surfaces, Sci. Rep. 6 (2016) 1–9.
[192] M. Hasan, G. Kumar, High strain rate thermoplastic demolding of metallic glasses, Scripta Mater. 123 (2016) 140–143.
[193] M. Hasan, J. Warzywoda, G. Kumar, Decoupling the effects of surface texture and chemistry on the wetting of metallic glasses, Appl. Surf. Sci. 447 (2018) 355–362.
[194] S. Ding, J. Kong, J. Schroers, Wetting of bulk metallic glass forming liquids on metals and ceramics, J. Appl. Phys. 110 (2011) 43508.
[195] Z. Liu, J. Schroers, General nanomoulding with bulk metallic glasses, Nanotechnology 26 (2015) 145301.

[196] Z. Hu, C. Uzun, Z. Dong, W. Li, A.A. Bernussi, G. Kumar, Elastocapillary bundling of high aspect-ratio metallic glass nanowires, Appl. Phys. Lett. 111 (2017) 23107.
[197] M. Hasan, N. Kahler, G. Kumar, Shape-controlled metal-metal and metal-polymer Janus structures by thermoplastic embossing, ACS Appl. Mater. Interfaces 8 (2016) 11084–11090.
[198] M. Hasan, G. Kumar, High-throughput drawing and testing of metallic glass nanostructures, Nanoscale 9 (2017) 3261–3268.
[199] Z. Hu, C.S. Meduri, J. Blawzdziewicz, G. Kumar, Nanoshaping of glass forming metallic liquids by stretching: evading lithography, Nanotechnology 30 (2018) 75302.
[200] N. Li, T. Xia, L. Heng, L. Liu, Superhydrophobic Zr-based metallic glass surface with high adhesive force, Appl. Phys. Lett. 102 (2013) 251603.
[201] Y. He, Y. Peng, Z. Li, J. Ma, X. Zhang, K. Liu, et al., Bio-inspired multifunctional metallic glass, Sci. China Chem. 59 (2016) 271–276.
[202] J. Ma, X.Y. Zhang, D.P. Wang, D.Q. Zhao, D.W. Ding, K. Liu, et al., Superhydrophobic metallic glass surface with superior mechanical stability and corrosion resistance, Appl. Phys. Lett. 104 (2014) 173701.
[203] M. Hasan, J. Schroers, G. Kumar, Functionalization of metallic glasses through hierarchical patterning, Nano Lett. 15 (2015) 963–968.
[204] G. Kumar, R.A. Staffier, R. Blawzdziewicz, R.D. Schwarz, J. Schroers, Atomically smooth surfaces through thermoplastic forming of metallic glass, Appl. Phys. Lett. 97 (2010) 851.
[205] R. Li, Z. Chen, A. Datye, G.H. Simon, J. Ketkaew, E. Kinser, et al., Atomic imprinting into metallic glasses, Commun. Phys. 1 (2018) 1–6.
[206] J. Ma, L.S. Huo, D.Q. Zhao, W.H. Wang, Micro mold filling kinetics of metallic glasses in supercooled liquid state, J. Appl. Phys. 113 (2013) 104505.
[207] G. Kumar, J. Blawzdziewicz, J. Schroers, Controllable nanoimprinting of metallic glasses: effect of pressure and interfacial properties, Nanotechnology 24 (2013) 105301.
[208] N. Li, X. Xu, Z. Zheng, L. Liu, Enhanced formability of a Zr-based bulk metallic glass in a supercooled liquid state by vibrational loading, Acta Mater. 65 (2014) 400–411.
[209] J. Schroers, C. Veazey, W.L. Johnson, Amorphous metallic foam, Appl. Phys. Lett. 82 (2003) 370–372.
[210] A.H. Brothers, D.C. Dunand, Ductile bulk metallic glass foams, Adv. Mater. 17 (2005) 484–486.
[211] S.Y. Kim, E.S. Park, R.T. Ott, T.A. Lograsso, M.Y. Huh, D.H. Kim, et al., Imprinting bulk amorphous alloy at room temperature, Sci. Rep. 5 (2015) 16540.
[212] F. Luo, F. Sun, K. Li, F. Gong, X. Liang, X. Wu, et al., Ultrasonic assisted micro-shear punching of amorphous alloy, Mater. Res. Lett. 6 (2018) 545–551.
[213] H. Li, Y. Yan, F. Sun, K. Li, J. Ma, Shear punching of amorphous alloys under high-frequency vibrations, Metals 9 (2019) 1158.
[214] F. Sun, B. Wang, F. Luo, Y.Q. Yan, H.B. Ke, J. Ma, et al., Shear punching of bulk metallic glasses under low stress, Mater. Des. 190 (2020) 108595.
[215] X. Li, X. Liang, Z. Zhang, J. Ma, J. Shen, Cold joining to fabricate large size metallic glasses by the ultrasonic vibrations, Scripta Mater. 185 (2020) 100–104.
[216] X. Liang, X. Zhu, X. Li, R. Mo, Y. Liu, K. Wu, et al., High-entropy alloy and amorphous alloy composites fabricated by ultrasonic vibrations, Sci. China Phys. Mech. Astron. 63 (2020) 116111.
[217] S. Sohrabi, M.X. Li, H.Y. Bai, J. Ma, W.H. Wang, A.L. Greer, Energy storage oscillation of metallic glass induced by high-intensity elastic stimulation, Appl. Phys. Lett. 116 (2020) 81901.
[218] J. Ma, X. Liang, X. Wu, Z. Liu, F. Gong, Sub-second thermoplastic forming of bulk metallic glasses by ultrasonic beating, Sci. Rep. 5 (2015) 17844.
[219] D.P. Yu, G.S. Hong, Y.S. Wong, Profile error compensation in fast tool servo diamond turning of micro-structured surfaces, Int. J. Mach. Tool Manufact. 52 (2012) 13–23.
[220] Y. Yang, Y. Pan, P. Guo, Structural coloration of metallic surfaces with micro/nano-structures induced by elliptical vibration texturing, Appl. Surf. Sci. 402 (2017) 400–409.
[221] M. Bakkal, A.J. Shih, R.O. Scattergood, C.T. Liu, Machining of a Zr-Ti-Al-Cu-Ni metallic glass, Scripta Mater. 50 (2004) 583–588.
[222] X. Chen, J. Xiao, Y. Zhu, R. Tian, X. Shu, J. Xu, Micro-machinability of bulk metallic glass in ultra-precision cutting, Mater. Des. 136 (2017) 1–12.
[223] N.K. Maroju, D.P. Yan, B. Xie, X. Jin, Investigations on surface microstructure in high-speed milling of Zr-based bulk metallic glass, J. Manuf. Process. 35 (2018) 40–50.
[224] D.X. Han, G. Wang, J. Li, K.C. Chan, S. To, F.F. Wu, et al., Cutting characteristics of Zr-based bulk metallic glass, J. Mater. Sci. Technol. 31 (2015) 153–158.
[225] M.Q. Jiang, L.H. Dai, Formation mechanism of lamellar chips during machining of bulk metallic glass, Acta Mater. 57 (2009) 2730–2738.
[226] Y. Zhao, J. Lu, Y. Zhang, F. Wu, D. Huo, Development of an analytical model based on Mohr-Coulomb criterion for cutting of metallic glasses, Int. J. Mech. Sci. 106 (2016) 168–175.
[227] C.D. Wu, R.H. Fang, J.K. Su, Nanometric mechanical cutting of metallic glass investigated using atomistic simulation, Appl. Surf. Sci. 396 (2017) 319–326.
[228] Z. Zhu, X. Zhou, Q. Liu, J. Lin, S. Zhao, Fabrication of micro-structured surfaces on bulk metallic glasses based on fast tool servo assisted diamond turning, Sci. Adv. Mater. 4 (2012) 906–911.
[229] R. Kobayashi, S. Xu, K. Shimada, M. Mizutani, T. Kuriyagawa, Defining the effects of cutting parameters on burr formation and minimization in ultra-precision grooving of amorphous alloy, Precis. Eng. 49 (2017) 115–121.
[230] S. Kuriakose, P.K. Patowari, J. Bhatt, Machinability study of Zr-Cu-Ti metallic glass by micro hole drilling using micro-USM, J. Mater. Process. Technol. 240 (2017) 42–51.
[231] N.K. Maroju, X. Jin, Vibration-assisted dimple generation on bulk metallic glass, Procedia Manuf. 26 (2018) 317–328.
[232] S.S. Park, Y. Wei, X.L. Jin, Direct laser assisted machining with a sapphire tool for bulk metallic glass, CIRP Ann. 67 (2018) 193–196.
[233] A. Pendurthi, S. Movafaghi, W. Wang, S. Shadman, A.P. Yalin, A.K. Kota, Fabrication of nanostructured omniphobic and superomniphobic surfaces with inexpensive CO_2 laser engraver, ACS Appl. Mater. Interfaces 9 (2017) 25656–25661.
[234] E. Williams, N. Lavery, Laser processing of bulk metallic glass: a review, J. Mater. Process. Technol. 247 (2017) 73–91.
[235] F.X. Ma, J.J. Yang, X.N. Zhu, C.Y. Liang, H.S. Wang, Femtosecond laser-induced concentric ring microstructures on Zr-based metallic glass, Appl. Surf. Sci. 256 (2010) 3653–3660.
[236] Y. Liu, M.Q. Jiang, G.W. Yang, Y.J. Guan, L.H. Dai, Surface rippling on bulk metallic glass under nanosecond pulse laser ablation, Appl. Phys. Lett. 99 (2011) 191902.
[237] Y. Zhu, J. Fu, C. Zheng, Z. Ji, Effect of nanosecond pulse laser ablation on the surface morphology of Zr-based metallic glass, Opt. Laser Technol. 83 (2016) 21–27.
[238] Y. Liu, M.Q. Jiang, G.W. Yang, J.H. Chen, Y.J. Guan, L.H. Dai, Saffman-Taylor fingering in nanosecond pulse laser ablating bulk metallic glass in water, Intermetallics 31 (2012) 325–329.
[239] M.Q. Jiang, Y.P. Wei, G. Wilde, L.H. Dai, Explosive boiling of a metallic glass superheated by nanosecond pulse laser ablation, Appl. Phys. Lett. 106 (2015), 021904.
[240] H. Huang, J. Noguchi, J. Yan, Shield gas induced cracks during nanosecond-pulsed laser irradiation of Zr-based metallic glass, Appl. Phys. A 122 (2016) 881.
[241] R. Yamada, N. Nomura, J. Saida, A. Kawasaki, Fabrication of optical gratings through surface patterning of zirconium-based metallic glass by laser irradiation, Intermetallics 93 (2018) 377–382.
[242] J. Fornell, E. Pellicer, E. Garcia-Lecina, D. Nieto, S. Surinach, M.D. Baró, et al., Structural and mechanical modifications induced on $Cu_{47.5}Zr_{47.5}Al_5$ metallic glass by surface laser treatments, Appl. Surf. Sci. 290 (2014) 188–193.
[243] H. Huang, N. Jun, M. Jiang, M. Ryoko, J. Yan, Nanosecond pulsed laser irradiation induced hierarchical micro/nanostructures on Zr-based metallic glass substrate, Mater. Des. 109 (2016) 153–161.
[244] H. Huang, J. Yan, Surface patterning of Zr-based metallic glass by laser irradiation induced selective thermoplastic extrusion in nitrogen gas, J. Micromech. Microeng. 27 (2017), 075007.
[245] Y. Yang, J.C. Ye, J. Lu, F.X. Liu, P.K. Liaw, Effects of specimen geometry and base material on the mechanical behavior of focused-ion-beam-fabricated metallic-glass micropillars, Acta Mater. 57 (2009) 1613–1623.
[246] P.C. Vella, S.S. Dimov, E. Brousseau, B.R. Whiteside, A new process chain for producing bulk metallic glass replication masters with micro- and nano-scale features, Int. J. Adv. Manuf. Technol. 76 (2014) 523–543.
[247] P.H. Loc, F.J. Shiou, Abrasive water jet polishing on Zr-based bulk metallic glass, Adv. Mater. Res. 579 (2012) 211–218.
[248] F.J. Shiou, P.H. Loc, N.H. Dang, Surface finish of bulk metallic glass using sequential abrasive jet polishing and annealing processes, Int. J. Adv. Manuf. Technol. 66 (2013) 1523–1533.
[249] W. Xu, J. Song, J. Sun, Y. Lu, Z. Yu, Rapid fabrication of large-area, corrosion-resistant superhydrophobic Mg alloy surfaces, ACS Appl. Mater. Interfaces 3 (2011) 4404–4414.
[250] S.H. Yeo, P.C. Tan, E. Aligiri, S.B. Tor, N.H. Loh, Processing of zirconium-based bulk metallic glass (BMG) using micro electrical discharge machining (Micro-EDM), Mater. Manuf. Process. 24 (2009) 1242–1248.
[251] Z. Huang, X. Liang, C. Chang, J. Ma, WEDM-LS processing sophisticated and durable Zr-based metallic glass mold insert for micro structure injection of polymers, Biomed. Microdevices 21 (2019) 13.
[252] X.H. Chen, X.C. Zhang, Y. Zhang, G.L. Chen, Fabrication and characterization of metallic glasses with a specific microstructure for micro-electro-mechanical system applications, J. Non-Cryst. Solids 354 (2008) 3308–3316.
[253] H. Huang, J. Yan, On the surface characteristics of a Zr-based bulk metallic glass processed by microelectrical discharge machining, Appl. Surf. Sci. 355 (2015) 1306–1315.
[254] C. Liu, N. Duong, M.P. Jahan, J. Ma, R. Kirwin, Experimental investigation and numerical simulation of micro-EDM of bulk metallic glass with focus on crater sizes, Procedia Manuf. 34 (2019) 275–286.
[255] B. Xu, X. Wu, J. Ma, X. Liang, J. Lei, B. Wu, et al., Micro-electrical discharge machining of 3D micro-molds from $Pd_{40}Cu_{30}P_{20}Ni_{10}$ metallic glass by using laminated 3D micro-electrodes, J. Micromech. Microeng. 26 (2016), 035004.
[256] L. Zhang, H. Huang, Micro machining of bulk metallic glasses: a review, Int. J. Adv. Manuf. Technol. 100 (2019) 637–661.
[257] S.F. Hsieh, S.L. Chen, M.H. Lin, S.F. Ou, W.T. Lin, M.S. Huang, Crystallization and carbonization of an electrical discharge machined Zr-based bulk metallic glass alloy, J. Mater. Res. 28 (2013) 3177–3184.
[258] H. Huang, J. Yan, Microstructural changes of Zr-based metallic glass during micro-electrical discharge machining and grinding by a sintered diamond tool, J. Alloys Compd. 688 (2016) 14–21.
[259] S. Horn, S. Oswald, M. Stoica, M. Uhlemann, A. Gebert, Complex micro-shaping of bulk metallic glass surfaces by electrochemical means, J. Mater. Res. 30 (2015) 3493–3501.

[260] L. Meng, Y. Zeng, D. Zhu, Wire electrochemical micromachining of Ni-based metallic glass using bipolar nanosecond pulses, Int. J. Mach. Tool Manufact. 146 (2019) 103439.
[261] H.Y. Erbil, A.L. Demirel, Y. Avci, O. Mert, Transformation of a simple plastic into a superhydrophobic surface, Science 299 (2003) 1377−1380.
[262] T Il Kim, D. Tahk, H.H. Lee, Wettability-controllable super water- and moderately oil-repellent surface fabricated by wet chemical etching, Langmuir 25 (2009) 6576−6579.
[263] N. Kawasegi, N. Morita, S. Yamada, N. Takano, T. Oyama, K. Ashida, et al., Rapid nanopatterning of a Zr-based metallic glass surface utilizing focused ion beam induced selective etching, Appl. Phys. Lett. 89 (2006) 143113−143115.
[264] K. Zhao, K.S. Liu, J.F. Li, W.H. Wang, L. Jiang, Superamphiphobic CaLi-based bulk metallic glasses, Scripta Mater. 60 (2009) 225−227.
[265] K. Liu, Z. Li, W. Wang, L. Jiang, Facile creation of bio-inspired superhydrophobic Ce-based metallic glass surfaces, Appl. Phys. Lett. 99 (2011) 261905.
[266] H.F. Li, Y.B. Wang, Y. Cheng, Y.F. Zheng, Surface modification of $Ca_{60}Mg_{15}Zn_{2}5$ bulk metallic glass for slowing down its biodegradation rate in water solution, Mater. Lett. 64 (2010) 1462−1464.
[267] S. Xiao, H. Zhang, S. Guo, Fabrication of a Zr-based bulk metallic glass surface with extreme wettability, J. Non-Cryst. Solids 536 (2020) 120001.
[268] K.I. Katsumata, T. Wada, A. Inoue, M. Sakai, A. Nakajima, A. Fujishima, et al., Control of wetting on Ti-based bulk metallic glass surfaces by a hydrothermal method, J. Mater. Sci. 46 (2011) 3430−3435.
[269] S. Wang, N. Li, L. Liu, Enhanced hydrogen generation performance of Pd-based micro/nano hierarchical porous structure, Mater. Lett. 228 (2018) 443−446.
[270] A. Yao, H. Yang, J.Q. Wang, W. Xu, J. Huo, R.W. Li, et al., Flexible supercapacitor electrodes fabricated by dealloying nanocrystallized Al-Ni-Co-Y-Cu metallic glasses, J. Alloys Compd. 772 (2019) 164−172.
[271] J. Jayaraj, B.J. Park, D.H. Kim, W.T. Kim, E. Fleury, Nanometer-sized porous Ti-based metallic glass, Scripta Mater. 55 (2006) 1063−1066.
[272] L. Battezzati, F. Scaglione, De-alloying of rapidly solidified amorphous and crystalline alloys, J. Alloys Compd. 509 (2011) S8−S12.
[273] K. Zhu, Z. Yang, X. Zhang, S. Yang, Y. Zeng, J. Jiang, Nanoporous Pd with tunable pore size prepared by dealloying $Pd_{30}Cu_{40}Ni_{10}P_{20}$ metallic glass and their catalytic performance, Mater. Res. 22 (2019).
[274] G. Doubek, R.C. Sekol, J. Li, W.H. Ryu, F.S. Gittleson, S. Nejati, et al., Guided evolution of bulk metallic glass nanostructures: a platform for designing 3D electrocatalytic surfaces, Adv. Mater. 28 (2016) 1940−1949.
[275] S. Shi, J. Markmann, J. Weissmüller, Synthesis of uniform bulk nanoporous palladium with tunable structure, Electrochim. Acta 285 (2018) 60−69.
[276] L. Mihaylov, A. Inoue, L. Lyubenova, D. Nihtianova, T. Spassov, Nanoporous metallic structures by de-alloying bulk glass forming Zr-based alloys, Intermetallics 98 (2018) 148−153.
[277] S. Mukherjee, M. Carmo, G. Kumar, R.C. Sekol, A.D. Taylor, J. Schroers, Palladium nanostructures from multi-component metallic glass, Electrochim. Acta 74 (2012) 145−150.
[278] S. Mukherjee, R.C. Sekol, M. Carmo, E.I. Altman, A.D. Taylor, J. Schroers, Tunable hierarchical metallic-glass nanostructures, Adv. Funct. Mater. 23 (2013) 2708−2713.
[279] H.S. Arora, Q. Xu, Z. Xia, Y.H. Ho, N.B. Dahotre, J. Schroers, et al., Wettability of nanotextured metallic glass surfaces, Scripta Mater. 69 (2013) 732−735.
[280] J Mater Res N. Chen, D. Wang, T. Feng, R. Kruk, K.F. Yao, D.V. Louzguine-Luzgin, et al., A nanoglass alloying immiscible Fe and Cu at the nanoscale, Nanoscale 7 (2015) 6607−6611.
[281] N. Chen, R. Frank, N. Asao, D.V. Louzguine-Luzgin, P. Sharma, J.Q. Wang, et al., Formation and properties of Au-based nanograined metallic glasses, Acta Mater. 59 (2011) 6433−6440.
[282] M.W. Glasscott, A.D. Pendergast, S. Goines, A.R. Bishop, A.T. Hoang, C. Renault, et al., Electrosynthesis of high-entropy metallic glass nanoparticles for designer, multi-functional electrocatalysis, Nat. Commun. 10 (2019) 1−8.
[283] N. Chen, D.V. Louzguine-Luzgin, K. Yao, A new class of non-crystalline materials: nanogranular metallic glasses, J. Alloys Compd. 707 (2017) 371−378.
[284] K.S. Nakayama, Y. Yokoyama, T. Wada, N. Chen, A. Inoue, Formation of metallic glass nanowires by gas atomization, Nano Lett. 12 (2012) 2404−2407.
[285] J. Yi, X.X. Xia, D.Q. Zhao, M.X. Pan, H.Y. Bai, W.H. Wang, Micro-and nanoscale metallic glassy fibers, Adv. Eng. Mater. 12 (2010) 1117−1122.
[286] D.W. Ding, J. Yi, G.L. Liu, Y.T. Sun, D.Q. Zhao, M.X. Pan, et al., The equipment for the preparation of micro and nanoscale metallic glassy fibers, Rev. Sci. Instrum. 85 (2014) 103907.
[287] C. Yang, C. Zhang, W. Xing, L. Liu, 3D printing of Zr-based bulk metallic glasses with complex geometries and enhanced catalytic properties, Intermetallics 94 (2018) 22−28.
[288] C. Zhang, X.M. Li, S.Q. Liu, H. Liu, L.J. Yu, L. Liu, 3D printing of Zr-based bulk metallic glasses and components for potential biomedical applications, J. Alloys Compd. 790 (2019) 963−973.
[289] D. Ouyang, N. Li, W. Xing, J. Zhang, L. Liu, 3D printing of crack-free high strength Zr-based bulk metallic glass composite by selective laser melting, Intermetallics 90 (2017) 128−134.
[290] N. Li, J. Zhang, W. Xing, D. Ouyang, L. Liu, 3D printing of Fe-based bulk metallic glass composites with combined high strength and fracture toughness, Mater. Des. 143 (2018) 285−296.
[291] J. Li, J. Fu, Y. Cong, Y. Wu, L. Xue, Y. Han, Macroporous fluoropolymeric films templated by silica colloidal assembly: a possible route to superhydrophobic surfaces, Appl. Surf. Sci. 252 (2006) 2229−2234.
[292] K. Askar, B.M. Phillips, Y. Fang, B. Choi, N. Gozubenli, P. Jiang, et al., Self-assembled self-cleaning broadband anti-reflection coatings, Colloids Surf. A Physicochem. Eng. Asp. 439 (2013) 84−100.
[293] Q. Wen, Z. Guo, Recent advances in the fabrication of superhydrophobic surfaces, Chem. Lett. 45 (2016) 1134−1149.
[294] D.J. Magagnosc, R. Ehrbar, G. Kumar, M.R. He, J. Schroers, D.S. Gianola, Tunable tensile ductility in metallic glasses, Sci. Rep. 3 (2013) 1096.
[295] M. Gopinadhan, Z. Shao, Y. Liu, S. Mukherjee, R.C. Sekol, G. Kumar, et al., Finite size effects in the crystallization of a bulk metallic glass, Appl. Phys. Lett. 103 (2013) 111912.
[296] X. Zhang, F. Shi, J. Niu, Y. Jiang, Z. Wang, Superhydrophobic surfaces: from structural control to functional application, J. Mater. Chem. 18 (2008) 621−633.
[297] S. Ghaffari, M. Aliofkhazraei, G.B. Darband, A. Zakeri, E. Ahmadi, Review of superoleophobic surfaces: evaluation, fabrication methods, and industrial applications, Surf. Interfaces 17 (2019) 100340.
[298] N. Valipour Motlagh, R. Khani, S. Rahnama, Super dewetting surfaces: focusing on their design and fabrication methods, Colloids Surf. A Physicochem. Eng. Asp. 484 (2015) 528−546.
[299] Y.C. Jung, B. Bhushan, Wetting transition of water droplets on superhydrophobic patterned surfaces, Scripta Mater. 57 (2007) 1057−1060.
[300] N.A. Patankar, Consolidation of hydrophobic transition criteria by using an approximate energy minimization approach, Langmuir 26 (2010) 8941−8945.
[301] J. de Ruiter, F. Mugele, D. van den Ende, Air cushioning in droplet impact. I. Dynamics of thin films studied by dual wavelength reflection interference microscopy, Phys. Fluids 27 (2015), 012104.
[302] Y.B. Wang, H.F. Li, Y.F. Zheng, S.C. Wei, M. Li, Correlation between corrosion performance and surface wettability in ZrTiCuNiBe bulk metallic glasses, Appl. Phys. Lett. 96 (2010) 251909.
[303] S. Sohn, Y. Jung, Y. Xie, C. Osuji, J. Schroers, J.J. Cha, Nanoscale size effects in crystallization of metallic glass nanorods, Nat. Commun. 6 (2015) 1−6.
[304] S. Sohn, Y. Xie, Y. Jung, J. Schroers, J.J. Cha, Tailoring crystallization phases in metallic glass nanorods via nucleus starvation, Nat. Commun. 8 (2017) 1−8.
[305] Y.F. Wang, H.Y. Li, L. Yang, Radiation-induced structural evolution in $Zr_{2}Cu$ metallic glass, J. Mater. Sci. 53 (2018) 10979−10986.
[306] S. Cheng, C. Wang, M. Ma, D. Shan, B. Guo, Mechanism for microstructural evolution induced by high temperature deformation in Zr-based bulk metallic glasses, J. Alloys Compd. 676 (2016) 299−304.
[307] J.C. Qiao, J.M. Pelletier, Dynamic mechanical relaxation in bulk metallic glasses: a review, J. Mater. Sci. Technol. 30 (2014) 523−545.
[308] Z. Liu, Y. Yang, J. Lu, G. Wang, P.K. Liaw, C.T. Liu, Stress induced atomic-scale damage and relaxation in bulk metallic glasses, J. Alloys Compd. 652 (2015) 185−190.
[309] Y. Zhang, W.H. Wang, A.L. Greer, Making metallic glasses plastic by control of residual stress, Nat. Mater. 5 (2006) 857−860.
[310] J. Pan, Y.X. Wang, Q. Guo, D. Zhang, A.L. Greer, Y. Li, Extreme rejuvenation and softening in a bulk metallic glass, Nat. Commun. 9 (2018) 1−9.
[311] M. Wakeda, J. Saida, J. Li, S. Ogata, Controlled rejuvenation of amorphous metals with thermal processing, Sci. Rep. 5 (2015) 10545.
[312] J. Saida, R. Yamada, M. Wakeda, S. Ogata, Thermal rejuvenation in metallic glasses, Sci. Technol. Adv. Mater. 18 (2017) 152−162.
[313] M. Liu, H.Y. Jiang, X.Z. Liu, L. Gu, Y.H. Sun, W.H. Wang, et al., Energy state and properties controlling of metallic glasses by surface rejuvenation, Intermetallics 112 (2019) 106549.
[314] L. Zhao, K.C. Chan, S.H. Chen, S.D. Feng, D.X. Han, G. Wang, Tunable tensile ductility of metallic glasses with partially rejuvenated amorphous structures, Acta Mater. 169 (2019) 122−134.
[315] Q.K. Jiang, P. Liu, Q.P. Cao, C. Wang, X.L. Li, X.Y. Gao, et al., The effect of size on the elastic strain limit in Ni60Nb40 glassy films, Acta Mater. 61 (2013) 4689−4695.
[316] Y. Fu, Q.P. Cao, S.Y. Liu, C. Wang, X.D. Wang, D.X. Zhang, et al., Anomalous deformation mode transition in amorphous Mg-Zn-Ca thin films, Scripta Mater. 149 (2018) 139−143.
[317] C. Wang, Q.P. Cao, T. Feng, X.D. Wang, D.X. Zhang, S.X. Qu, et al., Indentation size effects of mechanical behavior and shear transformation zone in thin film metallic glasses, Thin Solid Films 646 (2018) 36−43.
[318] Y. Shi, Size-independent shear band formation in amorphous nanowires made from simulated casting, Appl. Phys. Lett. 96 (2010) 121909.
[319] D. Şopu, A. Foroughi, M. Stoica, J. Eckert, Brittle-to-ductile transition in metallic glass nanowires, Nano Lett. 16 (2016) 4467−4471.
[320] J. Yi, W.H. Wang, J.J. Lewandowski, Sample size and preparation effects on the tensile ductility of Pd-based metallic glass nanowires, Acta Mater. 87 (2015) 1−7.
[321] K.S. Nakayama, Y. Yokoyama, G. Xie, Q.S. Zhang, M.W. Chen, T. Sakurai, et al., Metallic glass nanowire, Nano Lett. 8 (2008) 516−519.
[322] S. Mridha, H.S. Arora, J. Lefebvre, S. Bhowmick, S. Mukherjee, High temperature in situ compression of thermoplastically formed nano-scale metallic glass, JOM (J. Occup. Med.) 69 (2017) 39−44.

[323] K.S. Nakayama, Y. Yokoyama, T. Ono, M.W. Chen, K. Akiyama, T. Sakurai, et al., Controlled formation and mechanical characterization of metallic glassy nanowires, Adv. Mater. 22 (2010) 872–875.
[324] C.A. Volkert, A. Donohue, F. Spaepen, Effect of sample size on deformation in amorphous metals, J. Appl. Phys. 103 (2008) 83539.
[325] C.J. Lee, J.C. Huang, T.G. Nieh, Sample size effect and microcompression of $Mg_{65}Cu_{25}Gd_{10}$ metallic glass, Appl. Phys. Lett. 91 (2007) 161913.
[326] A. Donohue, F. Spaepen, R.G. Hoagland, A. Misra, Suppression of the shear band instability during plastic flow of nanometer-scale confined metallic glasses, Appl. Phys. Lett. 91 (2007) 241905.
[327] Y.B. Wang, C.C. Lee, J. Yi, X.H. An, M.X. Pan, K.Y. Xie, et al., Ultrahigh-strength submicron-sized metallic glass wires, Scripta Mater. 84–85 (2014) 27–30.
[328] W.H. Wang, Dynamic relaxations and relaxation-property relationships in metallic glasses, Prog. Mater. Sci. 106 (2019) 100561.
[329] Q. Zhang, Q.-K. Li, M. Li, Chemical segregation in metallic glass nanowires, J. Chem. Phys. 141 (2014) 194701.
[330] P. Zhang, J.J. Maldonis, Z. Liu, J. Schroers, P.M. Voyles, Spatially heterogeneous dynamics in a metallic glass forming liquid imaged by electron correlation microscopy, Nat. Commun. 9 (2018) 1–7.
[331] Q. Zhang, Q.-K. Li, M. Li, Processing dependence of mechanical properties of metallic glass nanowires, Appl. Phys. Lett. 106 (2015) 71905.
[332] D.J. Magagnosc, G. Kumar, J. Schroers, P. Felfer, J.M. Cairney, D.S. Gianola, Effect of ion irradiation on tensile ductility, strength and fictive temperature in metallic glass nanowires, Acta Mater. 74 (2014) 165–182.
[333] R. Liontas, X.W. Gu, E. Fu, Y. Wang, N. Li, N. Mara, et al., Effects of helium implantation on the tensile properties and microstructure of $Ni_{73}P_{27}$ metallic glass nanostructures, Nano Lett. 14 (2014) 5176–5183.
[334] R. Raghavan, K. Boopathy, R. Ghisleni, M.A. Pouchon, U. Ramamurty, J. Michler, Ion irradiation enhances the mechanical performance of metallic glasses, Scripta Mater. 62 (2010) 462–465.
[335] Q. Xiao, L. Huang, Y. Shi, Suppression of shear banding in amorphous ZrCuAl nanopillars by irradiation, J. Appl. Phys. 113 (2013) 83514.
[336] M.L. Rahaman, L. Zhang, M. Liu, W. Liu, Surface roughness effect on the friction and wear of bulk metallic glasses, Wear 332 (2015) 1231–1237.
[337] A.A. Burkov, P.G. Chigrin, Effect of tungsten, molybdenum, nickel and cobalt on the corrosion and wear performance of Fe-based metallic glass coatings, Surf. Coating. Technol. 351 (2018) 68–77.
[338] N. Hua, W. Chen, W. Wang, H. Lu, X. Ye, G. Li, et al., Tribological behavior of a Ni-free Zr-based bulk metallic glass with potential for biomedical applications, Mater. Sci. Eng. C 66 (2016) 268–277.
[339] Y. Liu, S. Pang, W. Yang, N. Hua, P.K. Liaw, T. Zhang, Tribological behaviors of a Ni-free Ti-based bulk metallic glass in air and a simulated physiological environment, J. Alloys Compd. 766 (2018) 1030–1036.
[340] Z. Liao, N. Hua, W. Chen, Y. Huang, T. Zhang, Correlations between the wear resistance and properties of bulk metallic glasses, Intermetallics 93 (2018) 290–298.
[341] M.L. Rahaman, L. Zhang, Size effect on friction and wear mechanisms of bulk metallic glass, Wear 376 (2017) 1522–1527.
[342] O.E. Dagdeviren, Nanotribological properties of bulk metallic glasses, Appl. Surf. Sci. 458 (2018) 344–349.
[343] C.T. Pan, T.T. Wu, C.F. Liu, C.Y. Su, W.J. Wang, J.C. Huang, Study of scratching Mg-based BMG using nanoindenter with Berkovich probe, Mater. Sci. Eng., A 527 (2010) 2342–2349.
[344] Q. Zhou, Y. Du, Y. Ren, W. Kuang, W. Han, H. Wang, et al., Investigation into nanoscratching mechanical performance of metallic glass multilayers with improved nano-tribological properties, J. Alloys Compd. 776 (2019) 447–459.
[345] B. Prakash, Abrasive wear behaviour of Fe, Co and Ni based metallic glasses, Wear 258 (2005) 217–224.
[346] M. Zhang, D. Yao, Z. Cao, P. Li, P. Zhou, X. Wang, Influence of oxidation on the performance of $Zr_{55}Cu_{30}Al_{10}Ni_5$ BMG, Intermetallics 79 (2016) 20–27.
[347] D. Guo, X. Chen, C. Zhang, X. Wu, Z. Liu, K. Li, et al., Nanoscale tunable reduction of interfacial friction on nano-patterned wear-resistant bulk metallic glass, Appl. Surf. Sci. 453 (2018) 297–308.
[348] H. Ida, M. Seiryu, N. Takeshita, M. Iwasaki, Y. Yokoyama, Y. Tsutsumi, et al., Biosafety, stability, and osteogenic activity of novel implants made of $Zr_{70}Ni_{16}Cu_6Al_8$ bulk metallic glass for biomedical application, Acta Biomater. 74 (2018) 505–517.
[349] W.H. Jiang, F. Jiang, B.A. Green, F.X. Liu, P.K. Liaw, H. Choo, et al., Electrochemical corrosion behavior of a Zr-based bulk-metallic glass, Appl. Phys. Lett. 91 (2007) 41904.
[350] M. Apreutesei, C. Boissy, N. Mary, M. Arab Pour Yazdi, A. Billard, P. Steyer, Binary Zr-Ni/Co metallic glass films: role of the structural state on their durability, Acta Mater. 89 (2015) 305–314.
[351] S. González, E. Pellicer, S. Suriñach, M.D. Baró, J. Sort, Mechanical and corrosion behaviour of as-cast and annealed $Zr_{60}Cu_{20}Al_{10}Fe_5Ti_5$ bulk metallic glass, Intermetallics 28 (2012) 149–155.
[352] M. Zhou, K. Hagos, H. Huang, M. Yang, L. Ma, Improved mechanical properties and pitting corrosion resistance of $Zr_{65}Cu_{17.5}Fe_{10}Al_{7.5}$ bulk metallic glass by isothermal annealing, J. Non-Cryst. Solids 452 (2016) 50–56.
[353] D.D. Liang, X.S. Wei, T.C. Ma, B. Chen, H.R. Jiang, Y. Dong, et al., Sliding tribocorrosion behavior of Fe-based bulk metallic glass under corrosive environments, J. Non-Cryst. Solids 510 (2019) 62–70.
[354] N. Espallargas, R.E. Aune, C. Torres, N. Papageorgiou, A.I. Muñoz, Bulk metallic glasses (BMG) for biomedical applications-A tribocorrosion investigation of $Zr_{55}Cu_{30}Ni_5Al_{10}$ in simulated body fluid, Wear 301 (2013) 271–279.
[355] G.H. Zhao, R.E. Aune, H. Mao, N. Espallargas, Degradation of Zr-based bulk metallic glasses used in load-bearing implants: a tribocorrosion appraisal, J. Mech. Behav. Biomed. Mater. 60 (2016) 56–67.
[356] J. Schroers, G. Kumar, Bulk metallic glass in micro to nano length scale Applications, Nano-Micro Interface Bridg Micro Nano Worlds Second Ed 1–2 (2015) 159–188.
[357] J. Schroers, Q. Pham, A. Desai, Thermoplastic forming of bulk metallic glass—a technology for MEMS and microstructure fabrication, J. Microelectromech. Syst. 16 (2007) 240–247.
[358] F. Wang, H. Zhang, X. Liang, F. Gong, J. Ma, Fabrication of metallic glass micro grooves by thermoplastic forming, J. Micromech. Microeng. 27 (2016) 25009.
[359] S.H. Chen, H.Y. Cheng, K.C. Chan, G. Wang, Metallic glass structures for mechanical-energy-dissipation purpose: a review, Metals 8 (2018) 689.
[360] E.R. Homer, M.B. Harris, S.A. Zirbel, J.A. Kolodziejska, H. Kozachkov, B.P. Trease, et al., New methods for developing and manufacturing compliant mechanisms utilizing bulk metallic glass, Adv. Eng. Mater. 16 (2014) 850–856.
[361] Y. Zhao, Stiction and anti-stiction in MEMS and NEMS, Acta Mech. Sin. Xuebao 19 (2003) 1–10.
[362] Z. Zhan, M. Elkabbash, J.L. Cheng, J. Zhang, S. Singh, C. Guo, Highly floatable superhydrophobic metallic assembly for aquatic applications, ACS Appl. Mater. Interfaces 11 (2019) 48512–48517.
[363] P. Sharma, N. Kaushik, H. Kimura, Y. Saotome, A. Inoue, Nano-fabrication with metallic glass—an exotic material for nano-electromechanical systems, Nanotechnology 18 (2007) 35302.
[364] S. Hata, K. Sato, A. Shimokohbe, Fabrication of thin film metallic glass and its application to microactuators, in: Device Process Technol. MEMS Microelectron., vol. 3892, 1999, pp. 97–108.
[365] Y.C. Lin, Y.C. Tsai, T. Ono, P. Liu, M. Esashi, T. Gessner, et al., Metallic glass as a mechanical material for microscanners, Adv. Funct. Mater. 25 (2015) 5677–5682.
[366] B.W. An, E.J. Gwak, K. Kim, Y.C. Kim, J. Jang, J.Y. Kim, et al., Stretchable, transparent electrodes as wearable heaters using nanotrough networks of metallic glasses with superior mechanical properties and thermal stability, Nano Lett. 16 (2016) 471–478.
[367] S.H. Chen, K.C. Chan, T.M. Yue, F.F. Wu, Highly stretchable kirigami metallic glass structures with ultra-small strain energy loss, Scripta Mater. 142 (2018) 83–87.
[368] L. Zheng, X. Su, X. Lai, W. Chen, H. Li, X. Zeng, Conductive superhydrophobic cotton fabrics via layer-by-layer assembly of carbon nanotubes for oil-water separation and human motion detection, Mater. Lett. 253 (2019) 230–233.
[369] M.S. Dambatta, S. Izman, B. Yahaya, J.Y. Lim, D. Kurniawan, Mg-based bulk metallic glasses for biodegradable implant materials: a review on glass forming ability, mechanical properties, and biocompatibility, J. Non-Cryst. Solids 426 (2015) 110–115.
[370] N. Hua, L. Huang, W. Chen, W. He, T. Zhang, Biocompatible Ni-free Zr-based bulk metallic glasses with high-Zr-content: compositional optimization for potential biomedical applications, Mater. Sci. Eng. C 44 (2014) 400–410.
[371] M.M. Khan, A. Nemati, Z.U. Rahman, U.H. Shah, H. Asgar, W. Haider, Recent advancements in bulk metallic glasses and their applications: a review, Crit. Rev. Solid State Mater. Sci. 43 (2018) 233–268.
[372] W. He, A. Chuang, Z. Cao, P.K. Liaw, Biocompatibility study of zirconium-based bulk metallic glasses for orthopedic applications, Metall. Mater. Trans. A Phys. Metall. Mater. Sci. 41 (2010) 1726–1734.
[373] A. Sagasti, A.C. Lopes, A. Lasheras, V. Palomares, J. Carrizo, J. Gutierrez, et al., Corrosion resistant metallic glasses for biosensing applications, AIP Adv. 8 (2018) 47702.
[374] S. Moradi, N. Hadjesfandiari, S.F. Toosi, J.N. Kizhakkedathu, S.G. Hatzikiriakos, Effect of extreme wettability on platelet adhesion on metallic implants: from superhydrophilicity to superhydrophobicity, ACS Appl. Mater. Interfaces 8 (2016) 17631–17641.
[375] E.R. Kinser, J. Padmanabhan, R. Yu, S.L. Corona, J. Li, S. Vaddiraju, et al., Nanopatterned bulk metallic glass biosensors, ACS Sens. 2 (2017) 1779–1787.
[376] A wettability gradient as a tool to study protein adsorption and cell adhesion on polymer surfaces, J. Biomater. Sci. Polym. Ed. 4 (2008) 467–481.
[377] D.G. Castner, B.D. Ratner, Biomedical surface science: foundations to frontiers, Surf. Sci. 500 (2002) 28–60.
[378] M. Shayan, J. Padmanabhan, A.H. Morris, B. Cheung, R. Smith, J. Schroers, et al., Nanopatterned bulk metallic glass-based biomaterials modulate macrophage polarization, Acta Biomater. 75 (2018) 427–438.
[379] L. Huang, Z. Cao, H.M. Meyer, P.K. Liaw, E. Garlea, J.R. Dunlap, et al., Responses of bone-forming cells on pre-immersed Zr-based bulk metallic glasses: effects of composition and roughness, Acta Biomater. 7 (2011) 395–405.
[380] L. Huang, C. Pu, R.K. Fisher, D.J.H. Mountain, Y. Gao, P.K. Liaw, et al., A Zr-based bulk metallic glass for future stent applications: materials properties, finite element modeling, and in vitro human vascular cell response, Acta Biomater. 25 (2015) 356–368.
[381] S.T. R, A. B, B. S, Cytocompatibility assessment of Ti-Nb-Zr-Si thin film metallic glasses with enhanced osteoblast differentiation for biomedical applications, Colloids Surf. B Biointerfaces 173 (2019) 109–120.

[382] A.M. Loye, E.R. Kinser, S. Bensouda, M. Shayan, R. Davis, R. Wang, et al., Regulation of mesenchymal stem cell differentiation by nanopatterning of bulk metallic glass, Sci. Rep. 8 (2018) 1–11.
[383] J. Wang, A.M. Loye, J. Ketkaew, J. Schroers, T.R. Kyriakides, Hierarchical micro-and nanopatterning of metallic glass to engineer cellular responses, ACS Appl. Bio. Mater. 1 (2018) 51–58.
[384] P. Meagher, E.D. O'Cearbhaill, J.H. Byrne, D.J. Browne, Bulk metallic glasses for implantable medical devices and surgical tools, Adv. Mater. 28 (2016) 5755–5762.
[385] X. Liu, Y. Shao, Y. Tang, K.-F. Yao, Highly uniform and reproducible surface enhanced Raman scattering on air-stable metallic glassy nanowire array, Sci. Rep. 4 (2014) 5835.
[386] S. Yang, P.J. Hricko, P.H. Huang, S. Li, Y. Zhao, Y. Xie, et al., Superhydrophobic surface enhanced Raman scattering sensing using Janus particle arrays realized by site-specific electrochemical growth, J. Mater. Chem. C 2 (2014) 542–547.
[387] H.J. Tarigan, N. Kahler, N.S. Ramos, G. Kumar, A.A. Bernussi, Low reflectance of nano-patterned Pt-Cu-Ni-P bulk metallic glass, Appl. Phys. Lett. 107 (2015) 21903.
[388] C. Uzun, C. Meduri, N. Kahler, L.G. de Peralta, J.M. McCollum, M. Pantoya, et al., Photoinduced heat conversion enhancement of metallic glass nanowire arrays, J. Appl. Phys. 125 (2019) 15102.
[389] L.L. Baranowski, G.J. Snyder, E.S. Toberer, Concentrated solar thermoelectric generators, Energy Environ. Sci. 5 (2012) 9055–9067.
[390] S.J. Kim, S.Y. Kim, J.M. Park, J.N. Heo, J.H. Lee, S.M. Lee, et al., Exploiting metallic glasses for 19.6% efficient back contact solar cell, Appl. Phys. Lett. 101 (2012) 64106.
[391] W. Diyatmika, L. Xue, T.-N. Lin, C. Chang, J.P. Chu, Thin film metallic glass as a diffusion barrier for copper indium gallium selenide solar cell on stainless steel substrate: a feasibility study, Jpn. J. Appl. Phys. 55 (2016) 80303.
[392] S.M. Kang, N. Ahn, J.-W. Lee, M. Choi, N.-G. Park, Water-repellent perovskite solar cell, J. Mater. Chem. 2 (2014) 20017–20021.
[393] J. Zhi, L.Z. Zhang, Durable superhydrophobic surface with highly antireflective and self-cleaning properties for the glass covers of solar cells, Appl. Surf. Sci. 454 (2018) 239–248.
[394] M. Carmo, R.C. Sekol, S. Ding, G. Kumar, J. Schroers, A.D. Taylor, Bulk metallic glass nanowire architecture for electrochemical applications, ACS Nano 5 (2011) 2979–2983.
[395] K. Ren, J. Zhou, H. Wu, Materials for microfluidic chip fabrication, Acc. Chem. Res. 46 (2013) 2396–2406.
[396] E.K. Sackmann, A.L. Fulton, D.J. Beebe, The present and future role of microfluidics in biomedical research, Nature 507 (2014) 181–189.
[397] C. Wu, R. Chen, Y. Liu, Z. Yu, Y. Jiang, X. Cheng, A planar dielectrophoresis-based chip for high-throughput cell pairing, Lab Chip 17 (2017) 4008–4014.
[398] W.K. Tomazelli Coltro, C.M. Cheng, E. Carrilho, D.P. de Jesus, Recent advances in low-cost microfluidic platforms for diagnostic applications, Electrophoresis 35 (2014) 2309–2324.
[399] D. Loke, T.H. Lee, W.J. Wang, L.P. Shi, R. Zhao, Y.C. Yeo, et al., Breaking the speed limits of phase-change memory, Science 336 (2012) 1566–1569.
[400] F. Rao, W. Zhang, E. Ma, Catching structural transitions in liquids, Science 364 (2019) 1032–1033.
[401] F. Rao, K. Ding, Y. Zhou, Y. Zheng, M. Xia, S. Lv, et al., Reducing the stochasticity of crystal nucleation to enable subnanosecond memory writing, Science 358 (2017) 1423–1427.
[402] S. Ding, Y. Liu, Y. Li, Z. Liu, S. Sohn, F.J. Walker, et al., Combinatorial development of bulk metallic glasses, Nat. Mater. 13 (2014) 494–500.
[403] T.S. Wong, S.H. Kang, S.K.Y. Tang, E.J. Smythe, B.D. Hatton, A. Grinthal, et al., Bioinspired self-repairing slippery surfaces with pressure-stable omniphobicity, Nature 477 (2011) 443–447.
[404] T. Verho, J.T. Korhonen, L. Sainiemi, V. Jokinen, C. Bower, K. Franze, et al., Reversible switching between superhydrophobic states on a hierarchically structured surface, Proc. Natl. Acad. Sci. U.S.A. 109 (2012) 10210–10213.
[405] J. Ma, C. Yang, X. Liu, B. Shang, Q. He, F. Li, et al., Fast surface dynamics enabled cold joining of metallic glasses, Sci. Adv. 5 (2019), eaax7256.
[406] C. Yuan, Z. Lv, C. Pang, X. Li, R. Liu, C. Yang, et al., Ultrasonic-assisted plastic flow in a Zr-based metallic glass, Sci. China Mater. (2020) 1–12.
[407] X. Li, D. Wei, J.Y. Zhang, X.D. Liu, Z. Li, T.Y. Wang, et al., Ultrasonic plasticity of metallic glass near room temperature, Appl. Mater. Today 21 (2020) 100866.
[408] H. Zhao, F. Sun, X. Li, Y. Ding, Y.Q. Yan, X. Tong, et al., Ultrastability of metallic supercooled liquid induced by vibration, Scripta Mater. 194 (2021) 113606.
[409] Z.Y. Huang, J.N. Fu, X. Li, W.X. Wen, H.J. Lin, Y. Lou, et al., Ultrasonic-assisted rapid cold welding of bulk metallic glasses, Sci. China Mater. (2021) 1–8.
[410] M. Gao, D.P. Wang, Y.F. Huang, S. Meng, W.H. Wang, Tunable hydrophobicity on fractal and micro-nanoscale hierarchical fracture surface of metallic glasses, Mater. Des. 95 (2016) 612–617.
[411] C. Ma, S. Suslov, C. Ye, Y. Dong, Improving plasticity of metallic glass by electropulsing-assisted surface severe plastic deformation, Mater. Des. 165 (2019) 107581.
[412] J. Fu, Y. Zhu, C. Zheng, R. Liu, Z. Ji, Enhanced plasticity of bulk metallic glass in different aspect ratios via laser shock peening with multiple impacts, Opt Laser. Technol. 83 (2016) 43–48.
[413] P. Luo, C.R. Cao, F. Zhu, Y.M. Lv, Y.H. Liu, P. Wen, et al., Ultrastable metallic glasses formed on cold substrates, Nat. Commun. 9 (2018) 1–7.
[414] Q. Yang, S.X. Peng, Z. Wang, H.B. Yu, Shadow glass transition as a thermodynamic signature of β relaxation in hyper-quenched metallic glasses, Natl. Sci. Rev. 7 (2020) 1896–1905.
[415] Q. Wang, A. Jain, A transferable machine-learning framework linking interstice distribution and plastic heterogeneity in metallic glasses, Nat. Commun. 10 (2019) 1–11.
[416] D. Wang, Q. Sun, M.J. Hokkanen, C. Zhang, F.Y. Lin, Q. Liu, et al., Design of robust superhydrophobic surfaces, Nature 582 (2020) 55–59.